ROYAUME DU MAROC
Université Mohammed V - RABAT -
جامعة محمد الخامس – الرباط –
Faculté des sciences
كلية العلوم
CENTRE D'ETUDES DOCTORALES - SCIENCES ET TECHNOLOGIES

N° d'ordre **3334**

THESE

En vue de l'obtention du : ***DOCTORAT***

Structure de Recherche : Laboratoire de Matière Condensée et Sciences Interdisciplinaires
Discipline : Physique Informatique
Spécialité : Sciences des matériaux

Présentée et soutenue le 12/09/2020 par :

Hind BENZIDI

Computational design of borohydride-based materials for hydrogen storage applications: Electronic structure and thermodynamics properties from first principles

JURY

Mohammed LOULIDI	PES, Faculté des sciences, Université Mohammed V-Rabat	Président
Abdallah El KENZ	PES, Faculté des sciences, Université Mohammed V-Rabat	Directeur de Thèse
Hassan LASSRI	PES,Faculté des Sciences, Université Hassan II-Casablanca	Examinateur/rapporteur
Mohamed BALLI	PES, Université Internationale de Rabat-Rabat	Examinateur/rapporteur
Abdelilah BENYOUSSEF	PES, Académie Hassan II des sciences et techniques-Rabat	Examinateur
Rachid BENCHRIFA	PES, Faculté des sciences, Université Mohammed V-Rabat	Examinateur
Abdelouahed EL FATIMY	Pr, Ecole Centrale of Casablanca - Casablanca	Examinateur
Omar MOUNKACHI	PA, Faculté des sciences, Université Mohammed V-Rabat	Invité
Abdel EL KHARBACHI	Chercheur, Helmholtz-Institut Ulm- Germany	Invité

ROYAUME DU MAROC
Université Mohammed V - RABAT -
جامعة محمد الخامس – الرباط –
Faculté des sciences
كلية العلوم

DOCTORAL THESIS

By

Hind BENZIDI[1]

Supervised by

Abdallah EL Kenz[2]

Computational design of borohydride-based materials for hydrogen storage applications: Electronic structure and thermodynamics properties from first principles

[1]E-mail:hind.benzidi@gmail.com
[2]E-mail:elkenz@fsr.ac.ma
Laboratory of Condensed Matter and interdisciplinary Sciences (LaMCScI)

"What you learn from a life in science is the vastness of our ignorance."

—J David Eagleman

Acknowledgments

This thesis was carried out at the Laboratory of Condensed Matter and Interdisciplinary Sciences (LaMCScI) of Faculty of Science, University of Mohammed V-Rabat,
Morocco under the supervision of Prof. **Abdallah EL KENZ**.

I owe a great deal of thanks to many people for their kind help during my PhD studies. First and foremost, many thanks to my supervisor Professor **Abdallah EL KENZ** for his invaluable guidance and support on everything from theoretical work to writing thesis. He is always generous with his time providing me with many inspiring discussions and much advice. I highly appreciate that he has given me the opportunities to participate in international scientific conferences, allowing me to learn a lot from other world-leading researchers and develop network for potential collaborations.

I would also thank the thesis committee for reviewing my work and giving their insightful and useful comments. It is an honor for me that they agree to judge this work.

I wish to thank Prof. **Mohammed LOULIDI** from University Mohammed V-Rabat, Faculty of Science, to be the president of the jury members of this thesis. And for his patience in revising my papers and thesis, for providing invaluable insight and constructive criticism to the work I have done.

I would like also to offer my thanks to Prof. **Hassan LASSRI** from The Faculty of Science Faculté des Sciences Ain Chock, University Hassan II, for reporting and reviewing this PhD thesis.

I would like also to thank Prof. **Mohamed BALLI** from International University of Rabat, for reviewing my Ph.D thesis.

I would like to express my very great appreciation, deep gratitude and sincere thanks to Prof **Abdelilah BENYOUSSEF**, for his indispensable practical teaching and supervision, for

extended discussions and valuable suggestions which have contributed greatly to the improvement of the thesis.

I would also like to extend my thanks to Prof. **Rachid BENCHRIFA** from University Mohammed V-Rabat, Faculty of Science, for reporting and reviewing this PhD thesis.

The thesis has also benefited from comments and suggestions made by Prof. **Omar MOUNKACHI**. I take this opportunity to thank him for all the encouragements and supports that he gave me, on my research works, on my publications.

I would like also to express my thanks to Prof. **Abdel EL KHARBACHI** from Ecole Nationale des Ingénieurs of Monastir, Tunisia, for reviewing this Ph.D thesis.

I would like to express my thanks to Prof. **Abdelouahed EL FATIMY**, from Ecole Central of Casablanca, for reviewing this thesis.

I am grateful for the assistance offered by members of the hydrogen materials group : **Marwan LAKHAL, Mourad GARARA, and Mustapha Abdellaoui**, for their useful discussions, contributions, and friendship.

Personal thanks and love to my family that supported me during these three years. Without their love and support I could never have achieved everything that I have in life.

Abstract

Hydrogen is the perfect fuel, it is abundant, the most efficient and produces no emissions when used in a fuel cell or combustion engine. However, hydrogen potential has not been realized even partially mainly because up of storage and commercial production difficulties. A complex hydride LiBH4 is a favorable prospect for solid-state hydrogen storage material capable of releasing the DOE target, because of the attractive volumetric capacity, and a high gravimetric capacity at room temperature exists 18.3 wt\%. Our studies have examined many properties; in which it shows that either the biaxial constraint or substitution of LiBH4 improves the de/hydrogenation properties of lithium borohydride; by the remarkable decrease in enthalpies of hydrogen desorption, and consequently the decrease in dehydrogenation temperature towards the ambient, either in kinetic point of view or the activation energies of diffusion of hydrogen atom in LiBH4 is also decreased. These thermodynamic and kinetic improvements could lead to the use of lithium borohydride LiBH4 in hydrogen storage applications.

KeyWords: Lithium borohydride, Hydrogen storage, First-principles calculation, Strain effect Desorption enthalpy, Activation energies

Résumé

L'hydrogène offre une solution élégante à le creuset de l'environnement. En tant que vecteur d'énergie très flexible, l'hydrogène peut offrir une approche énergétique globale, propre, intégrée et multisectorielle, qui permettra contribuer de manière décisive à la résolution du problème environnemental et à la garantie de l'avenir énergétique de la Terre. Cependant, l'adoption massive de l'économie de l'hydrogène est lente en raison d'un manque d'incitations et de difficultés techniques dans le stockage de l'hydrogène. Les complexes d'hydrures de LiBH4 suscitent un intérêt considérable pour plusieurs applications. Notamment, le stockage de l'hydrogène à l'état solide, en raison de leurs nombreuses propriétés remarquables. Basé sur ceci, nous avons décidé faire une étude approfondie sur l'influence des différentes stratégies utilisé pour améliorer les propriétés de LiBH4. Ces études ont examiné de nombreuses propriétés ; dont nous avons montré que soit le contrainte biaxiale ou substitution de LiBH4 améliore les propriétés de dé/hydrogénation de borohydrure de lithium soit par la diminution remarquable des enthalpies de désorption d'hydrogène, et par conséquent la diminution température de déshydrogénation vers l'ambiante, soit en point de vue cinétique ou les énergies d'activation de diffusion d'atome d'hydrogène en LiBH4 est également diminué. Ces améliorations thermodynamiques et cinétique pourraient conduire à utiliser le borohydrure de lithium LiBH4 dans les applications de stockage de l'hydrogène.

Mots-clefs : Stockage de l'hydrogène, Borohydrure de lithium, la théorie de la densité fonctionnelle, stockage des energies.

Résumé détaillé

En raison de la quantité limitée de combustibles fossiles et de leurs effets sur le climat et l'environnement, il devient une priorité mondiale d'explorer des sources d'énergie alternatives qui sont propres, abondantes et durables. Alors que les énergies durables telles que le solaire, l'éolien et l'hydrogène peuvent répondre à la demande d'énergie, les défis actuels demeurent pour trouver des matériaux capables de stocker et/ou de convertir l'énergie efficacement et à faible coût. L'hydrogène offre une solution élégante à le creuset de l'environnement. En tant que vecteur d'énergie très flexible, l'hydrogène peut offrir une approche énergétique globale, propre, intégrée et multisectorielle, qui permettra contribuer de manière décisive à la résolution du problème environnemental et à la garantie de l'avenir énergétique de la Terre. Cependant, l'adoption massive de l'économie de l'hydrogène est lente en raison d'un manque d'incitations et de difficultés techniques dans le stockage de l'hydrogène. L'objectif de notre projet est d'améliorer les conditions de stockage de l'hydrogène dans des réservoirs a base hydrure complexes. Selon la littérature, les hydrure complexes $LiBH_4$ suscitent un intérêt considérable pour applications de stockage de l'hydrogène à l'état solide. En raison de leurs grandes capacités d'hydrogène gravimétriques et volumétriques. Par exemple, le borohydrure de lithium (LiBH4) possède les capacités les plus élevées parmi les autres matériaux de stockage solides 18.3 % par poids. Néanmoins, la libération partielle d'hydrogène nécessite des pressions et des températures élevées (jusqu'à 600°K, 10 MPa). La décomposition d'hydrure complexe $LiBH_4$ se fait en deux étapes de désorption. Du bore et du LiH sont d'abord formés, suivis par le relâchement de l'hydrogène lié au lithium, donnant finalement du Li, du B et de l'hydrogène. Le LiH formé pendant la première réaction de la désorption est un composé très stable. Cet hydrure est difficilement décomposable, et en pratique, la décomposition du LiBH4 s'arrête après la formation de LiH, laissant un hydrogène lié dans les produits finaux. La capacité hydrogène accessible du LiBH4 est alors réduite à 13.8 % par poids. La mesure de la stabilité de l'hydrure est inversement proportionnelle à son énergie de formation. Lorsque l'enthalpie de formation augmente, la stabilité de l'hydrure diminue. Afin d'utiliser le borohydrure de lithium comme vecteur d'énergie dans les applications mobiles, il est nécessaire d'améliorer les propriétés thermodynamiques du stockage d'hydrogène dans $LiBH_4$ sans réduire sa haute capacité gravimétrique (18,3% en poids). Dans notre étude, le rôle de la contrainte mécanique bi-axiale sur la structure de $LiBH_4$ et leur effet sur la stabilité, les propriétés thermodynamiques et la cinétique d'hydrogénation ont été étudiés. Nos résultats montrent que :

• La contrainte de traction ou de compression bi-axiale à entraîner une déformation de la structure cristalline de $LiBH_4$, et la stabilisation de la structure devient sévère au sein de la contrainte bi-axiale croissante.

• Lorsque la contrainte de compression ou de traction appliquée sur la structure $LiBH_4$ les enthalpies désorbant l'hydrogène de l'hydrogène de LiBH4 sont réduites par rapport à celle de $LiBH_4$ pur, qui est bénéfique pour améliorer les propriétés thermodynamiques de $LiBH_4$.

• Les calculs DFT montrent que les barrières énergétiques pour différents trajets diminuent en fonction de la cinétique d'hydrogénation de LiBH4. La deuxième stratégie utilisée pour améliorer les propriétés de de/hydrogénation est la substitution du bore par l'atome de lithium dans la structure stable du borohydrure de lithium. Premièrement, la possibilité de fabrication de ces systèmes a été confirmée par la valeur négative des enthalpies de formation et les faibles modes imaginaire dans la dispersion des phonons de tous les systèmes. De plus, la température de déshydrogénation est réduite à 521,52 K pour l'hydrogène entièrement libéré pour le système $Li_{1.75}B_{0.25}H_4$. Les propriétés de stockage d'hydrogène considérablement améliorées des systèmes substitué sont attribuées à la diminution des atomes de bore dans le cadre du borohydrure de lithium, ce qui conduit à une hybridation plus faible entre les atomes de bore et d'hydrogène, et par la suite à une gravimétrie élevée capacités. Nos calculs théoriques fournissent une nouvelle approche pour un réglage efficace de la thermodynamique du $LiBH_4$, un candidat de premier plan pour le stockage d'hydrogène à haute capacité. La preuve expérimentale de ces prédictions théoriques peut ouvrir une nouvelle voie pour rechercher des propriétés améliorées de stockage d'hydrogène du $LiBH_4$ et d'autres hydrures complexes connexes.

En général, nous avons fait une étude approfondie sur l'influence des différentes stratégies utilisé pour améliorer les propriétés de $LiBH_4$. Ces études ont examiné de nombreuses propriétés ; dont nous avons montré que soit le contrainte bi-axiale ou substitution de $LiBH_4$ améliore les propriétés de dé/hydrogénation de borohydrure de lithium soit par la diminution remarquable des enthalpies de désorption d'hydrogène, et par conséquent la diminution température de déshydrogénation vers l'ambiante, soit en point de vue cinétique ou les énergies d'activation de diffusion d'atome d'hydrogène en $LiBH_4$ est également diminué. Ces améliorations thermodynamiques et cinétique pourraient conduire à utiliser le borohydrure de lithium $LiBH_4$ dans les applications de stockage de l'hydrogène.

Contents

General Introduction xiii

Energy storage: challenge and perspectives xvii

Research aims and scope xix

Research questions . . . xix

Research Aim . . . xix

Specific objectives . . . xx

Structure of this thesis . . . xx

I Review on hydrogen storage investigations 1

1 Hydrogen storage methods 3

1.1 Hydrogen . . . 3

1.1.1 History . . . 3

1.1.2 Properties of hydrogen . . . 4

1.1.3 Phase diagram . . . 4

1.2 DOE Technical Targets . . . 5

1.3 Established technologies of hydrogen storage . . . 6

1.3.1 Compressed Gaseous Hydrogen . . . 6

1.3.2 Cryogenic Liquid Storage . . . 7

1.3.3 Cryo-compressed Hydrogen . . . 8

1.4 Methods under Research and Development . . . 10

1.4.1 Physical storage . . . 10

Carbon based materials . . . 11

Metal-Organic Frameworks MOF's . . . 14

1.4.2 Reversible Metal Hydrides . . . 15
Metallic hydride formation process . . . 15
Pressure-composition-temperature isotherms (PCT) . . . 16
The different types of metal hydrides . . . 17
1.4.3 Complex metal hydride . . . 19
Amides . . . 20
Alanates . . . 21
Borohydrides . . . 23

II Theory and modeling **29**

2 Density Functional Theory: Concepts and Methods **31**
2.1 Introduction . . . 31
2.2 The Schrödinger equation . . . 31
2.2.1 Basic knowledge . . . 31
2.2.2 The Born-Oppenheimer Approximation . . . 33
2.2.3 Hartree-Fock approximation . . . 34
Hartree's approach . . . 34
Hartree-Fock Method (1930) . . . 35
2.2.4 Thomas-Fermi models . . . 35
2.3 The density functional theory . . . 36
2.3.1 The Kohn-Sham equation . . . 37
2.3.2 The exchange-correlation approximations . . . 38
2.3.3 Methods for electronic structure calculations . . . 40
2.4 Crystal structure and Bloch Theorem . . . 41
2.5 Plane-Waves . . . 42
2.6 Plane wave pseudopotential method . . . 43
2.7 Projector augmented wave method (PAW) . . . 45
2.8 Quantum Espresso . . . 46
2.9 Phonon calculation . . . 47
2.9.1 Crystal structure . . . 47
2.9.2 Lattice dynamics . . . 48

Beyond Harmonic Approximation 51
2.10 Molecular Dynamics calculation 52
2.10.1 Classical Molecular Dynamics 52
Introduction 52
Force calculation 52
2.10.2 Ab initio Molecular Dynamics 53

III Results and discussion **55**

3 Strain effect on dehydrogenation properties of $LiBH_4$ **57**
3.1 Introduction 57
3.2 Model and computational method 57
3.3 Orthorhombic and hexagonal structure of $LiBH_4$ 60
3.3.1 Crystalline structures 60
3.3.2 Electronic properties 60
3.3.3 Phonon dispersion 62
3.4 Thermodynamic properties 64
3.4.1 Vibrational enthalpy and Entropy 64
3.4.2 Heat capacity 64
3.4.3 Thermal expansion 66
3.5 Thermal decomposition of o-$LiBH_4$ 67
3.6 Strain effect on the o-$LiBH_4$ structure 68
3.6.1 Dehydrogenation propereties 70
3.6.2 Hydrogen diffusion 70
3.6.3 Electronic charge density 72

4 Improved dehydrogenation properties of doped $LiBH_4$ **75**
4.1 Motivation 75
4.2 Models and computational details 75
4.3 Li substituted Lithium borohydride 76
4.3.1 Structural properties and Formation enthalpies 76
4.3.2 De-hydrogenation properties 77
4.3.3 Electronic structure 79

4.3.4 Lattice dynamic stability 80
4.3.5 Lattice Thermodynamic properties 81
4.4 Conclusion 83

5 $LiBH_4$ substituted by halide **85**
5.1 Motivation 85
5.2 Model and computational method 85
5.3 Structural optimization 86
5.4 The heat of formation 87
5.5 Lattice dynamic stability 87
5.6 De/hydrogenation and pathways 89
5.7 Conclusion 92

General Conclusion **95**

Bibliography **99**

List of Figures

1.1 The primitive phase diagram of hydrogen [18] 5
1.2 Different types of hydrogen compressed tank [26] 7
1.3 Cryogenic tank (or cryostat) developed by linde [28] 8
1.4 Design schematic of the LLNL Gen-3 cryo-compressed H2 storage tank system [29] 9
1.5 Hydrogen density versus pressure and temperature from BMW [32] . 9
1.6 Common examples Porous MOFs prepared by several research groups (left) [58], H_2 uptake capacities at 77 K versus surface areas for some highly porous MOFs (right) [61] 15
1.7 P-C-T diagram and Van't Hoff plot: α– solid solution of hydrogen in α-phase; β–hydride; $\alpha+\beta$ two-phase [64] 16
1.8 Periodic system of elements with selected elements hydride and non-hydride forming 18
1.9 The desorption temperature as function of each additive 20
1.10 The elements M formed M(BH_4)n, their gravimetric hydrogen densities in the unit of mass%. The asterisks indicate the compounds stabilized at room temperature by coordination with ligands. The parentheses indicate that the compounds are declared unstable at room temperature but can be isolated at low temperature [95] 24
1.11 The desorption temperature T_d as a function of the Pauling electronegativity χ^P of the metal, M'. For the bimetallic borohydrides M' is the more electronegative of the two metals. 25

2.1 Diagram representing the Kohn-Sham equation solved in a self-consistent way 41

2.2 Schematic representation of pseudopotential and the pseudo wave function . . . 44
2.3 Example of a two-dimensional crystal structure (a) and associated reciprocal (b). . . . 48

3.1 Illustration of bi-axial strain . . . 57
3.2 Total energy versus primitive unit cell volume of o-$LiBH_4$ (left) and h-$LiBH_4$ (right) . . . 61
3.3 Total and partial DOS of free-strain, (a)o-$LiBH_4$ (b)h-$LiBH_4$ . . . 61
3.4 Phonon density of states of o-$LiBH_4$ (a) and h-$LiBH_4$ (b) . . . 62
3.5 Phonon band structure and PDOS of o-$LiBH_4$ (a) and h-$LiBH_4$(b) . . . 63
3.6 Vibrational enthalpy (a) and entropy (b) as function of temperature of both $LiBH_4$ structures . . . 65
3.7 Calculated heat capacity as function of temperature of o-$LiBH_4$ and h-$LiBH_4$ at constant pressure (a) and constant volume (b) . . . 66
3.8 The coefficient of thermal expansion as function of temperature of o-$LiBH_4$ and h-$LiBH_4$ . . . 67
3.9 Representation of a) c parameter and volume; b) energy as a function of biaxial strain on $LiBH_4$ . . . 69
3.10 The hydrogen desorption enthalpy according to biaxial strain ϵ(%) in the structure on $LiBH_4$ . . . 71
3.11 Energy curves for diffusing hydrogen between two interstitial sites along the first path and second path . . . 71
3.12 The hydrogen desorption enthalpy according to biaxial strain ϵ (%) in the structure $LiBH_4$ . . . 72
3.13 The three dimensional (3D) electron density contour maps for (100),(010),(001) planes according to rate strain . . . 73

4.1 Crystal structures of (a) pure, (b) $Li_{1.25}B_{0.75}H_4$ (c)$Li_{1.5}B_{0.5}H_4$(d) $Li_{1.75}B_{0.25}H_4$. Green, pink and blue balls represent respectively Li, B and H atoms. . . . 76
4.2 Formation enthalpies from the calculated static density-functional theory as function of atomic fraction of Li in $Li_{1+x}B_{1-x}H_4$ . . . 78

4.3 Desorption enthalpy and temperature as function of Li-substitution rate of $Li_{1+x}B_{1-x}H_4$ (x= 0, 0.25, 0.5, 0.75) 80
4.4 The calculated Total and partial DOS of $Li_{1+x}B_{1-x}H_4$ (x= 0, 0.25, 0.5, 0.75) 81
4.5 Phonon density of states of $Li_1{\equiv}xB_{1-x}H_4$ (x= 0, 0.25, 0.5, 0.75) 82
4.6 Temperature Helmholtz free energy F(V, T), vibrational entropy S, and heat capacity C_v of $Li_1{\equiv}xB_{1-x}H_4$ (x= 0, 0.25, 0.5, 0.75) 83

5.1 The optimized crystal structures of 2x2 supercells: Perspective views of LiBH4/LiX (with X= F, Cl, Br, I) systems 88
5.2 The calculated formation enthalpy of o-$LiBH_4$ and $LiBH_4$:LiX (with X= F, Cl, Br, I) 89
5.3 Total phonon density of states of $LiBH_4$:LiX (with X= F, Cl, Br, I) 90
5.4 Theoretical hydrogen storage capacity of $LiBH_4$:LiX (with X= F, Cl, Br, I) 91

List of Tables

1.1 Atomic and Molecular Hydrogen properties 4
1.2 The U.S. DOE hydrogen storage system performance targets [23, 24] . 6
1.3 Reported results on carbon nanostructure for hydrogen storage [39–46, 48–55] 13
1.4 Intermetallic Compounds and their types [72] 18
1.5 gravimetric capacity, enthalpy of desorption, and decomposition temperature of alkaline and alkaline earth alanates [60, 85–88] 22
1.6 Hydrogen storage properties of some borohydrides, $M(BH_4)_n$ [84, 88, 94–99] 26

3.1 Lattice parameters and positions for hexagonal and orthorhombic symmetries. Experimental results are included for comparison 59
3.2 Interatomic distances (Å) of hydrogen and other neighboring atoms. Experimental results are included for comparison 59
3.3 Comparison of vibrational enthalpy and entropy results with experimental data 64
3.4 Calculated heat capacity of o-$LiBH_4$ and h-$LiBH_4$ at constant pressure and constant volume compared with other calculated and experimental data 64
3.5 Lattice parameters, total energy of each component 68

4.1 Lattice parameter, volume, formation enthalpy, gravimetric and volumetric capacity of $Li_{1+x}B_{1-x}H_4$ (x = 0, 0.25,0.5, 0.75). 77
4.2 Desorption enthalpy and temperature of $Li_{1+x}B_{1-x}H_4$ (x= 0, 0.25, 0.5, 0.75) 78

5.1 Optimized equilibrium cell volume, lattice parameter and internal interatomic of $Li(BH_4)_{1-x}X_x$ where (X= F, Cl, I, Br) in HT phase 86
5.2 The enthalpy enthalpy and the corresponding desorption temperature of $LiBH_4$:LiX (with X= F, Cl, Br, I) 91

List of abbreviations

DoE	Department of Energy
CNTs	Carbon nanotubes
MOFs	Metal organic framework
TPES	Total primary energy supply
GHG	Greenhouse gas
PV	Photovoltaics
ICE	Internal combustion engine
PEM	proton exchange membrane
PEMFC	proton exchange membrane fuel cell
DMFC	Direct Methanol Fuel Cell
PAFC	Phosphoric Acid Fuel Cell
AFC	Alkaline Fuel Cell
SOFC	Solid Oxide Fuel Cell
MCFC	Molten Carbon Fuel Cell
COFs	Covalent organic frameworks
PIMs	Polymers of intrinsic micro-porosity
SWNT	Single wall structure
MWNT	Mmultiple wall structure
HCP	Hexagonal close-packed
DC	Direct current
RF	Radio frequency
UHV	Ultra-high vacuum
C_g	Gravimetric capacity
C_v	Volumetric capacity
wt.	Weight
T_{des}	Desorption Temperature
P	Equilibrium pressure
T	Temperature
R	The gas constant
E_a	Activation energy
K_β	Boltzmann constant
G	Free energy
ΔH	Heat of formation
ΔS	Entropy
E_{tot}	Energy total
DOS	Density of states
PDOS	Partial desnity of states
VB	Valence band
CB	Conduction band
TM	Transition metal

ab initio	First principal calculation
Ψ	Many-body wave function of electrons
$\hbar$	Planck's constant devised by 2π
e	Charge of the electron
m_e	Mass of the electron
M_I	Mass of the nucleus
Z_I	Charge of the nucleus
R_I	Position of the nuclei
r_i	Position of electron
T_e	Kinetic energies of the electrons
T_n	kinetic energies of the the nuclei
V_{int}	Internal potential
V_{ext}	External potential
V_{nn}	nucleus-nucleus potential
$n_H(z)$	Number of hydrogen in plan z
$n_S(z)$	Number of interstitial sites in plan z
$\rho(z)$	Density of Hydrogen in plan z
t_{eq}	Equilibrium time
t_f	Filling time
t_r	Relaxation time
V_{ee}	Electron electron potential
V_{KS}	Effective potential
$V_H(r)$	Hartree potential
$V_{xc}(r)$	Exchange-correlation potential
$\hat{H}$	Hamiltonian operator
Z	Partition function
LDA	Local density approximation
LSDA	Local Spin-Density approximation
GGA	Generalized gradient approximation
MC	Monte Carlo
MMC	Metropolis Monte Carlo
MCMC	Markov chain Monte Carlo
KMC	Kinetic Monte Carlo
ΔE	Energies difference
F	Hydrogen flux
M_{H_2}	Molecular mass of hydrogen
P_i	probability
R_i	The rate transition
R	Total rate transition
DFT	Density functional theory

I dedicate this manuscript to My parents and My sister Nawal

General Introduction

Energy storage: challenge and perspectives

The world population is exceeded 7.7 a billion inhabitants during the beginning of the 2018 year, and it is expected to reach 80 a million per year by 2050 [1]. The increase in the human population is simultaneously supported by a continual increase in energy consumption. Indeed, the viability of our economic models and quality of life are directly related to our ability to access energy, there is a strong connection between the availability of energy and the growth of a nation [2]. According to U.S. IEA [3] [3, 4], the energy consumption grows across all major end-use sectors. However, increases in efficiency, represented by declines in energy intensity [4] [5]. This was strengthened by a strong global economic augmentation in oil, gas, and coal which met most of the increase in demand for energy. Over 70% of global energy demand growth was met by oil, natural gas, and coal; renewable accounted for almost all of the remainder [6]. Fossil fuel based economy suffers from unrestrained release of greenhouse gas emissions and limited feedstock. Overwhelming reliant on the fossil fuels for the present energy needs is leading to air pollution [5] and global warming. Almost 70 percent CO_2 of rise was caused by the burning of fossil fuels like oil, coal, and gas, and the largest emissions estimated from buildings and industry [6–8]. As results, The global energy-related CO_2 emissions increased by 1.4% in 2017 [9], reaching a record level of 32.5 Gt. This rise comes after three years of stabilization of emissions. All countries need to increase their mitigation efforts and levels of ambition to reverse the tide of emissions growth, if decarbonisation pathways consistent with the climate targets of 1.5 °C and well-below 2 °C [10]. In the context of strengthening the global response

[3] Energy Information Administration Statistical Review of World Energy of 2019
[4] The amount of energy consumed per unit of potential demand
[5] CO, CO_2, NOx, SOx, or O_3

to the threat of climate change, creating a sustainable energy future is the world's greatest challenge that we are currently facing. To succeed in the energy transition, it is necessary to find alternative forms of energy to fossil resources. The exploitation of renewable energies theoretically generates few pollutants. In particular, electricity from renewable origin emits very little CO_2 especially when compared to fossil fuels such as coal [11]. For this reason, renewable energies are a particular vector of the fight against global warming. Indeed, renewable energies are sometimes criticized for their lower energy efficiency compared to fossil fuels. Production costs are also often considered higher in the short term. But above all, they are characterized by a more uncertain availability. This implies building batteries or complex storage systems that require many natural resources and increase pollution from renewable energies.

The hydrogen was initially used in the space industry as a fuel. Like other technologies used in advanced fields, studies and technical progress on transport, storage and more generally the use of hydrogen have discovered its potential as an energy carrier. It is today considered as future alternative to the use of fossil fuels in general, and petroleum in particular, for many reasons including the limited supply of readily accessible reserves, national security,and environmental impact [12]. It can be used in a full range of applications in all sectors of the economy: transportation, power, industry, and buildings. Across the world, researchers are trying to improve the efficiency and costs of producing, storing, transporting and using hydrogen in applications as diverse as heat and transport. The Hydrogen Council envisages that by 2030, 230–250 TWh of surplus solar and wind energy could be converted to hydrogen [13]. It suggests hydrogen could provide almost a fifth of total energy consumed by 2050, and cut carbon emissions by about six billion tonnes compared to today [13]. Moreover, it will tackle the air pollution that is the scourge of so many industrialized nations.

Research aims and scope

Once the hydrogen is produced in a cost-effective and environmentally friendly way, now comes the question of storage. It is necessary to develop techniques to transport it but specially to store it. Hydrogen has a very high energy content by weight, which presents about three times more than gasoline, but it has a very low energy content by volume, liquid hydrogen is about four times less than gasoline. This is a challenging goal because these physical characteristics that make it difficult to store in large quantities without taking up a significant amount of space. In the solid-state storage, there are several types of potential hydrogen storage materials. But there are always advantages and drawbacks, and the selection of a technology depends on the nature of the problem in a way that the disadvantages have less impact in the overall application.

Research questions

The main question is how to store hydrogen and move it around efficiently, which method of storage is the most efficient, is it possible to store hydrogen in complex hydride in effective way ?

Research Aim

The long-term goal of our research is on one hand to design a high capacity complex borohydride for storing hydrogen at room temperature and ambient pressure. On the other hand to develop strategies leading to a high-performance energy storage system based on complex borohydride materials.

Specific objectives

The objective of the current study is to provide a comprehensive review of literature and industry practices in relation to energy storage systems based on complex hydride materials and outline their drawbacks in order to improve it, which can be divided into two aspects namely strain engineering and substitution. The main objectives include:

- Increasing storage mass capacities
- Improving reversibility
- Carrying out cycling
- Improving kinetics of reaction
- Stabilizing the systems.
- Determine activation energy for ion diffusion

Structure of this thesis

The thesis is composed of three parts:

- The first part termed literature review is composed of two chapters, the first one gives an overview of Hydrogen storage methods, while the second is dedicated to benchmark results on hydrogen storage in complex borohydride especially Lithium borohydride based material.
- The second part is devoted to laying out theoretical analysis based on the density functional theory presented in the first chapter of this part. A detailled description of the code concerned with the methodology used for this study is also given in this part. The third part is devoted to the results and discussion the findings of the research:
  - In Chapter 3 the strain effect of $LiBH_4$ is developed. The reactants' ratio is varied to obtain different particle sizes and size effects are discussed. The effects of different reducing agents are also discussed in this chapter.

  - In chapter 4 a novel substitution approach to tune the problematic thermodynamic of $LiBH_4$ is considered. In addition, the vibrational and thermodynamic properties were investigated also to explore the possibility of lowering the hydrogen desorption temperature and reversibility of substituted lithium borohydride structure.

- Finally, the main conclusion gives a brief summary and criticism on our results. it includes a discussion of the impact of our findings to future research for the uses of $LiBH_4$ as solid-state hydrogen storage material.

Part I

Review on hydrogen storage investigations

1 Hydrogen storage methods

As described above Hydrogen storage is a key enabling technology for the advancement of hydrogen and fuel cell technologies in applications including stationary power, portable power, and transportation. However, its low ambient temperature density results in a low energy per unit volume. Therefore requiring the development of advanced storage methods that have potential for higher energy density. The aim of this chapter is to view various aspects on hydrogen storage, and describes advantages and disadvantages of the different techniques that are available for storing hydrogen.

1.1 Hydrogen

1.1.1 History

Hydrogen is the first chemical element of the periodic table with the symbol H, atomic number 1 and atomic weight of 1.00794. It is the lightest element on the periodic table and the most abundant chemical substance in the universe. The Hydrogen was discovered by Henry Cavendish in 1766 [14] via the mixing of metals with acids. Then, Antoine Lavoisier gave it the name of "Hydrogen" [1], due to its property to produce water when combusted. In 1932, Harold Urey reported the discovery of a stable isotope, deuterium (^{2}H or D) with an atomic weight of 2, deuterium is present in natural hydrogen to the extent of 0.015% [15]. Two years later, an unstable isotope, tritium (^{3}H), with an atomic weight of 3 was prepared by the group of by Ernest Rutherford in 1932 [16].

[1] which is a Greek name meaning "water forming"

TABLE 1.1: Atomic and Molecular Hydrogen properties

Atomic Hydrogen			
Atomic number	1	Atomic radius, non-bonded (Å)	1.10
Electron configuration	1s1	Electron affinity (eV)	0.7542
Density (g cm^{-3})	0.000082	Ionisation energies (eV)	13.595
Isotopes	1H, 2H, 3H	Electronegativity (Pauling)	2.1
Molecular Hydrogen			
Bond distance (Angstrom)	0.7416	Dissociation energy (25°C, kJ mol^{-1})	435.93
Ionization potential (eV)	15.427	Density of solid (g cm^{-3})	0.08671
Density of liquid (-252.78 °C,g cm^{-3})	0.07099	Heat of combustion to water (kJ mol^{-1})	-241.82

1.1.2 Properties of hydrogen

Hydrogen is a colorless, odorless gas. It is easily ignited. Once ignited it burns with a pale blue, almost invisible flame, the vapors are lighter than air. Hydrogen can form compounds with most elements and is present in water and most organic compounds. The Table 1.1 lists the important properties of atomic hydrogen and molecular hydrogen (H_2).

1.1.3 Phase diagram

At normal conditions, hydrogen is in gaseous state. It has the second lowest boiling point and melting points of all substances. Hydrogen liquefies below 20 K at atmospheric pressure. In these conditions, the liquid is 800 times denser than the gas at ambient temperature. Gas liquefaction processes involve techniques quite complex which combine cold intake and adiabatic relaxation [17]. The first liquefaction hydrogen was obtained by Claude using a cycle divided into several steps [18]. The gas is firstly cooled from the ambient to 230 K by a group mechanical refrigeration then up to 80 K using a liquid nitrogen ex-changer. Hydrogen then undergoes compression-expansion cycles which further reduce temperature before being subjected to Joule-Thompson relaxation which leads to the liquefaction[18]. Other processes can be envisaged such as the Brayton cycle which uses the liquid helium whose liquefaction temperature is lower than that of hydrogen or Magnetometer cycle refrigeration. The hydrogen is in solid state below its melting point of 259 °C (14 K) and atmospheric pressure. A phase diagram of hydrogen is shown in Figure 1.1, with a triple point at -259.1 °C and 0.07 bar and a critical point at -239.8 °C and 13 bars. At atmospheric pressure the boiling point (T_b) is at -253

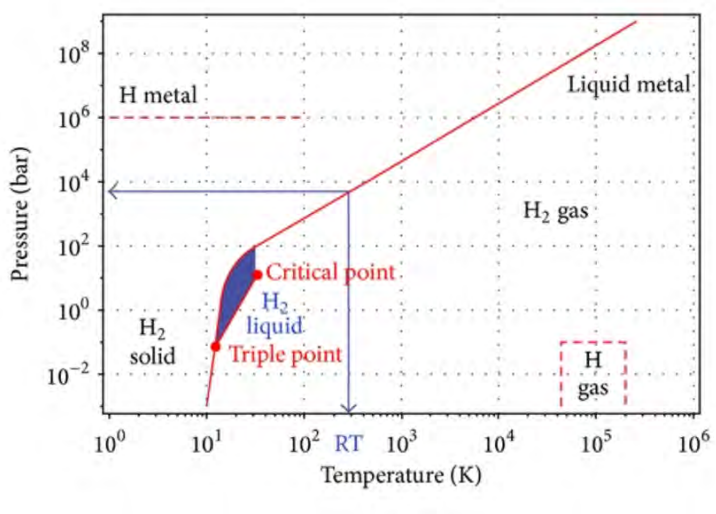

FIGURE 1.1: The primitive phase diagram of hydrogen [18]

°C and the melting point (T_m) at -259 °C. The boiling point of a fuel is a critical parameter since it defines the temperature to which it must be cooled in order to store and use it as a liquid [18].

1.2 DOE Technical Targets

Before the analysis of hydrogen storage methods, a perfect storage medium for mobility can be outlined by qualifying or quantifying the characteristics of every system. High volumetrical and gravimetrical energy densities are clearly fascinating for mobile applications [19]. Gasoline and diesel are presently the ever-present fuels for transportation, and that they may be used as a benchmark. The energy densities of those fuels vary as a result of complicated mixtures and totally different blends are on the market [20]. However, values near to 38 wt% try to 35 MJ L^{-1} are typical [21]. Pure H_2 at ambient temperature and pressure offers glorious measuring however poor volumetric energy densities of a 120 MJ kg^{-1} (100 wt %) and 0.01 MJ L^{-1}, respectively [22]. Furthermore, for a perfect storage technique, safety is important, particularly for general public use. Toxicity, flammability, danger of explosion or projections, etc., aren't recommendable. The U.S. Department of Energy (DOE) hydrogen storage system targets facilitates guide researchers by shaping system necessities to realize commercially hydrogen storage [23]. The table below summarizes the DOE performance targets for hydrogen storage systems

TABLE 1.2: The U.S. DOE hydrogen storage system performance targets [23, 24]

Storage Parameter	System Gravimetric Capacity (wt %)	System Volumetric Capacity ($MJ\,L^{-1}$)	Cost $/kWh
2020	4.5	2.9	10
2025	5.5	3.6	9
Ultimate	6.5	6.1	8

aboard light vehicles for a practice range quite three hundred miles [24]. These technical targets for 2020 and 2025. These targets' area unit supported equivalency to current fuel storage systems in terms capacity, cost, and different operational parameters. Regarding the reversible storage of hydrogen consistent with that the system gravimetric capacity ought to be 6.5 wt % and also the system volumetric capacity ought to be 6.1 $MJ\,L^{-1}$. To meet such need the main issues for hydrogen storage are [22–25]:

- Reducing weight, and volume of thermal parts is required;
- Operating temperature that may be vary between -40 and 60 °C;
- Operational cycle life of 1,500
- Charging/Discharging Rates of 3 to 5 min

1.3 Established technologies of hydrogen storage

1.3.1 Compressed Gaseous Hydrogen

The compressed H_2 gas (GH_2) in the storage tank is simplest method of reducing the volume of a gas, at a constant temperature, is to increase its pressure. This method is considered to be a solution for hydrogen storage due to the relative simplicity of gaseous hydrogen, rapid refueling capability, excellent dormancy characteristics, and low infrastructure impact. Under this form, hydrogen is contained in pressurized tanks. Higher pressure translate great amount of the hydrogen stored. For their design, the gas tanks are grouped under 4 types (figure 1.2) [26, 27]:

- **Type I** (pressure limited to 50 MPa)cylindrical metal tank

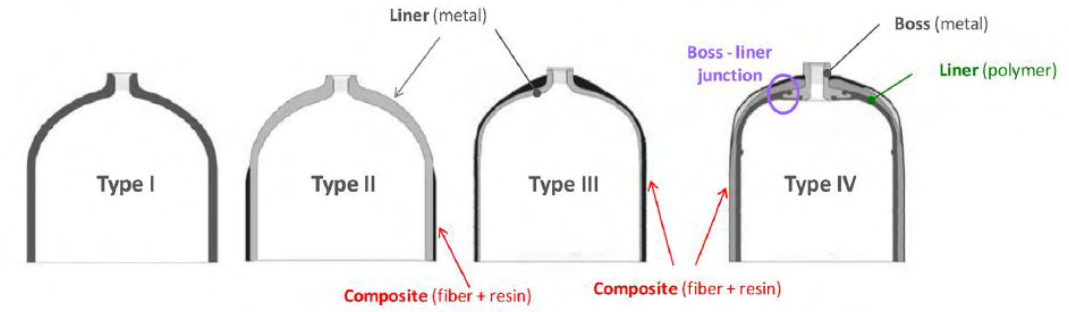

FIGURE 1.2: Different types of hydrogen compressed tank [26]

- **Type II** (pressure not limited) tank containing a metal envelope for mechanical strength, fretted by continuous fibers impregnated with resin.
- **Type III**(for P<45MPa) reservoir consisting of a metal shell to contain hydrogen and a continuous resin impregnated fiber envelope for mechanical holding.
- **Type IV** (For P<100MPa) reservoir consisting of a non-metallic envelope to contain the hydrogen and a continuous resin impregnated fiber envelope for mechanical latency.

For each type of tank, the choice of the envelope (liner) in contact with the hydrogen is of prime importance. In the case of Type I, the mechanical stresses are directly taken up by the liner; a material with a large elastic limit will therefore be preferred (steel). In the case of Type III and IV tanks, the liner serves as a hydrogen barrier. A material that is not very permeable to hydrogen will then be preferred (Aluminum in the case of type III). The shape of the vessels is generally cylindrical but they can also be polymorph or toroid. At pressure of 700 bar, the hydrogen has a density of 42 $kg\,m^{-3}$ against 0.090 $kg\,m^{-3}$ at normal pressure and temperature. Today most of the car manufacturers have retained the solution of high-pressure gas storage. This technology makes it possible to store the quantity of hydrogen required for a car fueled by a fuel cell to travel from 500 to 600 km between each fuel tank.

1.3.2 Cryogenic Liquid Storage

Low temperature liquid hydrogen is called cryogenic liquid hydrogen. The conversation Cryogenic hydrogen is organized in containers formed by several

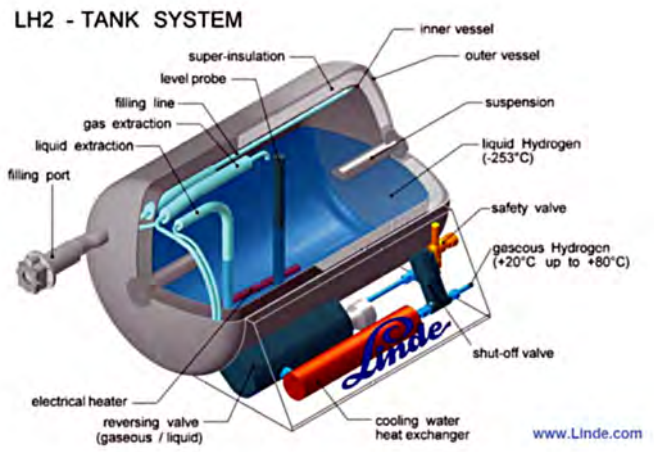

FIGURE 1.3: Cryogenic tank (or cryostat) developed by linde [28]

layers of thermal insulation ensured by the vacuum maintained in double walls and by sheets of insulating and metallic materials that reflect heat radiation. Everything is protected by a stainless steel or material casing composites(see figure 1.4) [29]. The Hydrogen is liquefied when cooled to a temperature below -252.87 °C and at 1.013 bar, the liquid hydrogen has a density of nearly 71 $kg\,m^{-3}$. At this pressure, 5 kg of hydrogen can be stored in a 75 L tank [30]. The critical pressure is 13 bar and critical temperature is -240 °C. In order to be able to keep liquid hydrogen at this temperature, the tanks must be perfectly insulated(figure 1.3). The storage of hydrogen in liquid form is for the moment reserved for certain particular applications of very high technologies such as space travel.

1.3.3 Cryo-compressed Hydrogen

The hybrid technologies; cryo-compression; consists on combining pressure and low temperature to increase the amount of hydrogen that can be stored by volume and avoid the energy cost linked to the liquefaction of hydrogen. The gaseous hydrogen compressed at cryogenic temperature is much denser than that of compressed gas tanks at room temperature. Figure 1.4 presents an example of prototype of the LLNL Gen-3 cryo-compressed tank system. These new reservoirs would be used to store hydrogen at low temperatures of 80 K and pressures between 200 and 400 bar [31]. This approach requires the development of composite tanks insulated under

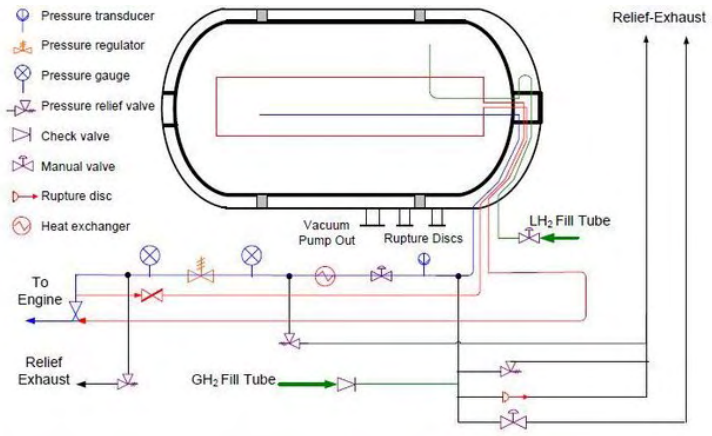

FIGURE 1.4: Design schematic of the LLNL Gen-3 cryo-compressed H2 storage tank system [29]

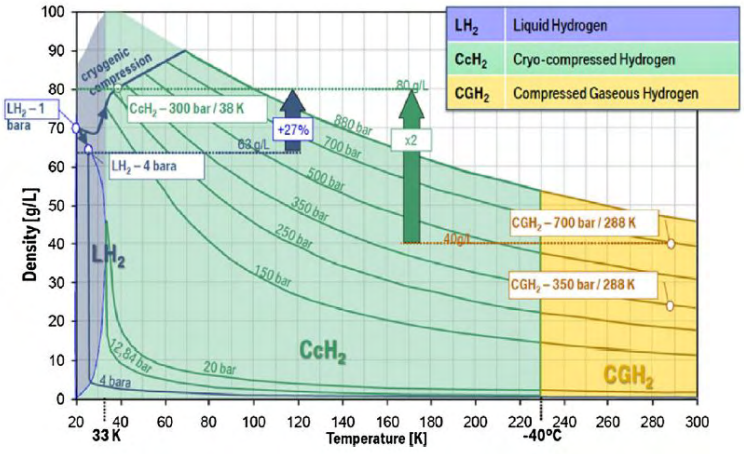

FIGURE 1.5: Hydrogen density versus pressure and temperature from BMW [32]

pressure. The use of cold hydrogen gas tanks requiring less cooling could also be considered. An optimal combination of pressure and temperature in the 80-200 K range is to be considered .

To sammury Indeed, in its gaseous form Hydrogen has a density of 0.09 kg m^{-3}. It seems impossible to store it at ambient pressure for a vehicle to have a range of 400 km, it would need a mass of Hydrogen of 4 kg, or a volume of 45000 L! With a current tank, it would cover 600 m. Recall that gasoline was chosen as fuel among other things for its quantity/volume ratio. It is obvious that Hydrogen will never be able to compete with it on this point, but it can still try to get closer to it, in particular by a high pressure: as indicated by Boyle's law, increase the pressure of a gas reduces its volume at constant temperature. In its liquid form, Hydrogen has

a density of 70.8 kg m^{-3}, which makes it advantageous for liquid storage compared to gas storage. But the main failure is the importance of the secondary systems necessary to reach a liquid form. The Hydrogen must be brought to a pressure of 10 bar and a temperature of about -253 °C. This involves tanks with very high thermal insulation, and therefore bulky, to maintain the Hydrogen at this temperature and avoid losses by evaporation. This does not prevent parasitic evaporation, of the order of 3% per day. In addition, the liquefaction of Hydrogen is an energy intensive operation: approximately 40% of the energy contained in the gas.

1.4 Methods under Research and Development

An alternative to the previous discussed method (gaseous,liquid, and hybrid storage methods) is materials-based hydrogen storage. Which is divided into three classes: first surface storage systems; second,metal hydride; and third, complex hydride. Most of these storage methods are still in development, and a numerous academic researchers have addressed this question.

1.4.1 Physical storage

The adsorption of a gas like hydrogen by solid, or physisorption, is the increase of the density of this gas on the surface of the solid [2] by the effect of the intermolecular forces. This adsorption increases with the pressure of the gas and the more important that the temperature is lower and the interaction surface with the solid is greater. Being purely physical, physisorption is perfectly reversible: it decreases when the pressure is lowered and/or the temperature increases. The phenomenon is based on the van der Waals interaction between carbon materials and hydrogen molecules. The interaction energy between solid material and hydrogen molecules can be estimated by [33]:

$$E = \frac{\alpha_{H_2}\alpha_{substrat}}{R^6} \tag{1.1}$$

where α is the polarizability and R is the interaction distance. The capacity of physisorption based hydrogen storage can be calculated as the sum of adsorption on solid surface and compression on slit pores. Adsorption of hydrogen occurs in

[2] Adsorbents

micropores where the density of hydrogen-adsorbed phase is higher than that of unadsorbed gaseous phase at above critical point. The hydrogen storage capacity of adsorbent material can be determined by micropore specific surface area (SSA), physisorption of latest nanoscale materials with high specific extent that is caused by weak Van der Waals forces between the adsorbate and therefore the adsorbent. The mix of a long-range engaging term and a short-range repulsive term offers rise to a shallow minimum within the potential energy curve at a distance of roughly one molecular radius of the gas molecule, this energy minimum corresponds usually to 1–10 $kJ\,mol^{-1}$ [18, 34]. As the forces involved in the interaction between adsorbate and adsorbent are very weak, physisorption usually takes place only at low temperature. There is no energy barrier to prevent the molecule approaching the surface from entering the physisorption well, therefore the process is non activated and fast kinetics is characteristic for physical adsorption.

Carbon based materials

Activated carbon(AC) is a form of processed carbon comprising graphite crystallites and amorphous carbon, fabricated from biomass resource and normally of less than 1 nm pore diameter possessing a SSA of 3000 $m^3\,g^{-1}$ [35]. The experimentally measured hydrogen storage capacity also depends on the material employed (doping, etc), which ranges between 0.5 and 5 wt% [36]. ACs possess low mass density and a high surface area. Weak van der Waal's forces enable the physisorption of hydrogen molecules as they get adsorbed and diffuse into the pores of the ACs [37]. It has been tested for AC having SSA of 2560 $m^3\,g^{-1}$ for hydrogen adsorption at room temperature and 77.4 K. The experimentally measured maximum hydrogen storage capacity was reported as 4.5 wt% at temperature of 77.4 K with high adsorption kinetics and reversibility [38]. Also, it is provided that hydrogen adsorption in AC it can be more efficient than compressed gas at cryogenic temperature by Bénard and Chahine [39].

Graphite is sp2 hybridized with a sheet like structure where in all atoms are weakly bonded and exist in a plane,and is held together by van der Waals forces to the sheets above and below. In spite of having high polarizability, graphite

possesses low hydrogen storage capacity due its small interlayer distance and low SSA. The interlayer gap (3.354 Å) of graphite is considerably small for intercalation of H_2 molecules (4.06 Å) [40]. Therefore, a several method have investigated to increase the interlayer distance, which can subsequently increase the SSA of graphite. For example, Doping by alkali-metal or metal increase distance between sheets and consequently increase hydrogen storage capacity (Ni(0.92wt%), Cu(0.97 wt%), Co(1.8 wt%), Al(3.48 wt%), Li(6.5 wt%) [41–45]).it is reported also that graphite nanofiber and ball-milling of graphite increases the SSA due to reducing of particle size.

Carbon aerogels(CAs) are another class of porous carbon materials with high surface areas and large mesopore volumes, the cost of supercritical drying is extremely high. that are derived from organic aerogels. They consist of interconnected clusters of carbon nanoparticles with diameters ranging from 3 to 20 nm. Due to their mesoporosity, low density, and high surface area, carbon aerogels are promising materials as adsorbent for hydrogen storage application.

Fullerene is a molecule composed of carbon that can take a geometric shape reminiscent of a sphere, an ellipsoid, a tube (called nanotube) or a ring. Fullerenes are similar to graphite, composed of linked hexagonal rings, but containing pentagonal and sometimes heptagonal rings, which prevents the leaf from being flat. Fullerenes are the third known form of carbon [46]. the most common is C60 which is constituted of 12 pentagons and 20 hexagons, with a shape comparable to that of a soccerball. Based on the calculations of C60 the theoretical hydrogen storage capacity reachs 8 wt% with the presence of transition metals as titanium and scandium [47].

Carbon nanotubes (CNT) are an allotropic form of carbon belonging to the family of fullerenes. They are composed of one or more layers of carbon atoms wounded on themselves forming a tube. The tube might or might not be closed at its ends by a half-sphere. We distinguish between single-walled carbon nanotubes (SWCNT). and multi-walled (MWCNT) [48, 49]. The hydrogen storage capacities

TABLE 1.3: Reported results on carbon nanostructure for hydrogen storage [39–46, 48–55]

Adsorbent	additive	Hydrogen storage(wt%	Condition T(K),P (bar)	Synthesis method
Activated carbon		5.40	77, 5	
		5.60	77, 3.2	KOH activation
		3.70	77 , 0.2	High temperature activation of precursor 900C in CO2 environment for 24 hours
		2.50	77, 3	Commercial
	F	4.50	77, 2.6	
	Ni	1.00	298, 10	metal doping
	Pt	1.20	298, 10	
Graphite	Cs	0.85	120, 1.0	Two bulb reaction,300 C at 60 Torr Ar
		1.24	77, 0.1	Two bulb reaction,300 C at 60 Torr Ar
	Li	0.06	293, 0.2	Wet chemistry
	Rb	1.03	100, 0.5	Two bulb reaction,300 C at 60 Torr Ar
Carbon Aerogel		5.30	77, 3.0	Sol-gel Synthesis/Activation
		0.90	298, 10	Sol-gel Synthesis/Activation
	Co	2.10	77, 3.0	Sol-gel Synthesis/Ion exchange doping
	Pt, H	1.70	77, 3.0	Sol-gel Synthesis/Ion exchange doping
	Pt, H	0.80	298, 10.0	Sol-gel Synthesis/Activation/Vapor phase deposition
Fullerene	C60 + Fe	0.5		Wet chemistry
	C60 +Li	0.47		Wet chemistry
Carbon Nanotube	CNT	0.54	77, 0.2	temperature Chemical Vapor Deposition 900C in CO and H2 mixture
	SWCNT	3.00	77, 2.0	Chemival Vapor Pulsed laser, chemical vapor deposition, 1100 to 1300K
Nanofibers	GNF	0.7	300, 10.5	
	CNF	6.5	300, 10	

of CNTs are mainly depending on its structure, pretreatments, geometry, structural defects,operating pressure, temperature, and so on.

Carbon nanofibers are cylindrical structures composed of graphene sheets organized in a precise geometry. CNF structures can be formed at elevated temperatures from the mixture of carbon-contained gases and hydrogen. It can also be formed from hydrocarbons alone using nickel andiron-based alloys as catalyst. Different types of CNF with difference in morphology, crystalline structure, and shape are possible by varying nature and geometry of catalyst as well as reaction condition. Hydrogen penetrates into the nanopores formed by the layers of CNF and the interior of CNT forming an intercalated layer of hydrogen.

To summary - The carbon materials are one of the most interesting materials for solid- state hydrogen storage due to its low atomic weight and microporous nature that adsorbs the hydrogen molecules at its surfave through Van der Waals interaction forces. Experimental studies beyond well-known physisorption lead to

a large set of various maximum hydrogen adsorption capacities. However, most of the results were obtained under special conditions either at 77 K or with high pressure (Table 1.3). The hydrogen storage capacity of carbon materials mainly depends upon surface area, which is affected by micropore size distribution that counts for presence of narrow micropores. However, the pure carbon surface cannot activate hydrogen molecule, concluded from the binding strength of hydrogen molecule which is almost the same for all kinds of carbon materials and the magnitude of interaction comes around 5 kJ mol^{-1}. Thermal treatments and metal doping on carbon nanostructures are observed to be useful for improving hydrogen storage capacities but unfortunatly, higher storage capacities can be obtained only at cryogenic temperature and higher pressure. The cost of these materials varies from very low for Expanded Natural Graphite (ENG) to very high for MWCNTs.

Metal-Organic Frameworks MOF's

The Metal-organic frameworks (MOFs) are the first and widely studied porous materials with regard to hydrogen economy. Thanks to their ultrahigh porosity and surface areas of well–designed which allows storing significant amounts of hydrogen at cryogenic temperatures. MOFs are crystalline porous frameworks that consist on two components secondary building units (clusters or metal ions) surrounded by organic molecules (linker). MOFs can be synthesized by the solvothermal reaction of metal ions and various carboxylic acids. Various metal sources are used within the synthesis of MOFs, such as Ni,Zn, Cr, Mn, Cu, Ni, rare-earth element metals, and alkali metals. A several MOFs types have been found in the last 20 years depending on the coordination number of secondary building units,linker type, different symmetry and pore sizes [17, 56–60]. The building blocks of the framework metals and organic linkers can be combined in almost infinite ways to create novel materials. Therefore, unique structural characteristics can be achieved by tuning the basic materials according to their specified application. Dillon et al [62] confirmed the adsorption of hydrogen molecule on the nanostructured carbon materials or metal organic frameworks (MOFs). They have potentially high gravimetric capability, as a result of they need high surface areas (4000 $m\,g^{-2}$), but their volumetrical capacity for H_2 storage

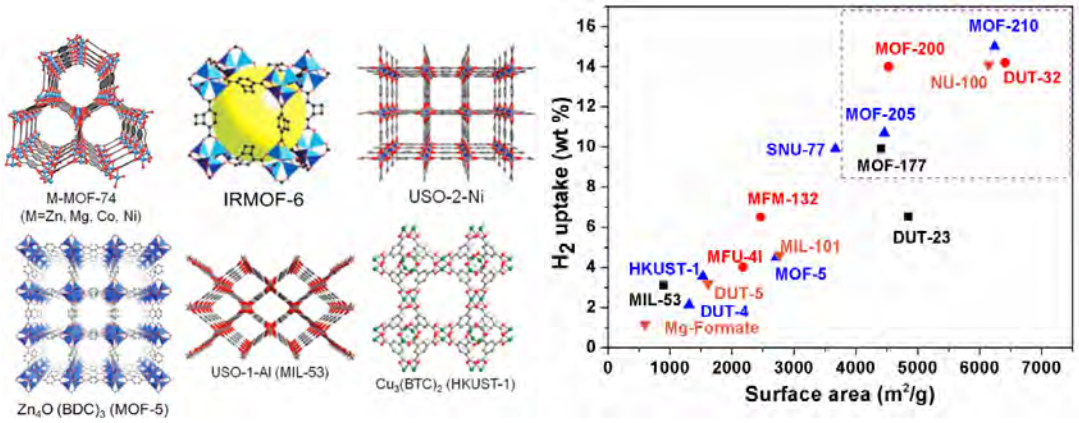

FIGURE 1.6: Common examples Porous MOFs prepared by several research groups (left) [58], H_2 uptake capacities at 77 K versus surface areas for some highly porous MOFs (right) [61]

can most likely be low [62, 63]. However, one advantage of these materials is that the binding of hydrogen is weak that the liberation of gas should not need high temperatures. Scientific efforts are made to develop and modify MOFs for H_2 storage. However, we might prefer to note that cryogenic (77 K) conditions at ambient pressure (1 bar) are impractical [62, 63] (figure 1.6)

1.4.2 Reversible Metal Hydrides

Another solution is to store hydrogen in the solid state which is the reversible hydrides based metal. Certain metals or alloys have the property of reacting spontaneously with hydrogen, depending on the next form:

$$M + xH_2 \Leftrightarrow MH_{2x} + \text{heat} \quad \{1\}$$

The product obtained from this reaction is a metal hydride plus heat. (Exothermic reaction). Hydrides are classified into three categories, according to the nature of the bond of hydrogen with metal, we find ionic, covalent and metallic hydrides.

Metallic hydride formation process

The hydriding process of an intermetallic compound is an exothermic reaction. It is described by a direct combination of the intemetallic compound and hydrogen, according to the following steps:

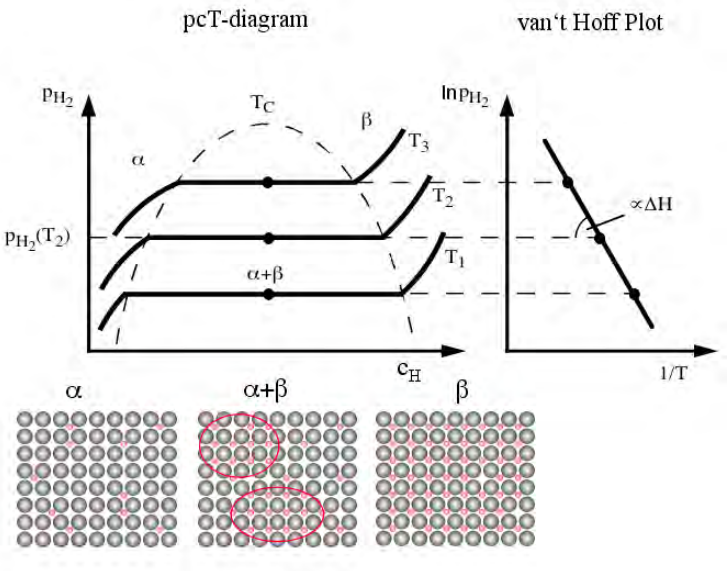

FIGURE 1.7: P-C-T diagram and Van't Hoff plot: α– solid solution of hydrogen in α-phase; β–hydride; α+ β two-phase [64]

1. Transport of hydrogen gas between pores;
2. Adsorption of hydrogen molecules on the surface;
3. Chemisorption and dissociation of hydrogen molecules into atoms;
4. Diffusion of hydrogen atoms in the solid phase;
5. Hydride formation.

These different stages can be treated as successive or simultaneous. Regarding of the desorption process, it can be described simply as the reverse of the mechanism of absorption which has just been described.

Pressure-composition-temperature isotherms (PCT)

The conditions of thermodynamic equilibrium between a metal and its hydride depend on the temperature, the pressure and the hydrogen composition of the system. At a given temperature, these equilibrium conditions can be plotted in a Pressure-Composition diagram. Figure 1.7 corresponds to the ideal case of a mono-hydride system. at low hydrogen pressure a solid solution is formed, the α phase, whose equilibrium pressure increases with the rate of hydriding. When the saturation rate of the α phase is reached, a structural transition leads to the

formation of a hydride of defined composition, the β phase. This transition takes place at constant pressure: there is coexistence of the α and β phases on an equilibrium plateau. Beyond this, the increase in pressure leads to saturation of the β phase, which is the preferred phase for the storage of hydrogen [65]. Although a phenomenon of hysteresis is generally observed between the absorption and desorption isotherms, the formation of a metal hydride is a reversible reaction: in theory, it suffices to lower the pressure of hydrogen at a value below the equilibrium pressure to desorb the hydride. The plate pressure increases with temperature. Determining the equilibrium pressure as a function of temperature makes it possible to represent in a Pressure-Temperature diagram the absorption and desorption domains (Figure 1.7). Using Van't Hoff's law which describes the relationship between temperature and free reaction enthalpy, the enthalpy and standard reaction entropy are then calculated, the values of which are characteristic of the stability of hydride. Hydrogen is chemically bonded in the metal hydrides. These bonds are much stronger than the physical bonds concerned within the adsorption of hydrogen. Consequently, additional energy is required to release the chemicals bonded hydrogen. On the opposite hand, the stronger bonding permits hydrogen to be stored at high density even at ambient conditions.

The different types of metal hydrides

The hydrogen is absorbed at moderate pressure (around 10 bars). Since the desorption reaction is endothermic; it is self-limiting. In the event of accidental leakage, the temperature of the tank drops rapidly to equilibrium temperature, interrupting the release of hydrogen. Some metallic elements, called type A (rare earths, Mg, Ti, Zr, ...), react spontaneously with hydrogen to form hydrides. These hydrides are thermodynamically stable and their decomposition can only take place at high temperature. On the contrary, the transition metals 3d, called type B (Cr, Mn, Fe, Co, Ni ...) [65–71], have a low affinity with hydrogen.They are unstable under standard pressure and temperature conditions. The intermetallic compounds thus formed may be sorted in step with their stoichiometry, shown in Table 1.4.

The volume capacities of the intermetallic compounds make solid-state hydrogen storage mode very competitive compared to the gaseous and liquid

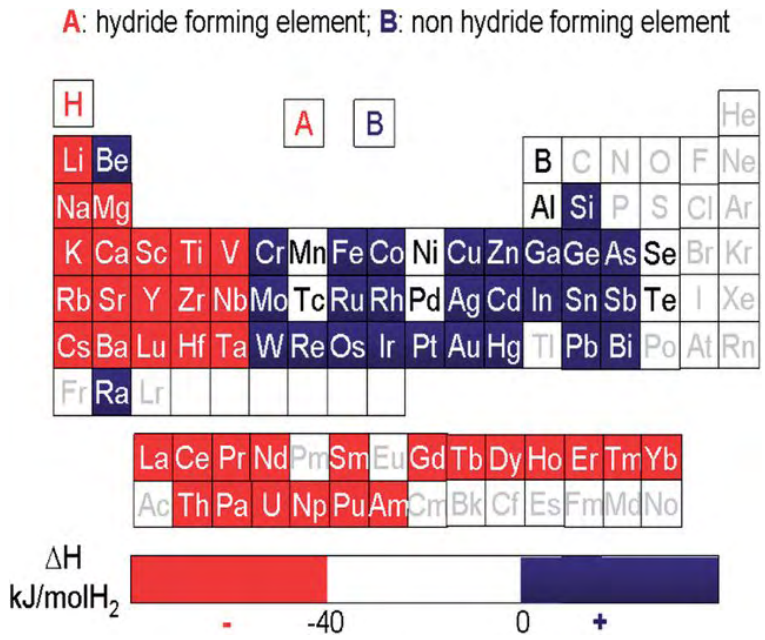

FIGURE 1.8: Periodic system of elements with selected elements hydride and non-hydride forming

TABLE 1.4: Intermetallic Compounds and their types [72]

Composition	Compound
AB_5	$CaNi_5, LaNi_5, CeNi_5, LaCu_5, LaPt_5, LaFe_5$
AB_2	$LaNi_2, YNi_2, YMn_2, ZrCr_2, ZrMn_2, ZrV_2, TiMn_2$
AB_3	$Co_3, YNi_3, LaMg_2Ni_9$
A_3B_7	Y_2Ni_7, Th_2Fe_7
A_6B_23	Y_6Fe_23
AB	$TiNi, TiFe, ZrNi$
A_2B	Mg_2Ni, Mg_2Co, Zr_2Fe

modes. On the other hand, the metallic matrix weighs considerably in the low gravimetric performances. The AB_5 category represented by the $LaNi_5$ alloy have the ability to absorb hydrogen already within the room temperature, however, the stored content is only 1.4% by weight. Another cluster are AB and AB_2 type materials, associate example of which might be FeTi, that has the capacity of 1.8 wt.% [70]. The materials during this group have good thermodynamic properties, however the flaw of these categories is that the activation of the hydrogenation itself is difficult. Therefore, the materials need to be subjected to initial cycles of absorption and decomposition in high temperatures and under high vacuum [73–76]. Following generations are A_2B type alloys, eg. Mg_2Ni, which have disadvantages like high temperature of the absorption and desorption process and slow reaction dynamics, however, they need good hydrogen storage capacities of about 3.6% by mass. They have comparatively low weight and relatively expensive [64, 70].

1.4.3 Complex metal hydride

Complex metal hydride is such class of compound having a general formmula of $M(XH_n)_m$, where M is generally a metallic cation and X is a metal or non-metallic element that sets up covalent or iono-covalent bond with H. $M[XH_n]_m$ is rich in Hydrogen and can decompose selectively in H_2 allowing complex hydrides of light weight potential hydrogen storage elements. The main series of complex hydrides considered of interest for hydrogen storage are the amides (based on the $[NH_2]^-$ anion, the alanates (based on the $[AlH_4]^-$ anion), and the borohydrides (based on the $[BH_4]^-$ anion). Unlike intermetallic hydrides, complex metal hydrides consist mainly of relatively light elements which allows to possess quite high gravimetric hydrogen capacity. Unfortunately, most complex hydrides rather require high temperatures for their dehydrogenation by thermolysis, and only a small quantity can be reversibly dehydrogenated, generally only in the presence of catalysts or additives.

FIGURE 1.9: The desorption temperature as function of each additive

Amides

Amide based storage systems consist of mixtures of two compounds: a metal amide ($[M][NH_2]_x$, M generally being Li (x=1), Na (x=1) or Mg (x=2)) and an elementary hydride. The addition of elemental hydride is crucial since the amide would otherwise liberates ammonia instead of hydrogen throughout its thermolysis [77]. However, most amide-based materials unleash traces of ammonia during thermolysis, that reduces reversibility through loss of active ingredient [78, 79]. One of the most interesting systems at present is represented by mixture of lithium amide ($LiNH_2$) and LiH. When mixed, these substances have a reversible hydrogen storage capacity of 6.5% wt, combined with a working temperature below 300 °C (285 °C) and attractive thermodynamic properties (ΔH_{des}= 44.5 kJ mol^{-1}) [80]. On the contrary, the pure lithium amide and the lithium hydride, separately, decompose at temperatures above 300°C and 550 °C, respectively [65, 81]. The poor sorption kinetics in both ab/desorption processes bloc practical application of Li-N-H system, It is necessary to lower the operation temperature [82]. A many strategies have been made to improve its performance, such as an excess of LiH to avoid the NH_3 formation and emission, or addition of different compounds to the Li-N-H system during ball milling process such us ($AlCl_3$, MgH_2, K-halide, $TiCl_3$, $MgCl_2$, LiCl,

$FeCl_3$...) [83]. The general desorption reaction is reported in reaction 2 [84]

$$Li_{(1+n)}(NH_2)X_n + LiH \rightarrow Li_{(2+n)}(NH)X_n + H_2 \quad \{2\}$$

Figure 1.9 presents the desorption temperature related to each mixture. In these systems, the effect of anion/cation substitution promotes N-H bond destabilization and induces structural defects into $LiNH_2$ lattice improving the Li^+ mobility [77]. The most efficient variant so far is the mixture of $LiNH_2$ with $AlCl_3$, When $AlCl_3$ is added the kinetic properties are improved, and the H_2 released bellow 230 °C. Another promising way to improve Li-N-H de/hydrogenation kinetics properties is the mixture of $LiNH_2$ with MgH_2 by replacing LiH with MgH_2, which systemically reduces the dehydrogention enthalpy from 51 $kJ\,mol^{-1}$ to 34 $kJ\,mol^{-1}$ [84]. Depending on the dopant, the $LiNH_2$ or $Mg(NiH_2)_2$ systems show different behaviors of thermodynamic properties and kinetics features. However, the activation energy of the dehydrogenation process of these systems is very high (arround 100 $kJ\,mol^{-1}$). By now, there is no amides-based system which can completely fits the specific targets fixed by DoE for 2020.

Alanates

Alanate are inorganic compounds formed by an anionic complex $[AlH_{(n+3)}]^{n-}$ and a metal cation M^{n+} (alkaline: Li^+, Na^+, K^+, or alkaline earth: Be^{2+}, Mg^{2+}, Ca^{2+}, Ba^{2+}, Sr^{2+}) assembled by an ionic bond. There are also transition metal alanates. They are too unstable for the storage of hydrogen. Lithium alanate crystallizes in the rhombohedral system while sodium and potassium alanates crystallize in the monoclinic system. the decomposition of the alanates gives rise to intermediate phases, of lower hydrogen content, due to the desorption of this gas. the stoichiometry of the intermediate phases and the quantity of hydrogen released are different for each family of alanates. The tetra-alkali metal alanates decompose and release hydrogen in three steps [85]:

$$3\,MAlH_4 \rightarrow M_3AlH_6 + 2\,Al + 3\,H_2 \quad \{3\}$$

TABLE 1.5: gravimetric capacity, enthalpy of desorption, and decomposition temperature of alkaline and alkaline earth alanates [60, 85–88]

Compound	Gravimetry (%wt)	ΔH_{des} ($kJ\,mol^{-1}H_2$)	Tdes
$LiAlH_4$	10.6	-2	120
Li_3AlH_6	11.2	29	120
$NaAlH_4$	7.5	37	150
Na_3AlH_6	5.9	47	150
$KAlH_4$	5.7		340
K_3AlH_6	4.0	135	340
Na_2LiAlH_6	7.0	53.5	220
K_2LiAlH_6	5.1	82	230
K_2NaAlH_6	5.3	97	260
$Ca(AlH_4)_2$	7.9	-7.4	250
$CaAlH_5$	7.0	32	250
$Mg(AlH_4)_2$	9.3	-18	150
$LiMg(AlH_4)_3$	9.7	<0	170
$LiMgAlH_6$	9.4	>0	170

$$M_3AlH_6 \rightarrow Al + 3\,MH + \frac{3}{2}\,H_2 \quad \{4\}$$

$$MH \rightarrow M + \frac{1}{2}\,H_2 \quad \{5\}$$

the quantity of hydrogen released in these stages, as well as the characteristic decomposition temperatures, T_{dec}, are collated in the table 1.5. Given that the alkali hydrides decompose at very high temperature, only the two first reactions are considered usable for the reversible storage of hydrogen. As an example, the $NaAlH_4$ whose hydrogen content is 7.5% by mass and the amount of potentially reversible hydrogen is 5.6% by mass. The difference corresponds to the formation of NaH [86]. The characteristic of the decomposition temperature of this hydride is of 500 °C. Therefore, the third reaction is not interesting for hydrogen storage.

On the other hand, the first two reactions, which correspond, respectively, to the decomposition of $NaAlH_4$ into Na_3AlH_6 and that into NaH, take place at moderate temperatures (T_{dec1} = 100 °C and T_{dec_2} = 150 °C) and, therefore, suitable for reversible hydrogen storage. The volume capacity of sodium alanate, deduced from its reversible absorption of hydrogen and its crystallographic structure, is 70 $kg\,m^{-3}$. Otherwise, the reaction path, during the decomposition of alkaline-earth alanates, is slightly different because of the formation of penta-alanates during the

first stage. Thus, the decomposition steps of tetra calcium alanate are:

$$Ca(AlH_4)_2 \rightarrow CaAlH_5 + Al + \frac{3}{2}H_2 \quad \{6\}$$

$$CaAlH_5 \rightarrow CaH_2 + Al + \frac{3}{2}H_2 \quad \{7\}$$

$$CaH_2 + 2\,Al \rightarrow CaAl_2 + H_2 \quad \{8\}$$

The reaction path during the decomposition of $Mg(AlH_4)_2$ is less obvious. Dymova et al. [67] claim that the decomposition of $Mg(AlH_4)_2$ follows the same reaction path as that of $Ca(AlH_4)_2$; but other authors have proved experimentally, and in agreement with theoretical calculations, that $Mg(AlH_4)_2$ breaks down directly into MgH_2 [89]. The enthalpies of decomposition of alkaline and alkaline earth alanates are collected in the table 1.5. alanates can be grouped into two families:

- A family, of which $NaAlH_4$, Na_3AlH_6, $KAlH_4$, K_3AlH_6, Na_2LiAlH_6, K_2NaAlH_6 belong, corresponds to fairly stable alanates. Their decomposition results in a change in enthalpy greater than 35 $kJ\,mol^{-1}H_2$. These compounds have a plateau pressure below 1 bar at room temperature. In order to release the hydrogen, the compounds must in practice be heated moderately. They are reversible because they can be rehydrogenated with low hydrogen pressures [90–93].

- The second family is made up of thermodynamically metastable alanates which of $LiAlH_4$, $Mg(AlH_4)_2$ and $MgLi(AlH_4)_3$ are among of them. These compounds have a negative change of the decomposition enthalpy (exothermic decomposition, $\Delta H < 0$) or slightly positive. They are considered irreversible [88, 89, 94].

Borohydrides

The borohydrides refer to metal-B-based complex hydrides. In the chemical storage of hydrogen, boron-based materials are quite promising because of their gravimetric density of hydrogen storage, varying from 10 to 20% by mass depending on the

1	2											13	14
Li 18.5	Be 20.8												
Na 10.7	Mg 14.9	3	4	5	6	7	8	9	10	11	12	[Al] 16.9	
K 7.5	Ca 11.6	Sc 13.5	III 13.1 IV 15.0 Ti	V 12.7	Cr 9.9	[Mn] 9.5	[Fe] 9.4	[Co] 9.1	[Ni] 9.1	[Cu]* 5.1	Zn 4.4	[Ga] 10.6	Ge 12.2
Rb 4.0	Sr 6.9	Y 9.1	Zr 10.7	Nb 8.8						[Ag]* 3.3	[Cd] 2.9	[In] 7.6	[Sn] 9.1
Cs 2.7	Ba 4.8	Ln	Hf 6.8							[Au] 1.9	Hg 1.8	Tl 4.9	
		Ac											

Ln	La 6.6	Ce 6.6		Nd 6.4		Sm 6.2	Eu 6.2	Gd 6.0	Tb 5.9	Dy 5.8	Ho 5.8	Er 5.7	Tm 5.7	Yb 5.6	Lu 5.5
Ac		Th 5.5	Pa 5.6	III 4.3 IV 5.4 U	Np 5.4	Pu 5.4									

FIGURE 1.10: The elements M formed $M(BH_4)n$, their gravimetric hydrogen densities in the unit of mass%. The asterisks indicate the compounds stabilized at room temperature by coordination with ligands. The parentheses indicate that the compounds are declared unstable at room temperature but can be isolated at low temperature [95]

material. The development of these boron-based materials for the chemical storage application of hydrogen involves meeting several challenges [88]

- The first is the dehydrogenation of these hydrides, which can be done by hydrolysis in the presence of a metal catalyst or by thermolysis according to different necessary approaches.

- The most blocking is the regenerability of boron-based materials or the recyclability of hydrolysis and thermolysis by-products. This step is crucial to close the hydrogen cycle that could be considered with boron-based materials.

Boron-based materials are a class of fascinating compounds with a remarkable variety in bonding characteristics, where hydrogen is covalently bound to the central atoms. In this way a crystal structure consisting of complex anions is formed. In general the complex hydrides have the formula $M(BH_4)_n$ (n indicates the valence of M). Here are numerous complex borohydride with high hydrogen content which are presented in Figure 1.10. The enthalpy change ΔH_{dec} of the dehydrogenation of $M(BH_4)_n$ correlates not only with itself stability but also with the stability of the products. The dehydrogenation reactions were assumed as the following equations:

$$M(BH_4)_n \rightarrow MH_n + B + \frac{3}{2} H_2 \qquad \{9\}$$

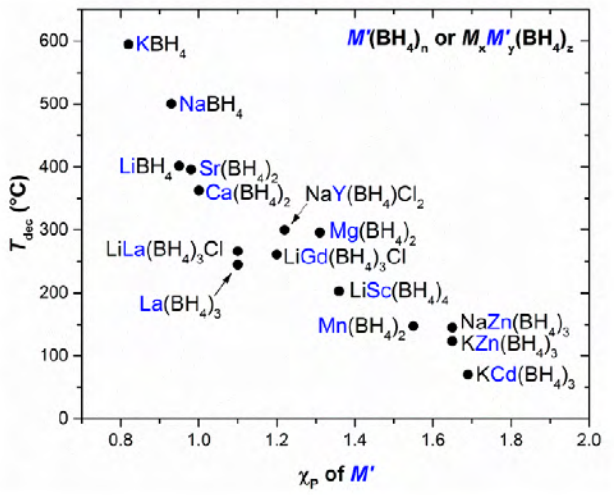

FIGURE 1.11: The desorption temperature T_d as a function of the Pauling electronegativity χ^P of the metal, M'. For the bimetallic borohydrides M' is the more electronegative of the two metals.

$$M(BH_4)_n \rightarrow MH_n + B + 2\,nH_2 \quad \{10\}$$

$$M(BH_4)_n \rightarrow MH_n + \frac{1}{2}B + nB_2H_6 \quad \{11\}$$

$$M(BH_4)_n \rightarrow M + \frac{1}{2}nB_2H_6 + \frac{1}{2}nH_2 \quad \{12\}$$

For the decomposition reaction, the Gibbs energy change ΔG_{dec} is:

$$\Delta G_{\mathrm{dec}} = \Delta H_{dec} - T_{dec}\Delta S_{dec} \quad (1.2)$$

the thermodynamic stability can be evaluated by the decomposition enthalpy change namely ΔH_{dec} : the difference in the formation enthalpies between the $M(BH_4)_n$ and its decomposition products:

$$\Delta H_{dec} = \Delta H_{products} - \Delta H_{borohydride} \quad (1.3)$$

The hydrogen desorption temperature (T_d) of $M(BH_4)_n$decreases with increasing the Pauling electronegativity χ^P value of M (Figure 1.11). The $M(BH_4)n$ with $\chi^P \geq 1.5$ (e.g. M = Mn, Ti and Al) are too thermodynamically unstable [84] and

TABLE 1.6: Hydrogen storage properties of some borohydrides, $M(BH_4)_n$ [84, 88, 94–99]

Compounds	Theoretical storage capacity (wt%)	Hydrogen density (kg/m3)	Decomposition temperature (K)	Heat of formation (kJ mol^{-1})
LiBH4	18.5	121	673	-194
NaBH4	10.7	114.5	838	-191
KBH4	7.47	87.8	913	-229
RbBH4	4.0	76.8		-48.52
CsBH4	2.7	65.3		
BeBH4	20.8	146.0		
Mg(BH2)2	14.9	147.4	533-553	
Ca(BH2)2	11.6	124.1	593	
Sc(BH4)3	13.5		435	
Ti(BH4)3	13.1		<298	
Zr(BH4)4	10.7	126.2	<523	
Hf(BH4)4	6.78	112.2	<523	
Mn(BH4)2	9.5	117.8		
Zn(BH4)2	8.49		358	
Al(BH4)3	16.9	133.5	<298	

are decomposed with the evolution of the toxic diborane in addition to hydrogen [95]. Therefore, M(BH_4)n ($\chi^P < 1.5$) were suggested as promising candidates with appropriate and without releasing diborane. Furthermore, it was found that multi-cation borohydrides MM'$(BH_4)_n$, where M and M' have different χ^P, exhibit moderate thermodynamic stabilities between $M(BH_4)_n$ and $M'(BH_4)_n$ [96, 97]. First-principles calculations of the electronic structures of $M(BH_4)_n$ show that they are nonmetallic and have relatively large energy gaps of 1.8 to 6.8 eV. A boron atom forms covalent bonds with four surrounding H atoms to form $[BH_4]^-$ anions of which the charge is compensated by metal cations M^{n+}. The electronic structures indicate that charge transfer from the metal cations M^{n+} to the $[BH_4]^-$ anions is a key feature determining the thermodynamic stability of $M(BH_4)_n$ [98].

The alkali metal borohydride compounds $LiBH_4$, $NaBH_4$,and KBH_4 are commercially available, the borohydrides of the alkaline earth and light transition metals, $Mg(BH_4)_2$, $Al(BH_4)_3$, $Zr(BH_4)_4$, $Ti(BH_4)_3$,$Mn(BH_4)_2$, $Zn(BH_4)_2$, and $Sc(BH_4)_3$ are for the most part known compounds and their solution synthesis has been described.For example, the aluminum borohydride ($A_1(BH_4)_3$) was prepared in 78% yield by reaction of purified A_1C_{13} with lithium borohydride, followed by distillation of the filtrate. The other alkali metal borohydrides MBH_4, M= Na,

K, Rb and Cs have higher thermal stability and all crystallize in the Rock salt structure. Sodium borohydride is also stable in basic aqueous solutions, which has been used as a hydrogen storage media. Alkali metal borohydrides are known to have the highest thermal stability [99]. The full series of alkaline earth metal borohydrides was completed with the discovery of $Ba(BH_4)_2$, $Sr(BH_4)_2$, and their chloride derivatives. The alkaline earth metal borohydrides show decreasing degree of covalent and directional bonding in the series, Mg > Ca > Sr> Ba. Magnesium borohydride is known in seven different polymorphs and, remarkably, one of these, γ-$Mg(BH_4)_2$, has permanent porosity and 30 % of open space in the structure. The heavier alkali earth metal borohydrides form three to four polymorphs. The material properties of typical single cation borohydrides are shown in Table 1.6. Within this class of compounds, alkali metal or alkaline earth metal borohydrides exhibit the higher hydrogen densities, e. g. 18.5 wt% and 121.5 kgH_2/m^3 for $LiBH_4$. However, these materials have decomposition temperature greater than 300 °C and exhibit poor reversibility [98].

Part II

Theory and modeling

2 Density Functional Theory: Concepts and Methods

2.1 Introduction

The understanding of the matter properties requires the study of the processes from macroscopic to microscopic scale. such as the molecular, atomic, electrons and atomic nuclei objects. Density functional theory (DFT) is a valuable tool to study physics and chemistry at this scale, and the applications of this theory, that is exact, are based on the approximation for the electron-electron interaction energy. The purpose of this chapter is to present the modeling of the physical problem that is posed to us. Since the DFT is based on of the Schrödinger equation, we will introduce approximations and different ways to solve it.

2.2 The Schrödinger equation

2.2.1 Basic knowledge

In this part, we consider the $\mathbb{R}^3 \times \mathbb{R}^+$ space, i.e. the three coordinates of space, and time. We denote by $\mathbf{q}$ the coordinates of a quantum system. $\mathbf{q}$ belongs to a space called the configuration space, composed of the spatial and temporal coordinates of the A nuclei and N electrons of the system ($\mathbb{R}^{3(K+N)} \times \mathbb{R}^+$). The state of a system is completely determined by its Ψ wave function, with values in $\mathbb{C}$[100]. By definition, the data of this function, at a given time, not only describes all the properties of the system at this moment, but also determines its behavior in all subsequent states. Mathematically, this translates into the fact that the value of the derivative $\frac{\partial}{\partial t}\Psi$ of the wave function with respect to time must, at every moment, be determined by the value of the wave function Ψ itself at this instant. In the most general form,

the Schrodinger equation, which describes the evolution of the function is given by [101]:

$$i\hbar\frac{\partial}{\partial t}\Psi = \mathscr{H}\Psi \tag{2.1}$$

where the Hamiltonian $\mathcal{H}$ is an hermitian linear operator, independent of time, $\hbar = \frac{h}{2\pi}$, h being the Planck constant (h=6.6260610^{-34} m^2 kg s^{-1}). At the stationary state the energy of the system is constant over time. Thus, the Schrodinger equation that depends on the time may be reduced to stationnary state Schrondinger equation:

$$\mathcal{H}\Psi_n = \varepsilon_n\Psi_n \tag{2.2}$$

ϵ_n being the eigenvalue or energy associated with the steady state Ψ_n. It's an eigenvalue equation where the eigenvalue of the Hamiltonian en is none other than the energy associated to the steady state psin that is independent of time. For many body systems, the information of all particles is contained in the wave function. Thus, the Schrodinger equation becomes complicated to solve in its standard form. In what follows, we will present the theory and the different approximations that simplify the problem. Considering a system of A nuclei and N electrons,the stationary state $|\Psi\rangle$ of this system can be described by a wave function:

$$\Psi\left(R_I, \vec{r}_i\right) = \left\langle \vec{R}_I, \vec{r}_i | \Psi \right\rangle = \Psi\left(\vec{R}_1, \vec{R}_2, \ldots, \vec{R}_N, \vec{r}_1, \vec{r}_2, \ldots, \vec{r}_n\right), \tag{2.3}$$

satisfying the equation of Schrödinger independent of the time [102]:

$$\widehat{\boldsymbol{H}}_{tot}\Psi\left(\vec{R}_I, \vec{r}_i\right) = E_{tot}\Psi\left(\vec{R}_I, \vec{r}_i\right) \tag{2.4}$$

where E_{tot} is the total energy of the system. The total Hamiltonian operator is given by:

$$\hat{H}_T = \hat{T}_n + \hat{T}_e + \hat{V}_{ne} + \hat{V}_{ee} + \hat{V}_{nn} \tag{2.5}$$

The first terms $\hat{T}_n$ and $\hat{T}_e$ designate the kinetic energy of A nuclei and N electrons respectively. while the terms $\hat{V}_{n-e}$, $\hat{V}_{e-e}$, and $\hat{V}_{n-n}$ describe Colombian interaction electron-nuclei, electron-electron and nuclei-nuclei respectively. Its

explicit expression can be written as follow:

$$\Psi = -\sum_{i}^{N} \frac{\hbar^2}{2m}\nabla_i^2 - \sum_{I}^{A} \frac{\hbar^2}{2M}\nabla_I^2 - \sum_{i,I} \frac{Z_I e^2}{\left|\vec{r}_i - \vec{R}_I\right|} + \sum_{i<j} \frac{e^2}{\left|\vec{r}_i - \vec{r}_j\right|} + \sum_{I<J} \frac{Z_I Z_J e^2}{\left|\vec{R}_I - \vec{R}_J\right|} \tag{2.6}$$

The first two terms of the Hamiltonian are the kinetic energy operators of N electrons (indexed i, j) and Atomic nuclei (indexed I, J) respectively. The other three terms represent the different electron-nucleus,electron-electron, and nucleus-nucleus interaction potentials. As an example of a many-body system, we may quote the case of a regular crystal. The electrons are not only affected by the nuclei in their lattice sites, but also by the other electrons. An exact solution of the Schrodinger equation is impossible in the case of poly-electronic systems. It is therefore necessary to implement simplifying procedures associated with some mathematical tricks in order to make possible the obtaining of an approximate solution.

2.2.2 The Born-Oppenheimer Approximation

Max Born and Robert Oppenheimer proposed an approximation to simplify the Schrödinger equation. This approach is today the basis of many calculations in the physics of matter. The Born-Oppenheimer approximation considers the position of atomic nuclei as fixed, from the simple observation that electrons are much lighter than nuclei($M_I \gg m_i$) [103]; their kinetic energy can therefore be neglected and the interaction term between nuclei considered as a constant. Then we can decouple the nuclear and electronic movements, and the wave function of the system becomes:

$$\Psi(\{r\},\{R\}) = \Psi_{\text{elec}}(\{r\};\{R\})\Psi_{\text{nucl}}(\{R\}) \tag{2.7}$$

However, the new equation obtained represents a N-body problem whose rigorous resolution can not be obtained analytically except in very simple cases like that of the hydrogen atom. Thus, the approximation of Born-Oppenheimer is important but still insufficient for solving the **Schrodinger** equation. Thus, other approximations should be introduced.

2.2.3 Hartree-Fock approximation

The Hartree-Fock method seeks to approximately solve the electronic Schrödinger equation, and it assumes that the wavefunction can be approximated by a single Slater determinant made up of one spin orbital per electron. The objective of the Hartree-Fock method is to produce the best possible one-electron wavefunctions for use in approximating the exact wavefunction for a multi-electron system. In these models, we consider the $\mathcal{H}_{el}$ operator composed of the three operators (The kinetic operator, the interaction of an electron-nuclei and the interaction between all the electrons):

$$H_{elec} = T_e + V_{ee} + V_{en} \tag{2.8}$$

Hartree's approach

The Hartree approximation consists of replacing the interaction of each electron of the atom with all the others by the interaction with a mean field created by the nuclei and all the other electrons, that is to say that the electron moves independently in a middle field created by other electrons and nuclei [104–106]. This makes it possible to replace the potential of the type $1/r_{ij}$ which depends on the coordinates of the two electrons by an expression defining the electronic interaction which depends on the coordinates of each isolated electron. Thus, within this approximation, the correlations are neglected allowing to write:

$$\Psi_H(\{\boldsymbol{r}\}) = \psi_1(\boldsymbol{r}_1)\,\psi_2(\boldsymbol{r}_2)\ldots\psi_N(\boldsymbol{r}_N) \tag{2.9}$$

Definition of Hartree Potential the potential of Hartree or Coulomb potential V_H is defined by [104]:

$$V_{\mathbf{H}}(\mathbf{r}) = \int \mathrm{d}\mathbf{r}' \frac{n(\mathbf{r}')}{|\mathbf{r}-\mathbf{r}'|} \tag{2.10}$$

Which describes the interaction pf an electron at a position $\mathbf{r}$ with an electronic cloud of density $\mathbf{n}(\mathbf{r}')$. We point out that, the equation Hartree's approximation ignores the anti-symmetry of the wave function, as long as the electron is a fermion then the total wave function must be antisymmetric with respect to the exchange of any two particles that is neglected by Hartree.

Hartree-Fock Method (1930)

To restore the wave function antisymmetry neglected in Hartree equation, Fock proposed to apply the Pauli's exclusion principle, therefore the electronic wave function is then written as a determinant of Slater [107–109]:

$$\Psi\left(r_1,\dots r_n\right)=\frac{1}{\sqrt{n!}}\begin{vmatrix}\psi_1\left(r_1\right) & \psi_1\left(r_2\right) & \dots & \psi_1\left(r_n\right)\\ \psi_2\left(r_1\right) & \psi_2\left(r_2\right) & \dots & \psi_2\left(r_n\right)\\ \vdots & \vdots & \ddots & \vdots\\ \psi_n\left(r_1\right) & \psi_n\left(r_2\right) & \dots & \psi_n\left(r_n\right)\end{vmatrix} \tag{2.11}$$

With $\frac{1}{\sqrt{n!}}$ the normalization constant. This approximation leads to good results, particularly in molecular physics. Moreover, solving the system of equations (2.11) remains difficult in the case of solids.

2.2.4 Thomas-Fermi models

Before Hohnberg and Kohn's theory of the functional density presented in the next section (2.3), Thomas and Fermi [110] independently demonstrated in the 1920s that the Y electronic density could be used as a central variable to solve the Schrödinger equation [101]. Compared with the previous expressions of energy, the calculation of kinetic energy is changed: it will also be a density function [111]. The ground state energy $\mathcal{E}^{TF}$ is obtained by minimizing according to Y:

$$\mathcal{E}^{TF}[\mathrm{Y}]=A_0\int_{\mathbb{R}^3}\mathrm{Y}(\mathbf{r})^{5/3}d\mathbf{r}+\int_{\mathbb{R}^3}V(\mathbf{r})\mathrm{Y}(\mathbf{r})d\mathbf{r}+\frac{1}{2}\iint_{\mathbb{R}^3\times\mathbb{R}^3}\frac{\mathrm{Y}(\mathbf{r})\mathrm{Y}\left(\mathbf{r}'\right)}{|\mathbf{r}-\mathbf{r}'|}d\mathbf{r}d\mathbf{r}' \tag{2.12}$$

Where $\int_{\mathbb{R}}\mathrm{Y}(r)dr=\lambda,\lambda\in\mathbb{R}^{+*}$,$A_0$ is a constant. In the general case, the density associated with the wave function of N electrons is written:

$$\mathrm{Y}(\mathbf{r})=N\int_{\mathbb{R}^{3(N-1)}}\left|\Psi\left(\mathbf{r},\mathbf{r}_2,\dots,\dots,\mathbf{r}_N\right)\right|^2d\mathbf{r}_2\dots d\mathbf{r}_N \tag{2.13}$$

But we will also have to define it from N orbitales $\psi_i(\mathbf{r})$:

$$\rho(\mathbf{r})=\sum_{i=1}^{N}\left|\psi_i(\mathbf{r})\right|^2 \tag{2.14}$$

Let's look at the physical meaning of the different terms of this energy:

- The first term would be the exact energy of a uniform gas of non-interacting electrons. When we consider a system with one nuclei, it then becomes necessary to introduce a correction, which von Weizsäcker did in 1935, thus allowing the stability of the molecules:

$$\mathcal{E}^{TFW}[\mathrm{Y}] = \mathcal{E}^{TF}[\mathrm{Y}] + A_2 \int_{\mathbb{R}^3} |\nabla\sqrt{\mathrm{Y}}|^2 d\mathbf{r} \tag{2.15}$$

- compared to the hartree $\mathcal{E}^H$ and Hartree-Fock $\mathcal{E}^{HF}$ potential. Only an electronic interaction of the Hartree type (2.10) is shown here. To correct this, Dirac added in 1930 [112] a so-called exchange term to better describe the interaction between electrons [109]:

$$\mathcal{E}^{TFD}[\mathrm{Y}] = \mathcal{E}^{TF}[\mathrm{Y}] - A_1 \int_{\mathbb{R}^3} \mathrm{Y}^{4/3}(\mathbf{r}) d\mathbf{r} \tag{2.16}$$

The model including the two corrections of Dirac and Von Weizsäcker is called TFDW. E. Lieb studies these different systems in detail, and P.-L. Lions demonstrates the existence and uniqueness of an electronic distribution for a neutral molecule or a positively charged ion [112–114]. The advantage of this method is that it is linear with respect to the number of electrons N.

2.3 The density functional theory

The DFT formalism was presented for the first time in an article by Hohenberg and Kohn in 1964. This article explains that the ground state is totally determined by the electronic density (*The details of density functional theory are explained in the book by R.G. Parr and W. Yang. [115]*). It is based on two theorems [116]:

Theorem 1 : The total energy of the fundamental state of the system is a single universal functional function of the electronic density for a given external potential; whether $E = E[\rho(\vec{r})]$. There are two classes of electrons, the spin-up electrons and the spin-down electrons. So the total energy is a functional (both electronic density

of spin up and spindown $E = E\left[\rho_{\uparrow}(\vec{r}), \rho_{\downarrow}(\vec{r})\right]$. The general expression of the total energy is:

$$E[\rho(\vec{r})] = F_{HK}[\rho(\vec{r})] + \int \hat{V}_{cert}(\vec{r})\rho(\vec{r})d\vec{r} \tag{2.17}$$

In which $F_{\mathrm{HK}}[\rho(\bar{r})]$ represents the universal functional of Hohenberg-Kohn.

Theorem 2 : A universal functional for the energy E[n] in terms of the density $n(r)$ can be defined, valid for any external potential $V_{ext}(r)$. The exact ground state energy of the system is the global minimum of this functional and the density that minimizes the functional is the exact ground state density $n_0(r)$. This reduces the very complex problem of finding all ground state physical properties of a system to finding the minimum of the energy with respect to the electron density. The energy functional is as follows:

$$E_{HK}[n] = T[n] + E_{int}[n] + \int V_{ext}(\mathrm{r})n(\mathrm{r})d\mathrm{r} \tag{2.18}$$

where $E_{HK}[n]$ is the total energy functional, T[n] its kinetic energy part and $E_{int}[n]$ the part coming from the electronic interactions. EN does not depend on the density and is due to the nuclei-nuclei interaction. It should be noted that although the first Hohenberg-Kohn theorem requires a nondegenerate ground state, degenerate ground states are also allowed by the Levy formulation. It should also be noted that using the Hohenberg- Kohn formulation of DFT implies that we are working at $T = 0\mathrm{K}$.

2.3.1 The Kohn-Sham equation

Kohn and Sham have shown that there is a way to map the problem of solving Eq. 2.18 to the one of solving a system of non-interacting electrons moving in an effective potential from all the (other) electrons. According to Theorem 2, the true electron density will minimize the total energy, but all means of finding it are valid. It could be guessed or, as suggested by Kohn and Sham, calculated from a reference system of non-interacting electrons moving in an effective potential. Thus, developing this variation with the full energy functional added (eq. 2.18), under the condition that the sum of the density throughout the molecule or solid should be constant and

equal to the number of electrons,

$$\int_V n(\mathbf{r})d\mathbf{r} = n_e \tag{2.19}$$

finally gives the Schrödinger-like equations called the Kohn-Sham equations:

$$\mathcal{H}\phi_i = \left[-\frac{1}{2}\nabla^2 + V_{eff}(\mathbf{r})\right]\phi_i = \epsilon_i\phi_i \tag{2.20}$$

$\mathcal{H}$ is the one electron Hamiltonian and $V_{eff}(r)$ the effective potential in which the electron moves. The effective potential is given by

$$V_{eff}(\mathbf{r}) = V_{ext} + V_H + V_{XC} = V_{ext}(\mathbf{r}) + \int \frac{n(\mathbf{r}')}{|\mathbf{r}-\mathbf{r}'|}d\mathbf{r}' + \frac{\delta E_{XC}[n(\mathbf{r})\mid}{\delta[n(\mathbf{r})]} \tag{2.21}$$

Since the electron density,

$$n(\mathbf{r}) = \sum_{i=1}^{\infty} |\phi_i(\mathbf{r})|^2 \tag{2.22}$$

is needed to calculate the last two terms, which are the Coulomb potential from all electrons and the exchange-correlation potential, the Kohn-Sham equations need to be solved self-consistently. The new term, the exchange correlation potential, appearing here contains all the many-body effects that are not present in the classical Hartree interaction term. The initial electron density can be chosen, for example, as a superposition of atomic densities. The Kohn-Sham equations can now be solved instead of finding the minimum of Eq. (2.18), and the orbitals $\phi_i(r)$ then give the electron density according to Eq. 2.22 above. These orbitals are often called Kohn-Sham orbitals and in the case of a non-spin-polarized system, each of these orbitals contain two electrons.

2.3.2 The exchange-correlation approximations

The functional LDA : The simplest physical way to approximate the exchange-correlation energy is the Local Density Approximation (LDA). In this approximation two assumptions are made: i) the local exchange-correlation energy per particle only depends on the local density (hence the name of the approximation) and ii) is equal to the exchange-correlation energy per particle of a homogeneous electron

gas, that has the same density, in a neutralizing positive background (jellium background). The total exchange-correlation energy EXC is then given by the sum of the contributions of each point in space, where it is assumed that the contribution of one point only depends on the density of that particular point, independent of the other points. So:

$$E_{XC}^{LDA}[n] = \int n(r)\epsilon_{XC}^{hom}[n(r)]dr \tag{2.23}$$

Where $E_{XC}[n(r)]$ is the exchange-correlation energy per particle of a uniform electron gas of density $n(r)$. The quantity $E_{XC}[n(r)]$ can be further split into exchange and correlation contributions,

$$\epsilon_{XC}(n(\mathbf{r})) = \epsilon_X(n(\mathbf{r})) + \epsilon_C(n(\mathbf{r})) \tag{2.24}$$

The exchange part, E_x, represents the exchange energy of an electron in a uniform electron gas and is given by:

$$\epsilon_X = -\frac{3}{4}\sqrt[3]{\frac{3n(\mathbf{r})}{\pi}} \tag{2.25}$$

The correlation part, E_C, is determined using quantum Monte-Carlo simulations of the homogeneous electron gas as proposed by Ceperly and Alder [117]. This approximation is more accurate for systems with slowly varying densities, as it is assumed that the density is locally a constant. While being a simple approximation, the results of this approximation are surprisingly good. In general, LDA almost always leads to a correct picture of binding trends across the periodic table. Also, structures, bond lengths, vibrational energies, phonon spectra and other properties are predicted correctly, or with a systematic deviation. Binding energies of solids and molecules are usually overestimated, which leads to an underestimation of the bond lengths. Band gaps are also underestimated (a notorious example of this is the bandgap of bulk Ge, which is predicted to be metallic).

Generalized Gradient Approximation (GGA) In LDA, one uses the knowledge of the density in a point r. In real systems the density varies in space. A logical improvement of the LDA approximation would be to include also information of

this rate of change in the functional. This can be done by adding gradient terms. This approach is called the gradient-expansion approximation. In this class of approximation, one tries to systematically calculate gradient-corrections of the form $|\nabla n(r)|, |\nabla n(r)|^2, \left|\nabla^2 n(r)\right|$, etc., to the LDA. In practice, the inclusion of low-order gradient corrections almost never improves on the LDA, and often even worsens it. Moreover, higher-order corrections are exceedingly difficult to calculate and little is known about them. It was realized that instead of power-series like systematic gradient expansions one could experiment with more general functions of $n(r)$ and $|\nabla n(r)|$ which needs not proceed order by order. Such functionals, of the general form:

$$E_{XC}^{GGA} = \int \epsilon x_C \left(n, |\nabla n|, \nabla^2 n\right) d\mathbf{r} \tag{2.26}$$

are known as generalized-gradient approximations (GGAs). The current GGAs seem to give reliable results for all main types of chemical bonds and are popular in computational chemistry. Overall, GGA type functionals, like PBE, are expected to be more accurate than LDA typefunctionals, meaning a GGA functional should give better results for a larger array of systems than an LDA functional. LDA functionals may perform better than GGA functionals for a particular system or a particular group of systems, but overall GGA functionals should give better result than LDAs functional.

2.3.3 Methods for electronic structure calculations

The Kohn-sham equation is solved self-consistent according to figure 2.1. This figure includes the following steps:

1. The first step consists in choosing an initial density in $n(r)$ based on the eigen densities of the free atoms of the solid
2. We then calculate the effective Kohn-Sham potential using the density defined in first step.
3. We solve the Schrodinger equation in order to obtain the wave functions of the system.
4. We recalculate the density

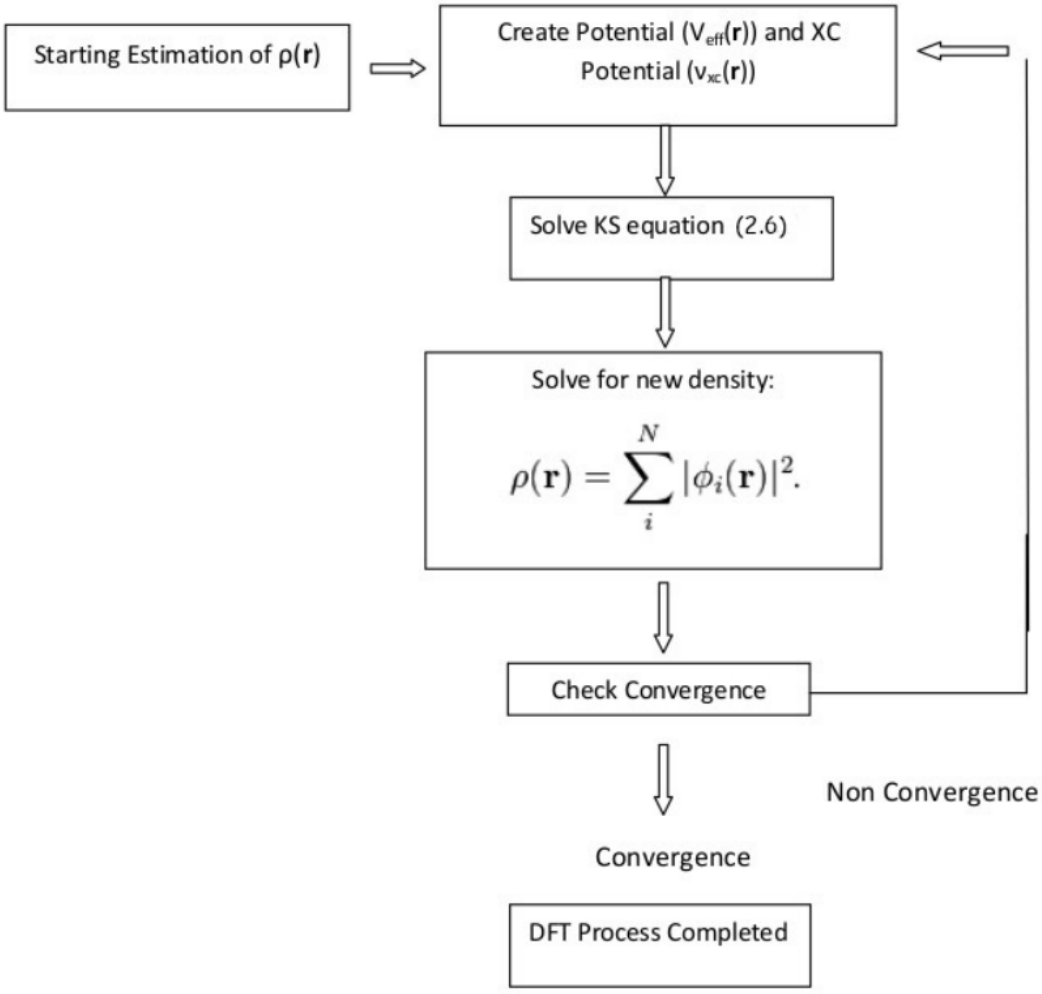

FIGURE 2.1: Diagram representing the Kohn-Sham equation solved in a self-consistent way

In the next sections we will briefly discuss themost popular methods that are used to calculate the electronic structure of materials.

2.4 Crystal structure and Bloch Theorem

In the case of solids, the situation is more complicated than that of a single atom or molecule, because the properties of the solid can depend on a very large number of electrons, since there are a large number of atoms distributed in a macroscopic volume. For standard calculation methods, that would be a huge cost in time, even for powerful computers if we were to try to calculate the electronic structure of the whole system. In the case of crystal structures, this process is greatly simplified because the network is periodic. Since the same structure, or supercell is generally

small, and has just repeated a large number of times, which allows to consider just this cell for the purpose of calculations (something that cannot be done in a non-crystalline structure). This is done in the calculation using periodic boundary conditions, which comes from the cell which are repeated again and again in the simulation, just like in a real solid. Another theorem useful for these solid state calculations is called Bloch's theorem. A Bloch wave is defined as the wave function of a particle (in terms of interest here an electron) inside a periodic potential. The definition of this theorem is given below;

Bloch theorem [118] : The proper function of such a system can be written as the product of a plane wave envelope function and a periodic function (of periodic function Bloch) $\mu_{nk}(r)$ which has the same periodicity as the potential:

$$\Psi_{nk}(r) = e^{ikr}\mu_{nk}(r) \tag{2.27}$$

The importance of this theorem is that the part of the envelope of the plane wave can be extended as a series of plane waves, allowing all functions of electrons to be expressed by plane-wave. It will become important and is discussed further in the following sections.

2.5 Plane-Waves

One of the most common methods for DFT when working in solids is the pseudopotential plane wave method [119]. It basically works out of a set of approximations and symmetries that work well in periodic boundary conditions of a crystal lattice. It is based on the theorem of Bloch identified as periodic boundary conditions as well as to create a set of basic wave plane. Returning to the previous section, it has shown that the electronic wave functions can be expressed as plane-waves. Another approximation, known as pseudopotential is also integrated to simplify the basic set plane wave and is discussed in the next section. The basis of the theory is that it could go to infinity, that the great values of k will result in electrons with high kinetic energy. Due since the DFT calculations are for the ground state, we can reasonably suppose that the wave functions of electrons can be

given with a reduced basic set which will contain only the plane waves lower than the cutting energy (denoted E_{cut}). Basically after a certain value of k (denoted k_{cut}), the coefficients for the plane-waves will become very low, and can be overlooked because they are higher than the energy of electrons. However, we must be careful to choose the right value of the cut-off energy, because a too low a value can lead to inaccurate values.

2.6 Plane wave pseudopotential method

Plane waves offer a natural choice as a basis set to expand the periodic functions $\mu nk(r)$ as:

$$u_{nk}(\mathrm{r}) = \sum_{\mathrm{G}} c_{n\mathrm{k},\mathrm{G}} e^{i\mathrm{G}\cdot\mathrm{r}} \tag{2.28}$$

where the summation is over all the reciprocal lattice vectors G of the system under study. Thus, the electronic wave functions can be written as:

$$\phi_{nk}(\mathrm{r}) = \sum_{G} c_{nk,G} e^{i(k+G)\cdot r} \tag{2.29}$$

The electronic wave functions at each k-point are now expressed in terms of a discrete plane wave basis set. In principle this Fourier series is infinite. However, in practice we cannot work with an infinite basis set, it has to be truncated. The number of plane waves can be restricted by placing an upper boundary to the kinetic energy of the plane waves. This boundary is called energy cut-off Ecut and only plane-waves satisfying the condition:

$$\frac{|\mathrm{k}+\mathrm{G}|^2}{2} < E_{\mathrm{cut}} \tag{2.30}$$

are considered in the computation. With DFT, the complexity of the problem has reduced appreciably. However, for systems with a large number of electrons, it still remains computationally very expensive. Pseudopotentials helped in a crucial way to make the calculations tractable. Using the fact that the physical properties of solids depend mainly on valence electrons, the computational effort can be minimized considerably. In the pseudopotential approximation, the core electrons

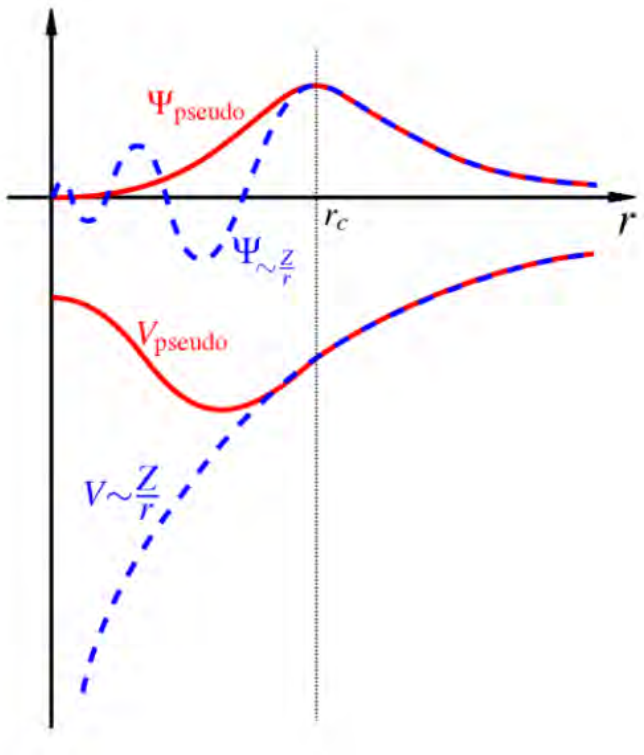

FIGURE 2.2: Schematic representation of pseudopotential and the pseudo wave function

are removed and the strong ionic potential is replaced by the weaker pseudo potential V_{pseudo} that acts on a set of pseudo wave functions Ψ_{pseudo} rather than the true valence wave functions (Ψ). The pseudopotential and pseudo wave functions are generated in such a way that they are identical to the true potential and wave function beyond a certain radius known as cut-off radius r_c. In the core region the pseudo wave function is constructed such that all the nodes are removed but the norm is conserved. Also, since the nodes of the core states are removed, the number of plane-wave basis functions required to describe this wave function in the core region is much less resulting in reduced computational effort. This leads to a popular plane wave pseudopotential method for electronic structure calculations. In this thesis, we use this method to calculate the DFT band structure within the GGA approximation. These calculations are performed using the Quantum espresso code.

2.7 Projector augmented wave method (PAW)

An approach that lies half-way between the LAPW and the pseudopotential methods has been introduced by Bloch 2.4 known as the projector augmented waves (PAW) method. This approach retains the all-electron character, but it uses a decomposition of the all-electron wave function in terms of a smooth pseudo-wave function, and a rapidly varying contribution localized within the core region. The true and pseudo-wave functions are related by a linear transformation:

$$\left|\Psi_n^{AE}\right\rangle = \left|\Psi_n^{PS}\right\rangle + \sum_i \left(\left|\phi_i^{AE}\right\rangle - \left|\phi_i^{PS}\right\rangle\right) \left\langle p_i^{PS} \mid \Psi_n^{PS}\right\rangle \tag{2.31}$$

The pseudo-wave functions Ψ_n^{PS}, where n is the band index, are the variational quantities and are expanded in plane waves. In the regions between the PAW spheres surrounding the atoms, the Ψ^{PS}, n are identical to the AE wave functions Ψ_n^{AE} , but inside the spheres Ψ^{PS} are only a bad approximation to the exact wave functions, they are used only as a computational tool. The AE partial waves ϕ_i^{PS} are solutions of the spherical scalar-relativistic Schrödinger equation for a non-spin-polarized atom at a reference energy E_i in the valence regime and for an angular momentum I_i,

$$\left(-\frac{1}{2}\nabla^2 + v_{eff}^{AE}\right)\left|\phi_i^{AE}\right\rangle = \varepsilon_i \left|\phi_i^{AE}\right\rangle \tag{2.32}$$

where V_{eff}^{AE} is the spherical component of the AE potential. The index i contains the reference energy ε_i the angular momentum quantum numbers (Ii, mi), and the atomic coordinates R_i. The PS partial waves ϕ_i^{PS} are nodeless and identical to the AE partial wave outside a core radius r_c (approximately equal to half the nearest-neighbor distance) and match continuously to ϕ_i^{AE} inside these spheres. The projector functions p_i^{PS} are constrained to be dual to the partial waves, they are constructed by a two-step procedure: First, intermediate functions χ_i are computed via

$$|\chi_i\rangle = \left(\varepsilon_i + \frac{1}{2}\nabla^2 - v_{eff}^{PS}\right)\left|\phi_i^{PS}\right\rangle \tag{2.33}$$

where V_{eff}^{PS} is the spherical component of the effective pseudopotential, which can be chosen arbitrarily inside the radius rc but must match V_{eff}^{PS} for $r \geq r_c$. The projector

functions are linear combinations of the $|\chi_i$ with

$$\left|\phi_i^{PS}\right\rangle = \sum_j \left(B^{-1}\right)_{ji} |\chi_j\rangle \, , B_{ij} = \left\langle \phi_i^{PS} \mid \chi_j \right\rangle \tag{2.34}$$

such that the ϕ_i^{PS} and p_i^{PS} are dual, $\left\langle p_i^{PS} \mid \phi_j^{PS} \right\rangle = \delta_{ij}$ and $\langle r \mid p_i^{PS} \rangle = 0$ for $r \geq r_c$

2.8 Quantum Espresso

In this thesis, all calculations were performed using the Quantum Espresso (PWSCF) code [120]. Quantum ESPRESSO stands for op**E**n **S**ource **P**ackage for **R**esearch in **E**lectronic **S**tructure, **S**imulation and **O**ptimization. It is a free software, released under the GNU General Public License. The code is designed to perform density functional theory calculations of the electronic structure. It uses plane wave basis sets and pseudopotential in its applications. Its features range from the calculation of ground-state energy and Kohn-Sham orbitals to the calculation of atomic forces, stresses, and structural optimization, molecular dynamics on the ground state Born-Oppenheimer surface, Nudged Elastic Band (NEB) and Fourier String Method Dynamics. Quantum ESPRESSO is also able to perform other calculations such as; phonon frequencies and eigenvectors at a generic wave vector, effective charges and dielectric tensors, electron-phonon interaction coefficients for metals, Infrared and Raman (non-resonant) crosssection etc. [121, 122]. The main advantages of QE over VASP in the context of this work are as follows: first, QE is able to characterize the vibrational frequencies into either Raman or infrared active modes. Secondly, QE assigns modes on the basis of the degeneracy of the vibrational frequencies (single, double or triple). In addition, QE tells you to which irreducible representation a mode belongs. This makes it easy to interpret the results of Raman and infrared spectra. Quantum Espresso is presently divided into several executable, performing different types of calculations, although some of them have overlapping functionalities. Typically, there is single set of functions or a single Fortran 90 module that perform each specific task, but there are still important exceptions to this rule, reflecting the different origin and different styles of the

original components. Quantum Espresso has in fact built out of the merging and re-engineering of different packages.

2.9 Phonon calculation

Crystallography is generally concerned with the static properties of crystals, describing features such as the average positions of atoms and the symmetry of a crystal. Solid state physics takes a similar line as far as elementary electronic properties are concerned [122, 123]. We know, however, that atoms actually move around inside the crystal structure, since it is these motions that give the concept of temperature. The static lattice model, which is only concerned with the average positions of atoms and neglects their motions, can explain a large number of material features. Calculating the phonon spectrum (=lattice vibrations) can provide you with an additional check. The phonon frequencies stand for the (effective) interatomic spring constants associated with vibrational normal modes. In a solely theoretical context, phonon calculations may indeed provide a hint towards the stability of the calculated structure. If some phonon frequency is particularly small, then this means that a distortion along this normal coordinate costs very little energy. In the extreme case, the energy curvature along some coordinate might turn out to be negative - then you know for sure that (within the chosen model) the structure is unstable. Otherwise, knowing the phonon spectrum, one can also compute the phonon contribution to specific heat, which could yet be another basic material property of interest. In conjunction with symmetry analysis, you can determine which phonons are Raman or IR active and which ones are "silent" modes.

2.9.1 Crystal structure

There are three types of heat carriers in solids: photons, phonons and electrons. The photons transport heat in semi-transparent media, such as glass, by radiation; electrons are mainly responsible for conduction in metals and phonons explain most of the thermal and dynamical stability behavior of semiconductors and insulators. Matter is generally found in three forms: solid, liquid and gas [1]. Within of

[1] We can also define a fourth state called plasma where the electrons are no longer linked to the nuclei atoms and a fifth state at temperatures close to absolute zero called "Bose-Einstein" condensate.

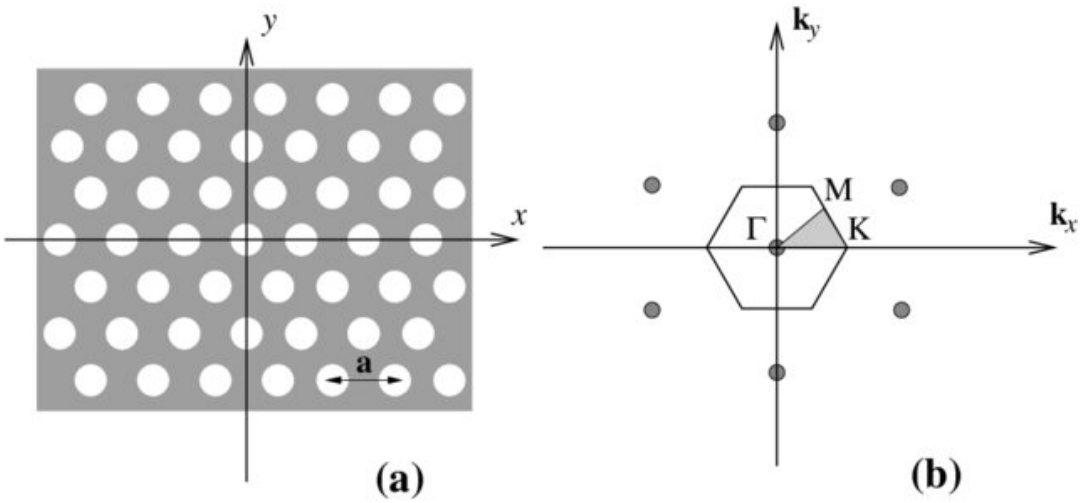

FIGURE 2.3: Example of a two-dimensional crystal structure (a) and associated reciprocal (b).

the solid state, we can also differentiate certain states according to their atomic organization. Crystals are structures for which the atoms (or ions) constituting the matter are organized according to an periodic pattern. Conversely, the amorphous state corresponds to a arrangement of atoms such that it is not possible to define periodicity. Depending on the pressure and temperature conditions, the number of covalent bonds, the charge static, the elements crystallize according to a particular elementary pattern. We distinguish in crystallography 14 Bravais networks; 14 ways to organize the material according to regular patterns. A crystal is usually described by its representation in reciprocal space, which corresponds to the Fourier transform of the real crystal structure. A basis of this space is defined by the vectors wave, K_x, K_y and K_z, as shown in Figure 2.3.

2.9.2 Lattice dynamics

Within the crystal, the atoms (ions) are not fixed. They vibrate, under the effect of thermal excitement , around an equilibrium position. These vibrations generate waves which can propagate in the structure. Within the framework of quantum theory, we can associate a particle with any wave and vice versa. A phonon is then the particle associated with a wave generated by the vibrations of atoms around their equilibrium position. In order to characterize these vibrations. To obtain the modes of vibration, we will follow a procedure similar to a classical one. Suppose we have a cell with a single atom in a cubic lattice. As a first approximation, we can represent

the interactions between adjacent sites by springs. Each atom is then connected only to its immediate neighbors. The main difference that we will find at the atomic scale is that we cannot consider only the first neighbors.The second neighbor has an effect, but as the force considered is due to the stretching of a cord, the influence of the more distant neighbors is only indirect through their influence on the position of the first neighbor. Since the force we now consider is the Coulomb force between two charges, an atom can be directly affected by the movement of a distant neighbor. The important point that remains is that we will still consider a linear relationship between displacement of an atom and the resulting force on another atom as in the equation of the exerted force. Force constants are generated based on finite displacement method. Crystal symmetry is used to reduce the calculation cost and numerical noise of the force constants. Firstly a symmetry reduced set of atomic displacements is generated. After the atomic force calculations, the set of atomic displacements are expanded using the symmetry and then all the elements of force constants between atoms in a primitive cell and the supercell are fit to the symmetry expanded forces of atoms in supercells. This procedure may considered as a variant of Parlinski-Li-Kawazoe method [124]. In case of 3D harmonic crystal the force constant matrix is presented by the folowing equation:

$$\Phi_{\alpha\beta}\left(il, jl'\right) = \frac{\partial^2 E}{\partial r_\alpha(l)\partial r_\beta\left(l'\right)} = -\frac{\partial F_\alpha(il)}{\partial r_\beta\left(jl'\right)} \tag{2.35}$$

where $r(jl)$ is the point of the $j_t h$ atom in the $l_t h$ unit cell. The α, β are the Cartesian indices, j, j' are the indices of atoms in a unit cell, and l, l', are the indices of unit cells. By convention, the dynamical matrix is used as follows:

$$D_{\alpha\beta}\left(jj', \mathbf{q}\right) = \frac{1}{\sqrt{m_j m_{j'}}} \sum_{l'} \Phi_{\alpha\beta}\left(j0, j'l'\right) \exp\left(i\mathbf{q} \cdot \left[\mathbf{r}\left(j'l'\right) - \mathbf{r}(j0)\right]\right) \tag{2.36}$$

Where m is the atomic mass and q is the wave vector, and the eigenvector of the band index at q is obtained by the diagonalization of D(q). After diagonalisation we get :

$$e(\mathbf{q}) \cdot \Omega(\mathbf{q}) = D(\mathbf{q}) \cdot e(\mathbf{q}) \tag{2.37}$$

The force constant matrix $\Phi_{\alpha\beta}\left(il, jl'\right)$ can be obtained either from finite-deplacement calculations, or by using the density-Functional Perturbation Theory (DFPT). In our calculaton, we carried out to extract the force matrix from the self-Consistent Field (SCF) calculation by quantum espresso code. The number of displacements which need to be evaluted to construct the dynamical matrix can be reduced by symmetry. The phonon density of state (or vibration spectrum) is calcualted either, as for the electrons one can define a density of states of modes:

$$g(\omega) = \frac{1}{N}\sum_{\lambda}\delta\left(\omega - \omega_{\lambda}\right) \tag{2.38}$$

where N is the number of unit cells and $\lambda = (\mu, q)$ with μ as the band index and q as the q-point, ω is frequency and k is Wave-vector . Based on the phonon frequencies, the thermodynamic functions can be also obtained. The Helmholtz free energy could be written as:

$$F = E + H_{vib} + TS_{vib} \tag{2.39}$$

where, E, H_{vib} and S_{vib} are the static electronic energy of the crystal, internal energy and entropy contributing to the lattice vibration. Within the harmonic approximation these contributions are given by:

$$H_{vib}(T) = \sum_{i}\frac{1}{2}\hbar\omega_i + \hbar\omega_i\left[\exp\left(\frac{\hbar\omega_i}{K_\beta T}\right) - 1\right]^{-1} \tag{2.40}$$

$$S_{vb}(T) = k_\beta\sum_{i}\frac{\frac{\hbar\omega_i}{K_\beta T}}{\exp\left(\frac{\hbar\omega_i}{k_\beta T}\right) - 1} - \ln\left[1 - \exp\left(-\frac{\hbar\omega_i}{k_\beta T}\right)\right] \tag{2.41}$$

Where the sums run over vibrational frequencies, K_β is the Boltzmann factor and T is the absolute temperature. The Constant volume heat capacity is gevin by the equation :

$$\begin{aligned} C_V &= \left(\frac{\partial E}{\partial T}\right)_V \\ &= \sum_{\mathbf{q}\nu} k_{\mathrm{B}}\left(\frac{\hbar\omega(\mathbf{q}\nu)}{k_{\mathrm{B}}T}\right)^2 \frac{\exp\left(\hbar\omega(\mathbf{q}\nu)/k_{\mathrm{B}}T\right)}{\left[\exp\left(\hbar\omega(\mathbf{q}\nu)/k_{\mathrm{B}}T\right) - 1\right]^2} \end{aligned} \tag{2.42}$$

Beyond Harmonic Approximation

The harmonic approximation is a very powerful tool for studying excitations in solids. In general, the assumption that the ions remain close to their equilibrium positions holds good in most materials below their melting points. Despite its undeniable qualities, the description harmonic of solids suffers from its inability to explain fairly common phenomena like thermal expansion of materials. It is very instructive to identify the reason for this failure of the model.

Thermal expansion and quasi-harmonic approximation The limitations of the Harmonic Approximation are well-known: zero thermal expansion, temperature independence of elastic constants and bulk modulus, equality of constant-pressure and constant-volume specific heats, infinite thermal conductivity and phonon lifetimes, etc. The simplest way for correcting most of the above mentioned deficiencies of the HA is represented by the QHA, according to which the Helmholtz free energy of a crystal is written retaining the same harmonic expression but introducing an explicit dependence of vibration phonon frequencies on volume:

$$G(T,p) = \min_{V} \left[U(V) + F_{\text{phonon}}(T;V) + pV \right] \tag{2.43}$$

Where U(V) electronic internal energy, F_{phonon} is the phonon Helmholtz free energy, T temperature, p pressure and, $\min_V[\,\text{function of } V]$ means to achieve unique minimum value in the brackets by changing volume. Since volume dependencies of energies in electronic and phonon structures are different, volume giving the minimum value of the energy function in the square brackets shifts from the value calculated only from electronic structure even at 0 K. By increasing temperature, the volume dependence of phonon free energy changes, then the equilibrium volume at temperatures changes. This is considered as thermal expansion under this approximation.

The heat capacity at constant pressure Cp are given by equation:

$$C_p(T,p) = -T\frac{\partial^2 G(T,p)}{\partial T^2} = C_v(T,V(T,p)) + T\frac{\partial V(T,p)}{\partial T}\frac{\partial S(T,V)}{\partial V}\bigg|_{V=V(T,p)} \tag{2.44}$$

The coefficient of thermal expansion (CTE) relates the change in volume of a material to change in temperature and it is given by:

$$\alpha_v = \frac{1}{V}\left(\frac{\partial V}{\partial T}\right)_p \tag{2.45}$$

2.10 Molecular Dynamics calculation

2.10.1 Classical Molecular Dynamics

Introduction

Molecular Dynamic (MD) is a microscopic form of computer simulation where the time evolution of a system of atoms is gouverned by Newton's laws of motion. Due to a lack of computational power, it was not until digital computers were invented that MD became a viable method of simulation. With the aid of modern computing, it is possible to numerically solve the equations of motion and use statistical mechanical theory to measure quantities of interest, such as temperature, pressure, and density. Thought the theory remains the same, MD simulations can be used for a variety of applications such as phase transition, polymers, biomolecules, and fluid dynamics. Numerical simulation consisting in calculating the temporal evolution of positions r_i and velocities v_i of a system composed of N interacting atoms, by numerically integrating the equations of classical Newtonian mechanics; F=ma; where F is the force exerted on the particle, m is its mass and a is its acceleration.

Force calculation

The most computationally intensive part of an MD simulation is calculating the forces between pairs of particles. For a potential function without a cutoff radius, it is necessary to evaluate forces for every pair within the simulation region. However, the use of a truncated potential function greatly reduces the number of interaction pairs, and subsequently the number of pairs worth investigating. Different numerical methods are used in MD simulations to find the trajectories of the particles. Besides, the size of the system should be set reasonably so the atoms

in the system can perform desired motions without any additional constraints. The initial settings of a simulation also include the dimension of simulation, boundary conditions, and the units of the parameters. In a soft sphere MD simulation, atomic interaction is calculated based on the potential energy between individual particles. The ineteractions are, in general, described by interatomic forces between particles . In the nature , these forces are :

$$f = -\nabla U(r) \tag{2.46}$$

Where U(r) is a potential energy function. The behavior of a simulation is largely based on the choice of potential function(s). Potential function of interest are largely based on the Born-Oppenhiemer approximation that electrons adjust to movement faster than the nuclei. Therefore, particle interaction based on the movement of nuclei is valid

2.10.2 Ab initio Molecular Dynamics

Since the founding article by Car and Parrinello [125], ab initio molecular dynamics (AIMD) has emerged from all of the atomic-scale simulation methods. Its success is intimately linked to its capacity to describe the temporal evolution of the nuclear but also electronic degrees of freedom of a system, including the rupture or the formation of covalent bonds. Another crucial aspect is the moderate computational cost of the method (compared to Born-Oppenheimer type molecular dynamics), an essential element for the study of biochemical systems. AIMD simulations thus provide reliable information on the structural, thermodynamic and dynamic properties of these systems, opening the door to a wide range of applications. We have applied this simulation technique to various solid-state hadrogen storage materials such as metal borohydride systems and their derivative. The difference betewen the Ab initio molecular dynamics and classical molecular dynamics is that the AIMD uses forces obtained from electronic structure theory calculations (typically density functional theory) to evolve the system's dynamics in time, while classical molecular dynamics uses forces obtained from (semi)empirical force fields. Ab initio molecular dynamics calculations are typically more accurate than

classical MD calculations, especially for systems where there is charge transfer, many body van der Waals, relativistic effects, strong spin orbit coupling, or strong electron correlation (note there are many materials and molecules where these effects are critical to include). Ab initio MD, however, is often limited to systems of much smaller size and shorter time scales than classical MD due to the computational expense. Note, classical force fields or machine learned potentials can be parameterized to highly accurate reference data, thus in some instances they can be very accurate.

Part III

Results and discussion

3 Strain effect on dehydrogenation properties of $LiBH_4$

3.1 Introduction

In order to use Lithium borohydride as an energy carrier in mobile applications, it is necessary to improve its thermodynamics properties of hydrogen storage in $LiBH_4$ without reducing its high gravimetric capacity (18.3 wt%). In this study, the role of bi-axial strain on the particles of $LiBH_4$ and their effect on the stability, thermodynamic properties, and hydrogenation kinetics was investigated.

3.2 Model and computational method

All calculations were carried out in the context of density functional theory (DFT). The generalized gradient approximation (GGA) in the form of the Perdew-Burke-Ernzerhof (PBE) functional [126] and plane wave pseudo potentiel method (PWSCF) implemented in the Quantum Expresso code are used to solve the Kohn-Shame

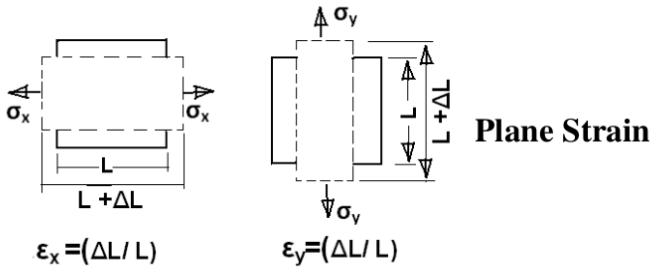

FIGURE 3.1: Illustration of bi-axial strain

equation [127]. Using the UltraSoft PseudoPotential (USPP) method, which provides a fast convergence of plane wave. Energy cut-off of 50 Ry and K-point samplings of 6x8x6 were used for all the calculations. To ensure a high accuracy in our performed computations, we have used both self-consistent criterions of the energy and the density together with a precision of 10^{-8} Ry and 10^{-6} respectively. All atomic positions and lattice vectors were fully optimized to obtain the unstrained configuration using the Broyden-Fletcher-Goldfarb-Shanno (BFGS) method. Atomic relaxation was performed with an energy convergence of 10^{-7} Ry and a force convergence of 10^{-4} Ry per Bohr. Once the converged structures for the both orthorhombic and hexagonal structure were obtained, in order to access the stability of materials, the vibrational density of states (VDOS) was calculated using the software PHONOPY [128] . The VDOS is evaluated using a finite displacement method based on the Parlinski-Li-Kawazoe method. Displacements of 0.02 Å were used for the calculation of the force constants in the displacement method. A larger displacement was used to avoid possible numerical inaccuracies in the system. A complete force constant matrix was obtained, and the phonon frequencies (ω) were then calculated by diagonalization of the dynamical matrix, then phonon eigenmode frequencies are obtained.

The lattice constant c was completely relaxed in the ab-biaxial strain. The strain rate for each direction defined by equation (eq.3.1, figure 3.1) [129]

$$\epsilon_{xx}(\epsilon_{xx}) = \frac{a(b) - a_0(b_0)}{a_0(b_0)} \tag{3.1}$$

Where $a_0(b_0)$ and $a(b)$ indicate the lattice constants in the x(y) axis of the strain-free and strained unit cell of $LiBH_4$ respectively. In general, the negative value of $\epsilon_{xx}(\epsilon_{yy})$ represents the compression strain state in the x and y axes, although positive value of $\epsilon_{xx}(\epsilon_{yy})$ indicates that the model under a tensile strain [130].

TABLE 3.1: Lattice parameters and positions for hexagonal and orthorhombic symmetries. Experimental results are included for comparison

	Parameters			Positions							
		Calculated	Experimented [131]	Calculated				Experimented [131]			
o-$LiBH_4$	a	7.2145	7.1785	Li	0.1567	0.250	0.1015	0.157	0.250	0.1015	
	b	43.652	44.368	B	0.3092	0.250	0.4275	0.304	0.250	0.4305	
	c	6.6180	6.8032	H	0.8090	0.250	0.9275	0.900	0.250	0.9560	
				H	0.4102	0.250	0.2719	0.404	0.250	0.2800	
				H	0.2085	0.024	0.4270	0.172	0.054	0.4280	
h-$LiBH_4$	a	4.1898	4.2763	Li	1/3	2/3	0.1107	1/3	2/3	0	
	b	41.898	42.763	B	1/3	2/3	0.5362	1/3	2/3	0.5530	
	c	73.072	69.484	H	1/3	2/3	0.3697	1/3	2/3	0.3700	
				H	0.174	0.349	0.5927	0.172	0.344	0.6240	

TABLE 3.2: Interatomic distances (Å) of hydrogen and other neighboring atoms. Experimental results are included for comparison

System	Interatomic distances (Å)							
	Calculated (at 0 K)				Experimented			
	Li-H	B-H	H-H	Li-B	Li-H	B-H	H-H	Li-B
o-$LiBH_4$	19.831	12.234	19.691	23.408	1.980	1.25	1.80	2.475
	20.516	12.273	19.934	25.229	2.090	1.28	1.73	2.521
	20.516	12.289	20.167	25.237	2.150	1.04	2.13	2.542
	22.499				2.289			
	23.162				2.380			
h-$LiBH_4$	18.924	12.164	19.919	24.796	2.300	1.27	2.13	2.496
	20.999	12.219	21.978		2.570	1.29	2.74	3.106
	20.999		29.138		2.629			
	29.922				2.870			

3.3 Orthorhombic and hexagonal structure of $LiBH_4$

3.3.1 Crystalline structures

Using first principle calculations, two $LiBH_4$ phases (o-$LiBH_4$ and h-$LiBH_4$) have been built by using crystallographic data in ref [131], and then, their cell parameters and atomic positions have been optimized. As a result, the corresponding total energies as function of the unit cell volume have been obtained, and are plotted in figure 3.2. The relaxed lattice constants, atom positions of two $LiBH_4$ phases along with the experimental and theoretical data are summarized in table 3.1. The difference between the experimental and calculated unit cell parameters a, b and c are around 0.38% using PWSCF method. This difference is in good agreement with previous first principles studies[132–135]. Furthermore, the bond length between two different atoms is also calculated and the results are listed in Table 3.2. This result is in good agreement with recent theoretical results obtained by ab-initio calculations [136–139] where the relative differences between the theoretical and experimental of the interatomic distances are essentially due to the larger difference of the temperature factors. It should be mentioned also that the orientation of the BH_4^- anion is different in these structures. The orientational disorder of the threefold rotation of BH4 have an important influence of the stabitlity of the system and also in the strentgh of each single B-H bond. Thus, the orientation of the tetrahedral BH_4^- units is of crucial interest in understanding the with occasional exchange between rotationally disordered H atoms and the fixed H atom.

3.3.2 Electronic properties

The projected density of states and band structures of o-$LiBH_4$ and h- $LiBH_4$ calculated are shown in figure 3.3. The electronic structure of the o-$LiBH_4$ and h-$LiBH_4$ exhibits a non-metallic character with a large energy band gap of 6.8 and 6.98 eV respectively. Which is closer to the theoretical and experimental values [136–139]. The Total DOS of o-strain $LiBH_4$ (Figure 3.3) is divided into three distinct regions, two regions in the valence band, region I from -7.15 to -5.76 eV, region II from -2.67 eV to fermi level and the third one is the conduction band (region III: from 7 to 16.2 eV). Region I is mainly constitued by B-s and H-s states while the region

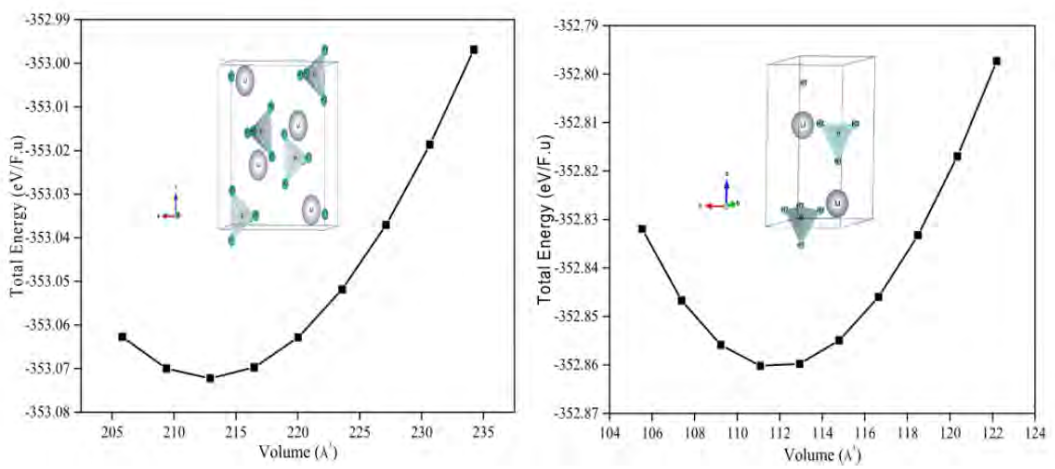

FIGURE 3.2: Total energy versus primitive unit cell volume of o-$LiBH_4$ (left) and h-$LiBH_4$ (right)

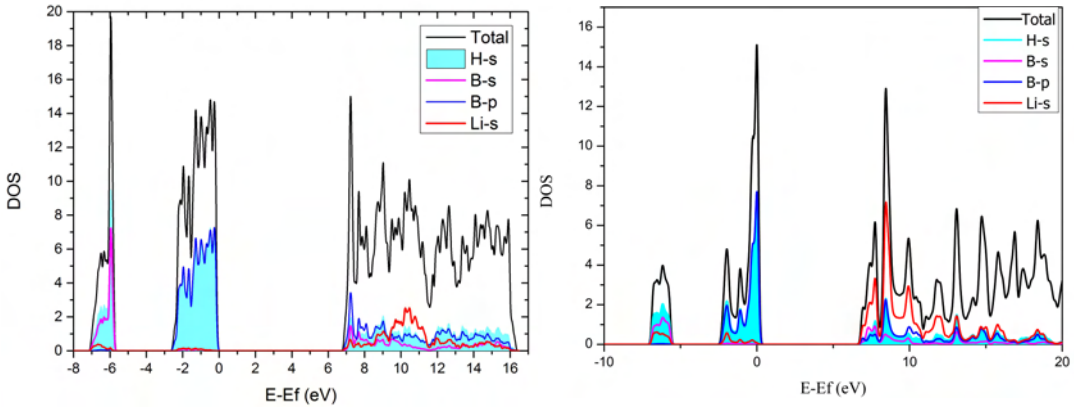

FIGURE 3.3: Total and partial DOS of free-strain, (a)o-$LiBH_4$ (b)h-$LiBH_4$

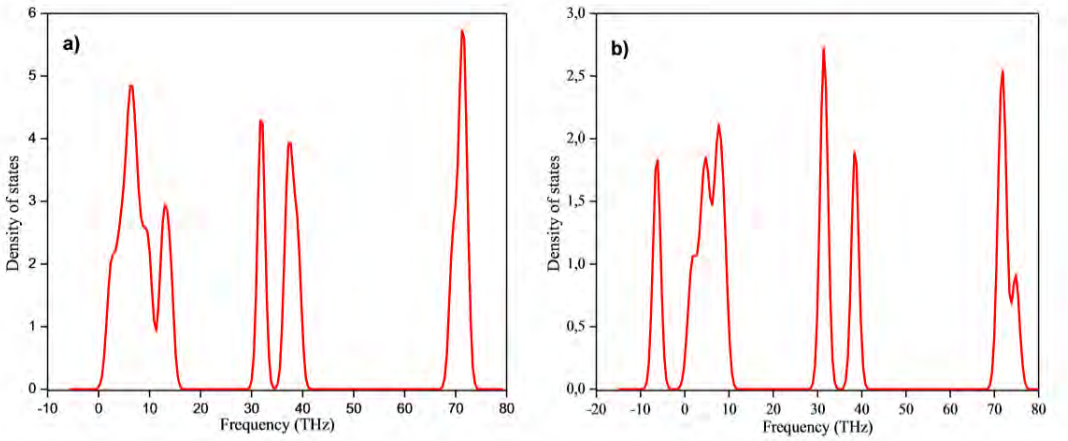

FIGURE 3.4: Phonon density of states of o-$LiBH_4$ (a) and h-$LiBH_4$ (b)

II is occuppied by H-s and B-p states. The Partial Dos in region III shows a high hybridization of the orbitals by B-p, B-s and Li-s with orbital H-s, which contributes to covalent mixed ionic interactions between $[BH_4]^-$ and Li^+. The B-p and H-s states are energetically degenerate in region II, which clearly facilitates the formation of the hybridization condition for the appearance of the complex covalent bonds of the hydride structure. The DOS of h-$LiBH_4$ shows almost the same behavior, were the occupied states splites into two peaks whose states are composed of B-s, B-p and H-s orbitals. Generaly, the boron atom constructs sp^3 hybrids and most likely forms covalent bonds with surrounding H atoms.

3.3.3 Phonon dispersion

Once the converged structures for each phase were obtained, we directly evaluate the vibrational density of state (VDOS). The method uses a phonon calculation at 0 K to see if there are imaginary phonon modes, also called soft mode. The unit cell of orthorhombic (o-$LiBH_4$) structure holding four formula units have 72 modes, while the hexagonal (h-$LiBH_4$) structure holding two formula units have 36 modes. The figure 3.4 shows the density of states of phonons in both structures of $LiBH_4$ which is divided into three and four regions for o-$LiBH_4$ and h-$LiBH_4$ Hexagonal phase respectively. Similar to the previous works[140–143], the present study also shows that h-$LiBH_4$ has a phonon with an imaginary frequency which indicates that the hexagonal structure is unstable. The absence of any imaginary phonon frequencies in the entire Brillion zone of Figure 3.4 confirms that o-$LiBH_4$ (Pnma) structure are

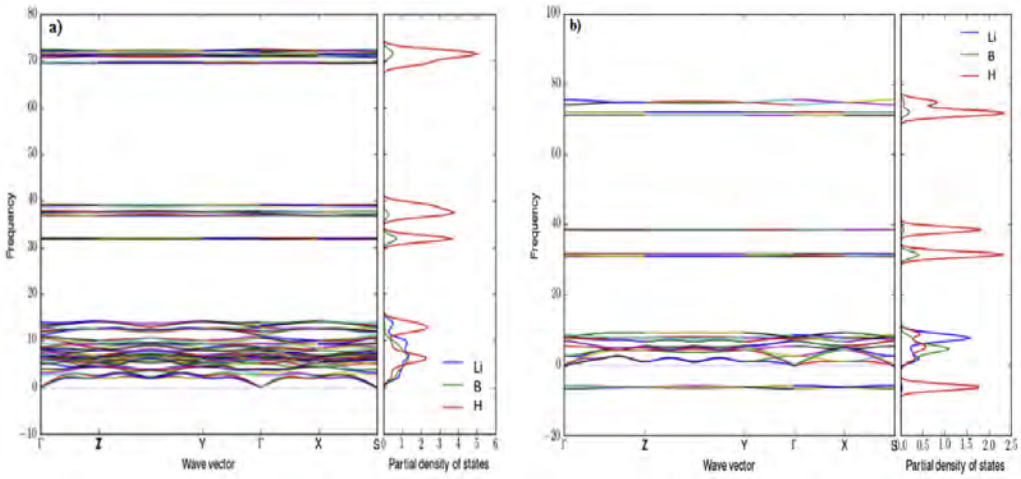

FIGURE 3.5: Phonon band structure and PDOS of o-$LiBH_4$ (a) and h-$LiBH_4$(b)

dynamically stable. In addition, it is shown that two divided regions of phonon bands are distinctly recognized, by reason of the heavy weight of B and Li which are greater than hydrogen atoms and the vibration frequency of these atoms is visibly below than that of the hydrogen atom. The low-frequency bands are from the B and Li atoms, although higher-frequency modes are due to the light H atoms. In the phonon PDOS (Figure 3.5) for o-$LiBH_4$ and h-$LiBH_4$, the region at low frequencies are composed of Li, B and H atoms states, while between 30 and 40 THz, two peaks composed of H atoms and a small fraction of states of B atoms are observed. The apparent peak at high frequencies are mostly composed of H states since its atomic mass is much lighter than those of the other atoms. The only noticeable difference between the orthorhombic phase and hexagonal is that the peak composed of H atoms appear at negative frequencies for h-$LiBH_4$. The phonon band structure could be classified into three regions; the first one (less than 15 THz); region II(from 30 to 40 THz); and region III (68-72 THz). The eigenmodes in group I are due to the displacements of Li^+ cations and $[BH_4]^-$ anion, while those in region II and III originate from the internal H-B-H bending and B-H stretching vibrations of $[BH_4]^-$ anion, respectively.

TABLE 3.3: Comparison of vibrational enthalpy and entropy results with experimental data

System	ZPE=H_{vib}(T=0) ($J\,mol^{-1}$)	ZPE other works [144, 145]	Evib=H_{vib}ZPE	Evib [144]	S_{vib} (T=300 K) ($J\,mol^{-1}\,K^{-1}$)	S_{vib} [144]
o-$LiBH_4$	106.03	107.1, 106.5, 108.1	10.8(300K)	10.8	73.97	63.6
h-$LiBH_4$	99.9		21.2(450K)		75.57	

TABLE 3.4: Calculated heat capacity of o-$LiBH_4$ and h-$LiBH_4$ at constant pressure and constant volume compared with other calculated and experimental data

System	Cp($J\,mol^{-1}\,K^{-1}$)	Cp other	Cv ($J\,mol^{-1}\,K^{-1}$)	Cv other
o-$LiBH_4$	69.03 (300K)	76.6 ± 0.9 (285.6 K) [146] 81.51 (298K)[147]	59.45 (300K)	
h-$LiBH_4$	86.87 (450K)	95.43 (450 K)[147]	85.23 (450K)	

3.4 Thermodynamic properties

3.4.1 Vibrational enthalpy and Entropy

The thermodynamic properties of $LiBH_4$ phases were obtained Within the harmonic approximation listed in the Chapter 2. The Figure 3.6 plots the calculated H_{vib} and S_{vib} of $LiBH_4$ both phases as a function of temperature. Although having different structures, the H_{vib} and S_{vib} exhibit similar temperature dependencies for both structures. From Figure 3.6, it is noticed that the ZPE of h-$LiBH_4$ is about 7 $kJ\,mol^{-1}$ lower than that of o-$LiBH_4$. Above 300 K, the internal energies H_{vib} increase almost linearly with temperature, tending to display k_BT behavior. Even more, at low temperature, the entropy S_{vib} of h-$LiBH_4$ is higher than that of o-$LiBH_4$, while increasing the temperature the o-$LiBH_4$ entropy becomes superior (see Figure 3.6). The zero-point, enthalpy and entropic contributions to the free energy of the different phases are summarized in Table 3.3. As a further test of our computational methodology, there, our calculations results are compared to other values reported in the literature and find good agreement.

3.4.2 Heat capacity

The molar heat capacity has importance in terms of energy, time and costs involved in changing temperatures of objects. Hence it is important as it will present a notion of how much energy will be appropriate to heat or cool an object of a given mass by

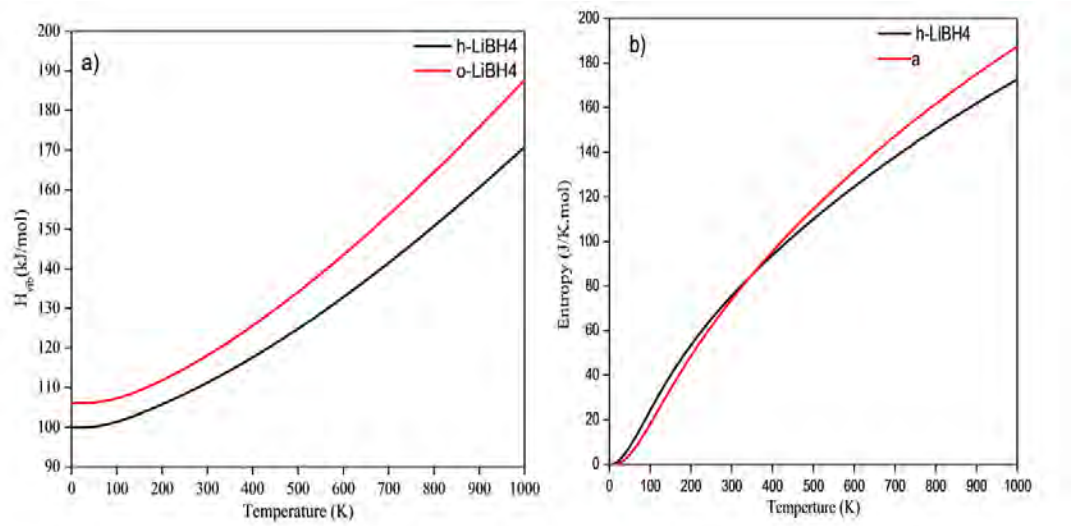

FIGURE 3.6: Vibrational enthalpy (a) and entropy (b) as function of temperature of both $LiBH_4$ structures

a given supply. This will give information as to how long the heating or cooling process will take under a given supply. The heat capacity at constant volume Cv and at constant pressure are presented in Figure 3.7, At constant pressure, some of the heat goes into expanding the system, which does external work, and therefore leaves less energy available for raising the temperature. The heat capacity depends on the temperature, it increases with increasing temperature and this translates an accumulation of energy in the vibrational movement. In the interest of $LiBH_4$ changes in the crystal structure is expected to observe discontinuities in this case. Beyond room temperature, experimental values for the molar heat capacity of orthorhombic and hexagonal phases of $LiBH_4$ have been realized by many authors. ElKharbachi et al. [146, 147] deliberates the heat capacity from ambient temperature to approaching the melting point of the compound at 553 K using calorimetric measurements and found the following values Cp(285.6 K) =76.6±0.9 $J\,mol^{-1}\,K^{-1}$. At lower temperatures (i.e. 15–303 K), the standard molar heat capacity and entropy at 298.15 K is 82.563 $J\,mol^{-1}\,K^{-1}$ and S(298.15 K)= is about 75.860 ± 0.125 J/mol/K(Table3.4). The agreement with the experimental data is limited, mainly at high temperatures. In fact, at room temperature, the value of Cp for the orthorhombic phase is around 10 $J\,mol^{-1}\,K^{-1}$ lower than that desoluted experimentally, while for the hexagonal phase at 450 K there is a difference about 23. At constant volume, all the heat that goes into the system increases the temperature

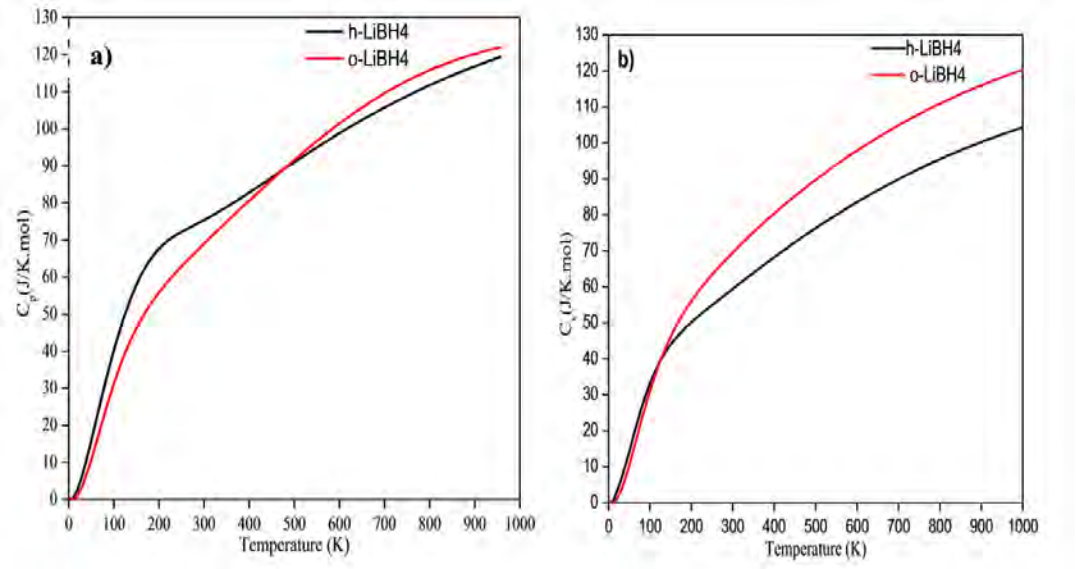

FIGURE 3.7: Calculated heat capacity as function of temperature of o-$LiBH_4$ and h-$LiBH_4$ at constant pressure (a) and constant volume (b)

of the system and no external work is done. According to the phase diagram for $LiBH_4$ composition [148], at the high temperature a coexistence of different phase (H_2 gas, LiH solid, B solid) can be observed between 450 K and 850 K then the LiH decomposes and transforms to Li-liquid. A regular theory of the heat capacity for liquids has not been accomplished and is still a rich area of research. Thus, we find that we need more heat to raise the temperature of unit mass of the system over 1 K under constant pressure conditions, compared to the heat required to increment the temperature of the same unit mass of the system through 1 K and under constant volume conditions.

3.4.3 Thermal expansion

The coefficient of thermal expansion (CTE) relates the change in volume of a material to change in temperature and is given by the negative value for CTE indicates a contraction on negative thermal expansion (NTE) while a positive value indicates a positive thermal expansion (PTE). From Figure 3.8, it is found to be strongly dependent on temperature but remains negative for o-$LiBH_4$ ($-2.5 * 10^{-5}$) and positive for h-$LiBH_4$ ($1.6 * 10^{-4}$) until 500 K, above which both phases are near ZTE. DFT calculations combined with a quasiharmonic approximation method have been used to investigate phonon contribution of $LiBH_4$ polymorphs. Computed

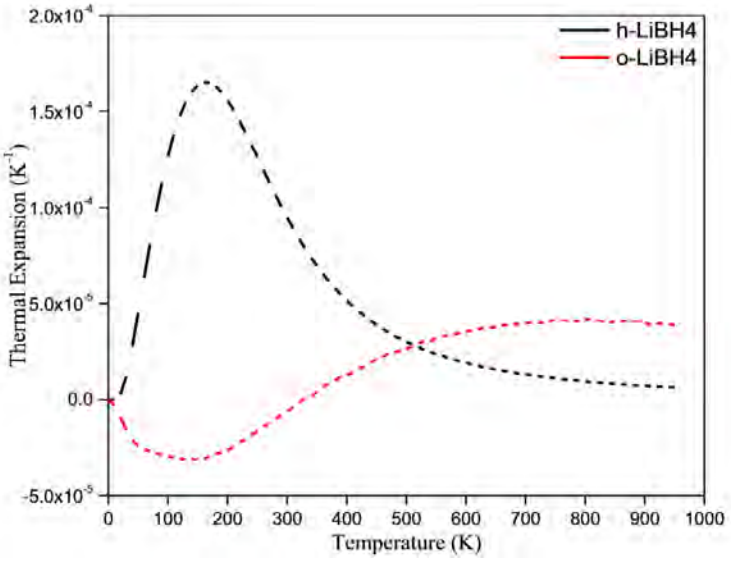

FIGURE 3.8: The coefficient of thermal expansion as function of temperature of o-$LiBH_4$ and h-$LiBH_4$

vibrational properties were used to illustrate thermodynamic properties. They, allowed us to understand some properties of a small atom like hydrogen which are not observable experimentally.

3.5 Thermal decomposition of o-$LiBH_4$

The decomposition of complex hydride $LiBH_4$ takes place in two principal steps. The first desoption proceeds trough the following reaction accompanied by the fomation Boron and LiH hydride:

$$LiBH_4 \rightarrow LiH + B + \frac{3}{2} H_2 \quad \{13\}$$

The release of total content of hydrogen bonded to lithium, giving in the end Li, B and H through the final reaction:

$$LiBH_4 \rightarrow Li + B + 2\,H_2 \quad \{14\}$$

The LiH formed during the first reaction of the desorption is a very stable compound. This hydride is difficult to decompose. Generaly, the decomposition of $LiBH_4$ stops after the formation of LiH, leaving a hydrogen bonded in the final products. The accessible hydrogen capacity of LiBH4 is then reduced to 13.8% weight. The desorption enthalpy for the reaction 13 is calculated from the following

equation:

$$\Delta H_{des} = E_{tot}(B) + E_{tot}(LiH) + \frac{3}{2}E_{tot}(H_2) - E_{tot}(LiBH_4) \quad (3.2)$$

Where $E_{tot(LiBH4)}$ presents the total energy of $LiBH_4$, $E_{tot(B)}$, $E_{tot(LiH)}$, and $E_{tot(H2)}$

TABLE 3.5: Lattice parameters, total energy of each component

Component	LiH	B	H_2	$LiBH_4$
Crystalline structure	Cc	α-Rhomo	hcp	Ortho
Parameter a(Å)	4.01	4.90	3.64	7.21
Parameter b(Å)	4.01	4.90	3.64	4.36
Parameter c(Å)	4.01	12.55	3.43	6.61
Total energy($Ry/f.u$)	16.06	6.288	2.330	-25.93
Desorption Enthalpy(kJ mol^{-1}H$_2$)				**75.73**

are the total energy of boron, lithium hydride and hydrogen molecule respectively. The used lattice parameters and total energy are given in Table 3.5. The calculated desorption enthalpy of the $LiBH_4$ is 75.73 kJ mol^{-1}.H_2 which is close to other value obtained experimentally and theoretically [134, 135, 146, 149]. The calculated desoption enthalpy is too high compared to the traget range ΔH mointioned in Section 1.2. Thus, we demonstrated that $LiBH_4$ is thermodynamically too stable to desorb hydrogen at ambient conditions.

3.6 Strain effect on the o-$LiBH_4$ structure

The previous results show that the lithium borohydride presents a high desorption enthalpy and reduce it we applied a biaxial tensile/compressive strains along the a[100] and b[010] directions (eq.3.1).

The effects of the strain on the lattice parameter c and volume of $LiBH_4$ are represented in Figure 3.9. This Figure shows that for the maximum biaxial compressive strain of -6% the lattice parameter c of complex hydride $LiBH_4$ takes the highest values then decreases by increasing strain rate applied by 1%. On the other side the volume increases in the opposite direction by increasing the strain applied to $LiBH_4$. So we may conclude that the biaxial tensile or compressive strain is likely cause deformation of the crystal structure of $LiBH_4$ and its lattice distortion becomes severe with increasing the biaxial strain. As well, Figure 3.9 shows the total

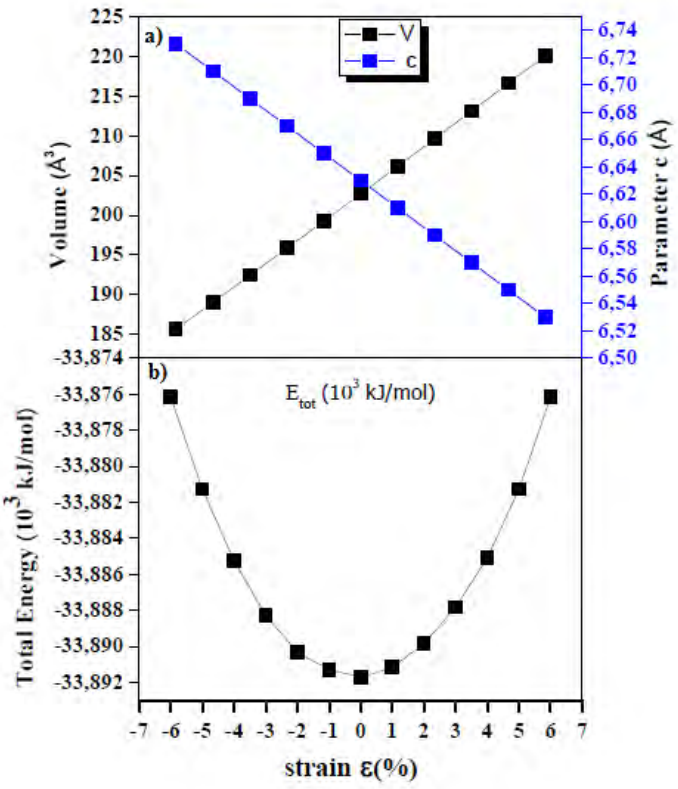

FIGURE 3.9: Representation of a) c parameter and volume; b) energy as a function of biaxial strain on $LiBH_4$

energy as a function of biaxial strain in $LiBH_4$ unit cell respectively. Generally, the structural stability of crystal is associated with its total energy, and the minimum total energy indicates the most stable crystal structure. We can notice that the total energy of strained $LiBH_4$ increased compared to total energy of pure-strain $LiBH_4$. We can consider that either compression or biaxial tensile cause destabilization of the $LiBH_4$ structure.

3.6.1 Dehydrogenation properetie

The measurement of the hydride stability is inversely proportional to its formation energy. As the enthalpy of formation increases, the stability of the hydride decreases. According to Figure 3.10 it is noted that the desorption enthalpy decreases during the application of biaxial strain on the $LiBH_4$ structure relative to that of strain-free of $LiBH_4$. This suggests that either the tensile or compressive strain is applied improve the thermodynamic dehydrogenation because of the contribution of strain energy. The results show that hydrogen desorption enthalpy reduced from 75.73 kJ/mol.H_2 for free-strain $LiBH_4$ structure to 65 kJ/mol.H_2 for $LiBH_4$ structure under of -6% strain rate. Therefore we may have a gain of 20.73 kJ/mol.H_2 by application of biaxial strain on the $LiBH_4$ structure.

3.6.2 Hydrogen diffusion

After dissociation, the hydrogen atoms can move from one site to interstitial site according to the corresponding activation energies. based on our model, each hydrogen atom has four nearest neighbors available sites in the same distance, which is represented by the first path and the second path is the hydrogen atom displacement anion $[BH_4]^-$ to another anion $[BH_4]^-$ neighbors. Figure 3.11 shows the diffusion of energy barriers of H corresponding to the first path 3.11a and second path 3.11b respectively in the (un)strain structure of $LiBH_4$. The free-strain diffusion activation energy of hydrogen atom for the first path is 665.702 kJ mol^{-1}but for the second path the energy diffusion activation of hydrogen atom is 92.873 kJ mol^{-1}which is lower. We can conclude that the hydrogen atom easily moves along the second path relative to the first path. Particularly Figure 3.12

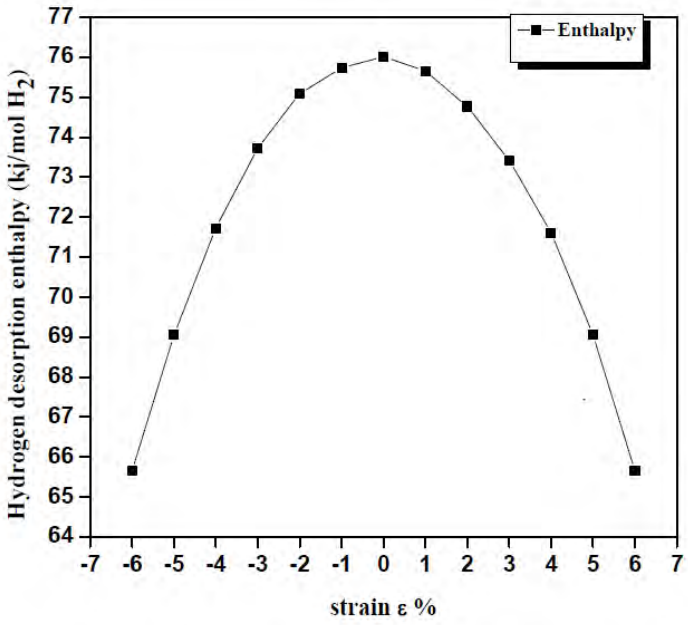

FIGURE 3.10: The hydrogen desorption enthalpy according to biaxial strain $\epsilon(\%)$ in the structure on $LiBH_4$

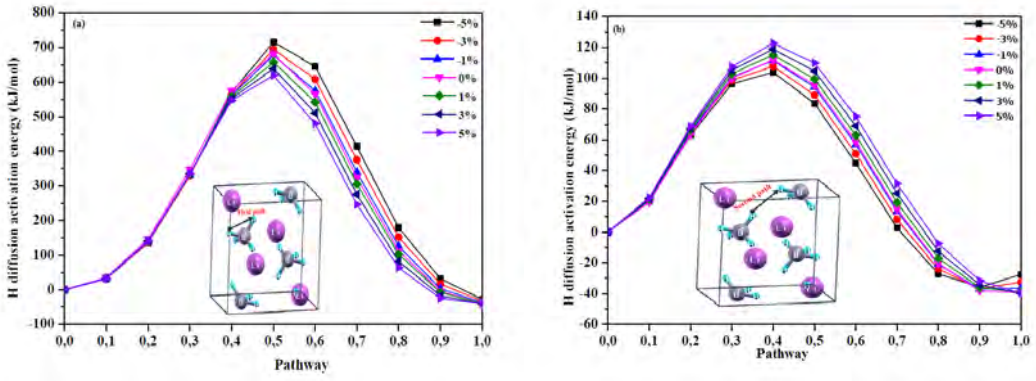

(A) First path (B) Second path

FIGURE 3.11: Energy curves for diffusing hydrogen between two interstitial sites along the first path and second path

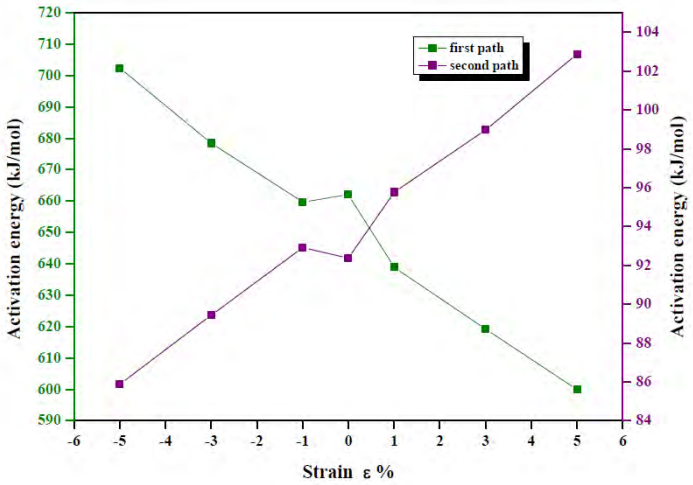

FIGURE 3.12: The hydrogen desorption enthalpy according to biaxial strain ϵ (%) in the structure $LiBH_4$

shows that the diffusion activation energy of hydrogen atom along the first path decreases under tensile strain from 665.702 kJ $mol^{-1}$to 603.241 kJ/mol. Otherwise, for the second path, the diffusion activation energy of hydrogen atom decreases by increasing the compression, from 92.873 kJ mol^{-1}value to 86.361 kJ mol^{-1}. This increases favorably the kinetics of hydrogen desorption in complex hydride $LiBH_4$.

3.6.3 Electronic charge density

The calculation of the electronic charge density which is usually presented in a plane or in a direction, informs us about the charge transfer and therefore on the ionic or covalent nature of the liaisons. Therefore, to see the bond's nature of considred hydrides, we calculated the charge density in the (001) plane, (100) and (010). Figure 3.13 shows a contour map of the charge distribution for most stable state (0%) and strained state (5%, -5%). The amount of electronic charge at every point in space is determined and all points having the same value for the electron density in the plane are joined by a line, a contour line. On one hand for free-strained state we have equal sharing of the charge density between bore and hydrogen atoms which is interpreted by covalent binding. In anion $[BH_4]^-$ the electronic charge is heavily concentrated in the internuclear region where it forms a bridge of high density between the three nuclei. On the other hand the anion $[BH_4]^-$ and Li^+ cations form an ionic bonding

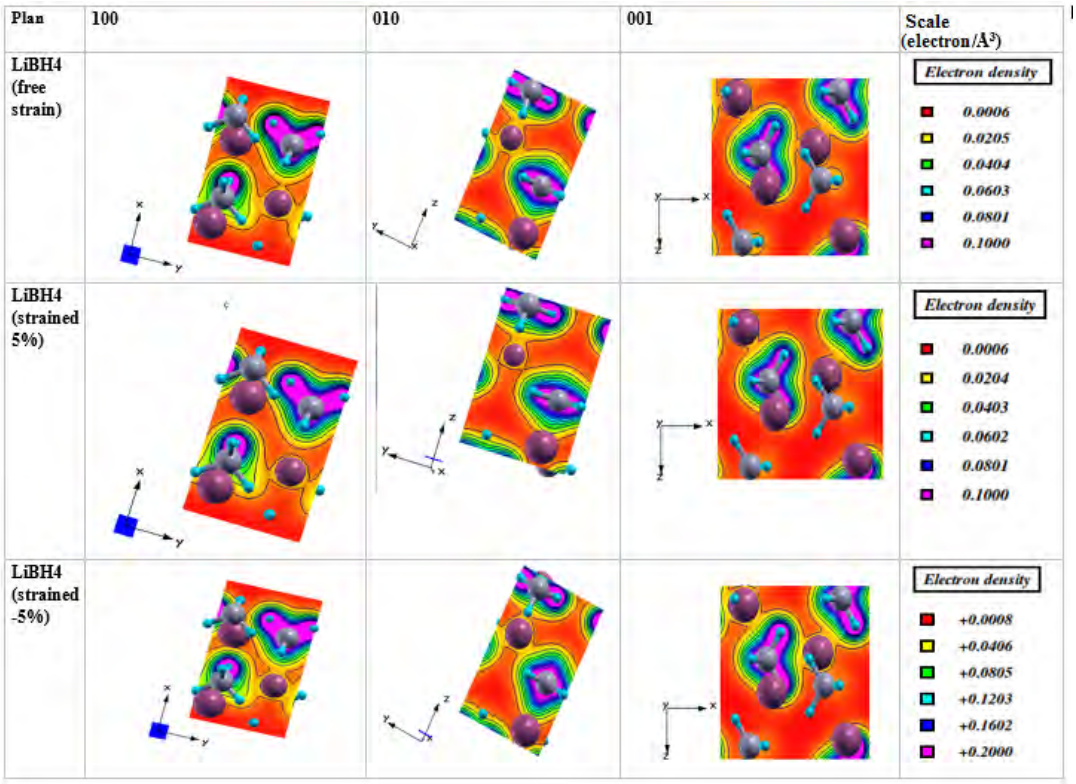

FIGURE 3.13: The three dimensional (3D) electron density contour maps for (100),(010),(001) planes according to rate strain

because the bond formed between the anion and cations have very different affinities for the electronic charge density. The calculation shows that there is a continuous distortion of the original atomic density distributions, a distortion which increases as the internuclear distance decreases. The contours maps demonstrate that the compressive strain (-5%) causes the greatest decrease in electron density of $[BH_4]^-$ and Li^+ bonds of complex hydride $LiBH_4$. Due to these effects, the transfer of charge density from lithium cation to anion $[BH_4]^-$ is very evident, in this case the system becomes unstable and it's easy to remove hydrogen atoms which could explain the decrease of desorption enthalpy under compressive strain.

Conclusion

The first-principles plane-wave pseudopotential method based on density functional theory was used to study strain effect on complex hydride $LiBH_4$. Improving thermodynamic properties and kinetics hydrogenation in the hydride $LiBH_4$ are summarized in the following:

- Biaxial tensile or compressive strain tends to result in the deformation of the crystal structure of $LiBH_4$, and the destabilization of the structure becomes severe with increasing biaxial strain.
- When the compressive or tensile strain applied on the $LiBH_4$ structure the enthalpies desorbing Hydrogen of hydride $LiBH_4$ are reduced relative to that of free-strain $LiBH_4$, which is beneficial to improve the thermodynamic properties of $LiBH_4$.
- The DFT calculations show that the energy barriers for different paths decrease according to the hydrogenation kinetics of $LiBH_4$.

4 Improved dehydrogenation properties of doped $LiBH_4$

4.1 Motivation

The theoretical analyses for the electonic, thermodynamic and vibrational properties suggest that BH4- anion complex forms the table covalents bonds similar to a CH4 molecule and a deficient electron to form them is compensated by Li+ cation. Therefore, it is expexted, from our previous work that the charge transfer from Li^+ to BH_4^- is a key feature for the stability of $LiBH_4$, the high stability of the system $LiBH_4$ is mainly due to the high hybridization between B and H atoms. For this reason, it was thought to have substituted the B by light elements such as Lithium to reduce this hybridization and consequently reduce the energy of formation of the system. To the best of our knowledge, there are no theoretical and experimental works performed previously for the current approach of doping boron by lithium in the lithium borohydride framework. Additionally, the negative formation enthalpy values and the calculated lattice dynamics stability confirms the possibility of the fabrication of the studied systems. Also, the calculated dehydrogenation properties show an interesting decrease relative to the pure structure of $LiBH_4$, which may lead to a compound for high-capacity hydrogen storage.

4.2 Models and computational details

To study the decomposition reaction of doped $LiBH_4$, the cell of $Li_{1+x}B_{(1-x)}H_4$ (x = 0, 0.25, 0.5, 0.75) (see figure 4.1) was used to model the substitution of Li at B site in $LiBH_4$ bulk. This method consists on the study of the generation of doped structures has been widely accepted in the field. In addition, it is technically difficult to

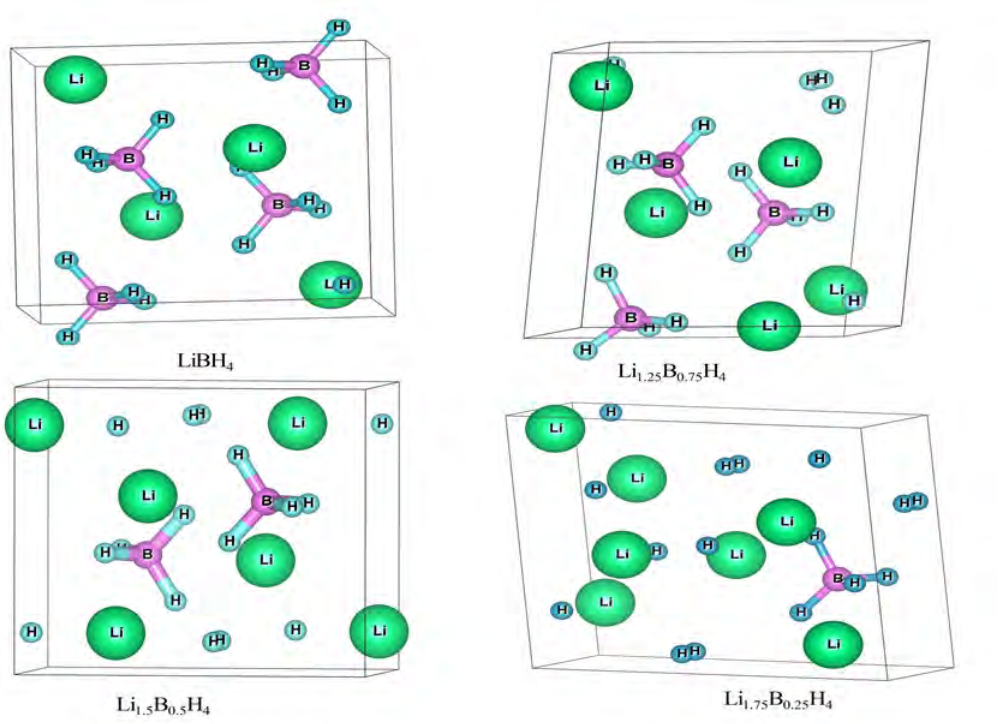

FIGURE 4.1: Crystal structures of (a) pure, (b) $Li_{1.25}B_{0.75}H_4$ (c)$Li_{1.5}B_{0.5}H_4$(d) $Li_{1.75}B_{0.25}H_4$. Green, pink and blue balls represent respectively Li, B and H atoms.

develop random structure, because it needs a large supercell and several calculations of doping in different position of this supercell which takes several times of calculations and effort; if any, into account. Therefore, we have used the classical model of doping following the best practice in the field. Additionally, regarding the phases stability, the calculated formation enthalpies and lattice phonon dispersion confirm the stability of all studied systems.

4.3 Li substituted Lithium borohydride

4.3.1 Structural properties and Formation enthalpies

In order to investigate the substitution of boron by lithium, the geometries of $Li_{(1+x)}B_{(1-x)}H_4$ (with x= 0.25, 0.5, 0.75) were fully relaxed. This substitution breaks the symmetry of $LiBH_4$ because of the different atomic radii of Li (1.52 Å), B (0.85 Å), which leads to different lattice parameters and cell volumes for pure $LiBH_4$ and substituted $LiBH_4$ and then creates changes on the periodicity of the crystal. As shown in figure 4.1. The relaxed lattice parameters and volume of all the systems

TABLE 4.1: Lattice parameter, volume, formation enthalpy, gravimetric and volumetric capacity of $Li_{1+x}B_{1-x}H_4$ (x = 0, 0.25,0.5, 0.75).

System	Parameters(Å)			Volume (Å^3)	Formation enthalpy (kJ mol^{-1})	Gravimetric capacity (wt%)	Volumetric capacity (g l^{-1} H_2)
	a	b	c				
$LiBH_4$	7.05	4.33	6.74	205.75	-192.12	18.5	146.37
$Li_{1.25}B_{0.75}H_4$	6.50	4.32	7.18	200.88	-174.44	18.88	132.3
$Li_{1.5}B_{0.5}H_4$	7.54	4.03	6.67	203.1	-141.87	19.36	130.86
$Li_{1.75}B_{0.25}H_4$	7.93	3.93	6.65	206.59	-119.95	20.31	128.65

are listed in table 4.1. The possibility of the structure of $LiBH_4$ substituted by Li was evaluated by calculating the formation enthalpy of $LiBH_4$ and the related $Li_{1+x}B_{1-x}H_4$(with x= 0.25, 0.5, 0.75). The formation enthalpies are calculated based on the equation:

$$Li_{1+x}B_{1-x}H_4 \rightleftharpoons (1+x)\,Li + (1-x)\,B + 2\,H_2 \quad \{15\}$$

Where (x=0,0.25,0.5,0.75) the formation enthalpy for each structure is determined with respect to the most stable structure of the pure elements. The calculated enthalpies are presented in figure 2, and reported in (kJ mol^{-1}) unit in table 4.1. In all cases, the substitution of B by Li in the $LiBH_4$ lattice is an exothermic process. By virtue of, negative heats of formation, the complex hydride is thermodynamically stable with respect to the complete decomposition into its basic constituents (B, Li, and H_2).

4.3.2 De-hydrogenation properties

To further investigate the effects of the substitution on the de-hydrogenation behavior of $LiBH_4$, the desorption enthalpy E_{des}, which is the most important thermodynamic parameter, has been calculated and used to predict de-hydrogenation proprieties. As seen in table 4.2, for pure $LiBH_4$, the computed desorption enthalpies for the first reaction (partial decomposition) is 75.7 kJ mol^{-1} H_2. In view of, the de-hydrogenation enthalpy ΔH is significantly less than 30 kJ mol^{-1} H_2, the material will not be easily reversible. However, for an ideal material for hydrogen-storage, the heat of formation ΔH should be around 40 kJ mol^{-1} (H_2) [21]. The temperature of de-hydrogenation can be reliably estimated by $\Delta H = T\Delta S$, where ΔH and ΔS are the enthalpy and entropy change of the

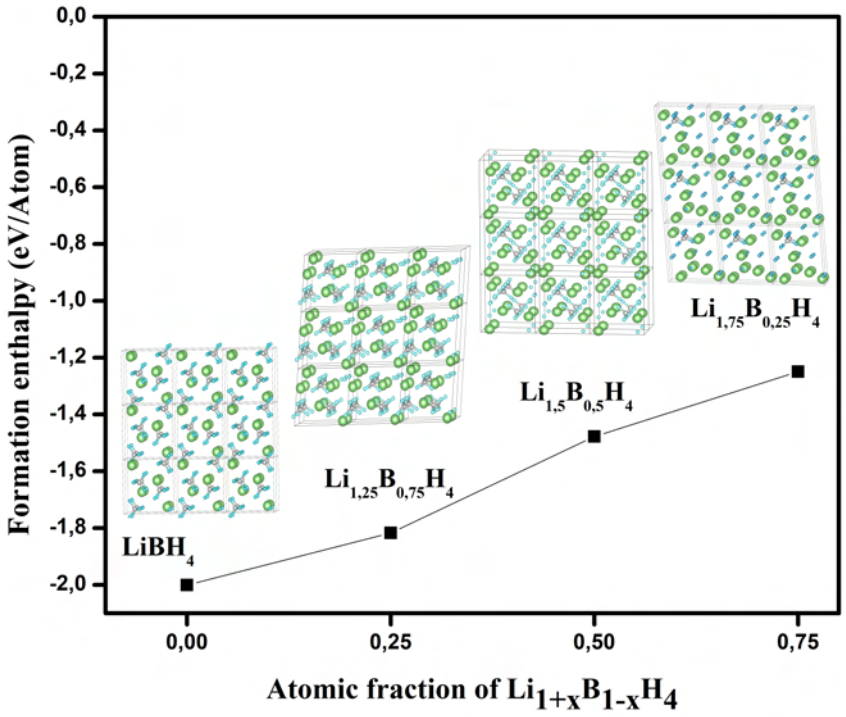

FIGURE 4.2: Formation enthalpies from the calculated static density-functional theory as function of atomic fraction of Li in $Li_{1+x}B_{1-x}H_4$

TABLE 4.2: Desorption enthalpy and temperature of $Li_{1+x}B_{1-x}H_4$ (x= 0, 0.25, 0.5, 0.75)

System	First reaction:$LiBH4 \rightarrow LiH + B + 3/2H_2$		Second reaction: $LiBH4 \rightarrow Li + B + 2H_2$	
	E_{des} (kJ mol^{-1})	T_{des}(K)	E_{des} (kJ mol^{-1})	T_{des} (K)
$LiBH_4$	75.75	658.75	96.06	835.31
$Li_{1.25}B_{0.75}H_4$	62.38	542.49	87.22	758.44
$Li_{1.5}B_{0.5}H_4$	61.46	534.48	70.93	616.81
$Li_{1.75}B_{0.25}H_4$	46.854	407.42	59.97	521.52

de-hydrogenation reaction. The entropy changes estimate that $95 \leq \Delta S \leq 140$ $J\,mol^{-1}$. For almost all the intermetallic hydride the variation entropy reaction is $\Delta S = 130\ J\,mol^{-1}\,K.H_2$ corresponding to the change entropy of hydrogen gas to solid hydrogen. The stability of the hydride can be described and compared with the enthalpy of reaction only. For complex hydrides, the situation is a bit more complicated and entropy of the reaction appears to be lower and variable for different complex hydrides. Based on the theoretical calculation, the value of ΔS has been estimated to $115\ J\,mol^{-1}\,K.H_2$ [150]. The predicted decomposition temperature is 658.75 K for the first reaction. This temperature is still too high for practical applications. According to the calculated desorption enthalpies listed in table 4.2, the modified crystal structures after Li doping for the first equation is nearly reduced to 62.38, 61.46 and 46.85 $kJ\,mol^{-1}$ H_2 with increasing the substitution level from x = 0.25 to 0.75. Likewise, the de-hydrogenation temperature is reduced by 150 K for 20.31 wt% for $Li_{1.75}B_{0.25}H_4$. Therefore, the decomposition reaction following Eq. **??** is thermodynamically favorable than the process following Eq. **??**. Generally, the stabilities of the reaction products are dramatically reduced with increasing the percentage of Li. Our calculations show that substitution of B by Li in $LiBH_4$ structure results in a favorable modification of the thermodynamics that essentially constrains the potential of $LiBH_4$ for hydrogen-storage application.

4.3.3 Electronic structure

To understand and explain the improved performance of de-hydrogenation process during application of substitution with lithium, the density of states of pure and modified of $LiBH_4$ structure have been carried out. This study will clarify the effect of the substitution with Lithium on the hydrogenation performance of this system. Figure 4 presents the total and partial densities of states for $Li_{1+x}B_{1-x}H_4$ with x varied from 0 to 0.75. In these figures, the Fermi level (E_F) is set to zero and used as a reference. The Valence band split into two regions: The region I (low-energy states) which composed of B-2s and H-1s orbitals and the region II (high-energy states) consists of B-2p and H-1s orbitals, which show a high hybridization. Boron atoms form covalent bonds with surrounding four H atoms. Because there is a little contribution of Li orbitals to the occupied states, Li atoms are thought to

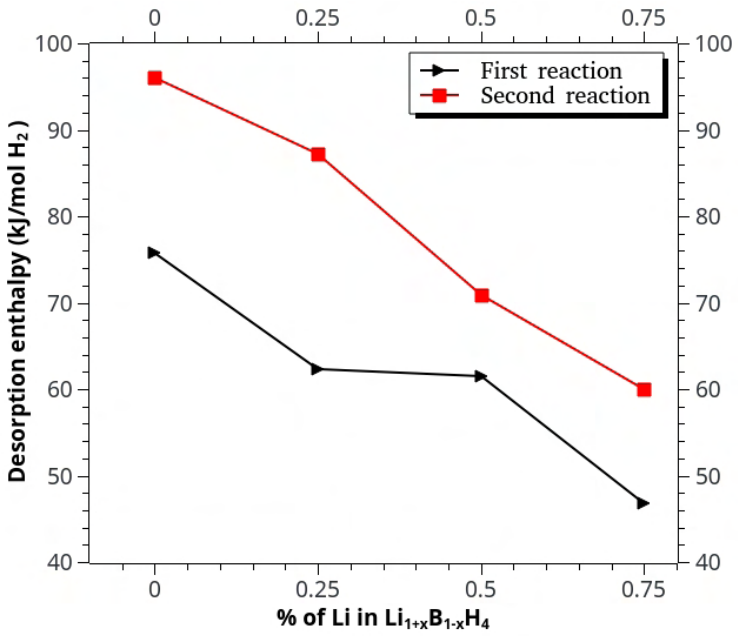

FIGURE 4.3: Desorption enthalpy and temperature as function of Li-substitution rate of $Li_{1+x}B_{1-x}H_4$ (x= 0, 0.25, 0.5, 0.75)

be ionized as Li^+ cations. As expected, after the substitution of boron by Li, the strong hybridization between B and H atoms begins to weaken by increasing the rate of substitution, and other states of individual hydrogen begin to appear, it can be explained that the covalent band between B and H has broken and other binding begins to appear to form hydrogen molecules in interstitial sites. this translates the release of the desorption enthalpy by adding the percentage of Li in the $LiBH_4$ structure. We should note also that the energy band gap decreases with increasing the percent of Li inside the $LiBH_4$ framework.

4.3.4 Lattice dynamic stability

To further study of the lattice stability of $Li_{1+x}B_{1-x}H_4$ (x =0, 0.25, 0.5, 0.75) compounds first-principles phonon calculations are carried out. According to harmonic approximation, this is possible when all the phonons have real and positive frequencies. Negative or imaginary frequencies of phonons indicate that crystal is dynamically unstable. In our present study, from figure 4.5 any negative frequencies are not observed for the pure $LiBH_4$ compound. This means the compound is mechanically stable. The phonon density of state shows three branches of optical phonons separated from the phonon branches of lower frequencies. The

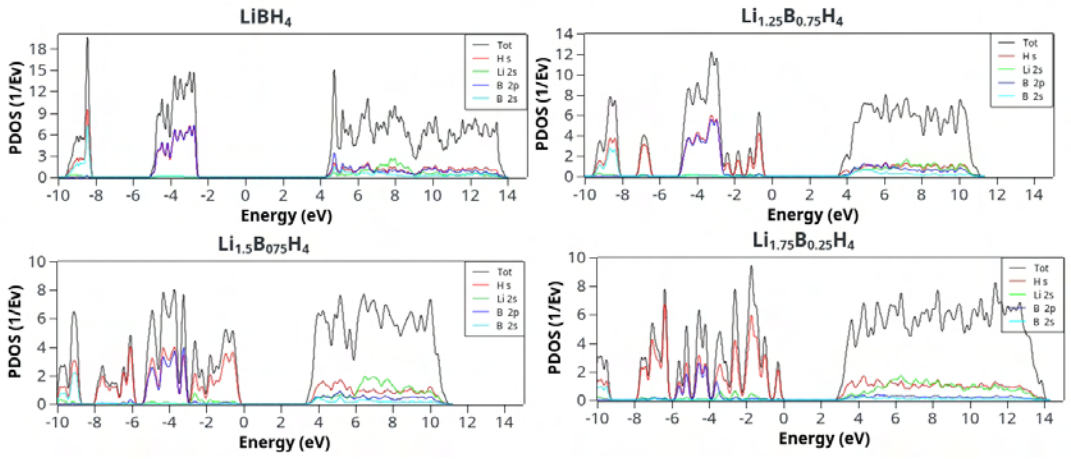

FIGURE 4.4: The calculated Total and partial DOS of $Li_{1+x}B_{1-x}H_4$ (x= 0, 0.25, 0.5, 0.75)

reason for the separation of these branches comes from the lower mass H present in the compound. The peak in the lower energy region corresponds to the acoustic branches in the dispersion plot. The next separated higher energy peaks represent the coupled optical phonon branches. In the case of the modified $LiBH_4$ structure figure 4.5 a small phonon branches in the negative frequency range of -15 THz (negative frequencies are representative of imaginary frequencies. The vibration of the hydrogen is more independent than that of the complex bond of BH_4 explains the reduction of desorption enthalpies for modified $LiBH_4$ lattice. We believe applying external pressure can eliminate these imaginary phonons.

4.3.5 Lattice Thermodynamic properties

Thermal properties such as Helmholtz free energy, entropy and constant-volume specific heat (C_V) as a function of temperature are computed using phonopy. It can be seen from figure6 that the lattice heat capacity increases slowly with the temperature in the initial stage. The lattice heat capacity approaches almost linear when the temperature exceeds 400 K. Besides, with the increasing of Li-substitution concentration, the lattice heat capacities of the modified systems have small increases. Although Li-substitution has slight effects on the lattice heat capacity of $LiBH_4$, and the current framework can be useful to characterize complicated crystal structures of complex hydrides materials. Finally, the present framework is beneficial to optimize the material composition or to design a new

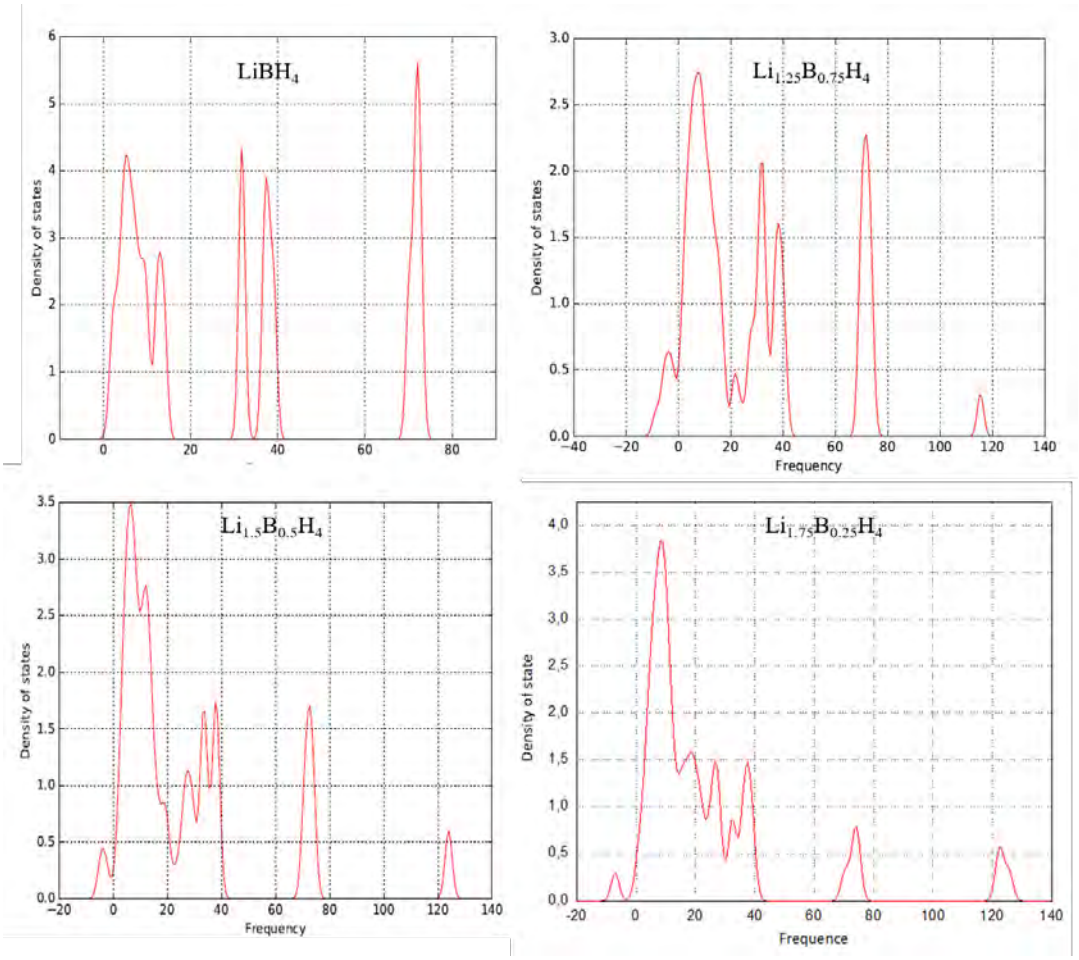

FIGURE 4.5: Phonon density of states of $Li_1{\equiv}xB_{1-x}H_4$ (x= 0, 0.25, 0.5, 0.75)

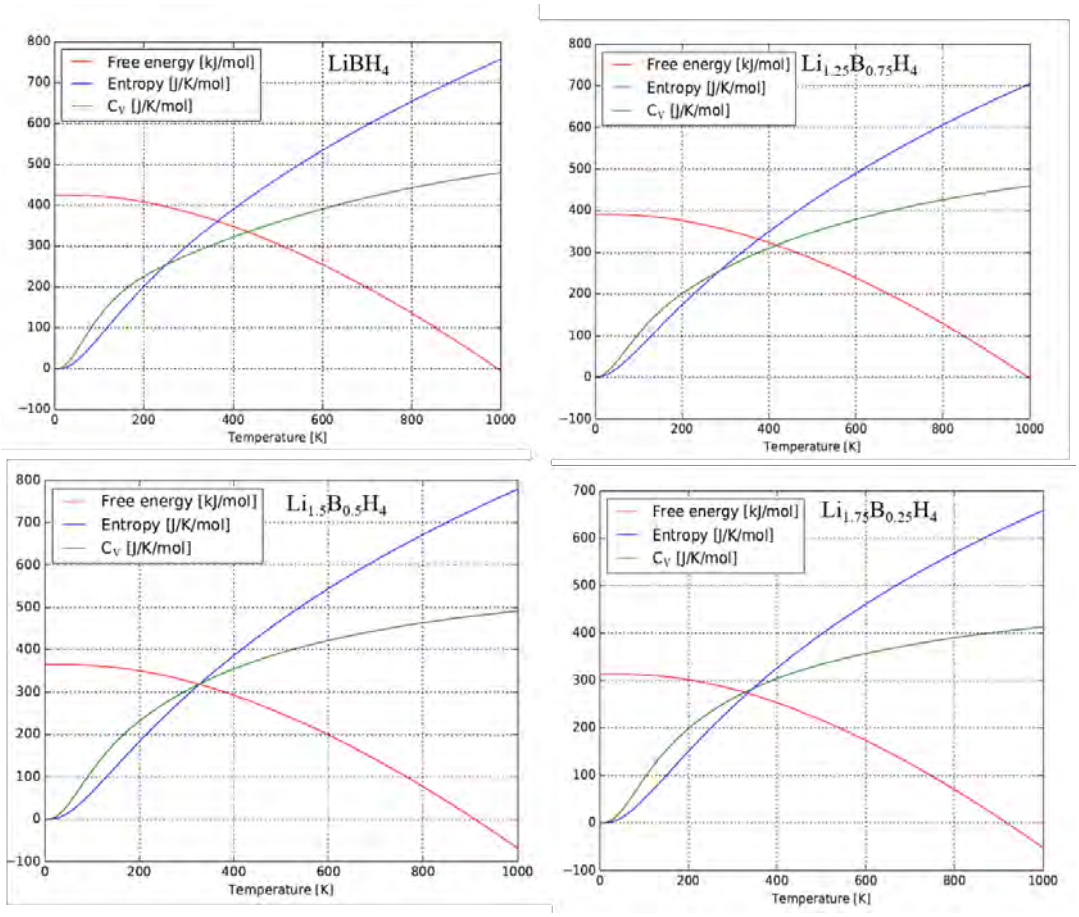

FIGURE 4.6: Temperature Helmholtz free energy F(V, T), vibrational entropy S, and heat capacity C_v of $Li_1{\equiv}xB_{1-x}H_4$ (x= 0, 0.25, 0.5, 0.75)

modified crystal of $LiBH_4$, which could be applicable as solid-state hydrogen-storage materials.

4.4 Conclusion

To sum up, this study points towards the idea of the substitution of boron by lithium atom in the lithium borohydride $Li_{(1+x)}B_{(1-x)}H_4$ (x = 1⁄4 0, 0.25, 0.5, 0.75) framework. Firstly, the possibility of the fabrication of these systems was confirmed by the negative value of formation enthalpies and the weak soft modes in phonon dispersion of all the systems. Furthermore, the de-hydrogenation temperature is reduced to 521.52 K for fully released hydrogen for Li 1.75 B 0.25 H 4 system. The significantly enhanced hydrogen-storage properties of the $Li_{(1+x)}B_{(1-x)}H_4$ (x 1⁄4 0, 0.25, 0.5, 0.75) systems are attributed to the decrease of the boron atoms in the lithium borohydride framework, which leads to a weaker hybridization between Boron and

Hydrogen atoms, and subsequently high gravimetric capacities. Our theoretical calculations provide a novel approach for effectively tuning thermodynamics of $LiBH_4$, a leading to a potential candidate for high hydrogen-storage capacity. Experimentally evidencing these theoretical predictions may pave a new way to pursue improved hydrogen-storage properties of $LiBH_4$ and other related complex hydrides. Another important point is the cyclic properties after thermodynamic tuning. However, the cyclic properties are difficult to be evaluated by the first principle density functional theory calculation. To address this concern, the dynamic molecular and kinetic Monte Carlo are the best choices. Unfortunately, it takes several times of calculations and it will be addressed in our future works.

5 $LiBH_4$ substituted by halide

5.1 Motivation

At atmospheric pressure, two lithium borohydride polymorphs are known, with a first-order transition at 380 K, the low-temperature (orthorhombic) phase, which has a low ionic conductivity ($10^{-8}S/m$ at 303 K) and the high-temperature (hexagonal) phase, which has a remarkable high ionic conductivity ($10^{-3}S/cm$ at 393 K). It has been proven that mixtures of metal borohydrides with halides can stabilize the h-LiBH4 phase at lower temperatures. This has led several authors, for example yin et al. [151] and Corno et al. [152] to investigate anion substitution by F in the o-$LiBH_4$ (space group Pnma) [153]. Moreover, Maekawa et al. [154] proposed a superionic solid solution phase at room temperature by doping with lithium halides and also demonstrated that $Li(BH_4)_{0.667}Br_{0.333}$ conserves the hexagonal structure (space group P63mc) from 293 to 573 K [155]. Further, Gulino et al. [156] studied the mixed halide anions (Cl/Br) substitution resulting in additional optimization of the electrochemical properties of the hexagonal phase. In this chapter the substitution of $[BH_4]^-$ by halide anions (F^-, Cl^-, Br^-, I^-) has also been investigated considering three compositions (molar fraction) equal to 0.125, 0.25 and 0.375 in the hexagonal framework. Our study aims to identify the microscopic behaviour during the replacement of the $[BH_4]^-$ anion by halide (F^-, Cl^-, Br^-, I^-) into the $h-LiBH_4$ phase.

5.2 Model and computational method

To study the decomposition reaction of the solid-solution the $LiBH_4/LiX$ (with X= F, Cl, Br, I), first peinciples calculations have been performed based on a density functional theory approach. The exchange and correlation energy corrections have been included through a generalized gradient approximation (PBE-GGA),

TABLE 5.1: Optimized equilibrium cell volume, lattice parameter and internal interatomic of $Li(BH_4)_{1-x}X_x$ where (X= F, Cl, I, Br) in HT phase

System	Parameters (Å)			Interatomic distances ()					Volume
	a	b	c	Li-H	B-H	H-H	Li-B	Li-X	($Å^3$/f.u)
$Li(BH_4)_{0.875}F_{0.125}$	4.08	4.08	6.25	1.90	1.22	1.96	2.46	2.03	90.40
$Li(BH_4)_{0.75}F_{0.25}$	4.08	4.08	6.12	1.92	1.22	1.99	2.48	1.94	84.24
$Li(BH_4)_{0.625}F_{0.375}$	4.01	4.01	5.84	1.93	1.22	1.99	2.50	1.80	79.73
$Li(BH_4)_{0.875}Cl_{0.125}$	4.12	4.12	6.62	1.87	1.22	1.95	2.46	2.47	97.14
$Li(BH_4)_{0.75}Cl_{0.25}$	4.13	4.13	6.47	1.91	1.22	1.97	2.46	2.45	93.29
$Li(BH_4)_{0.625}Cl_{0.375}$	4.10	4.10	6.40	1.92	1.22	1.98	2.46	2.42	91.18
$Li(BH_4)_{0.875}Br_{0.125}$	4.14	4.14	6.66	1.90	1.22	1.96	2.46	2.60	99.11
$Li(BH_4)_{0.75}Br_{0.25}$	4.11	4.11	6.63	1.87	1.22	1.96	2.45	2.60	98.16
$Li(BH_4)_{0.625}Br_{0.375}$	4.17	4.10	6.36	1.91	1.22	1.97	2.45	2.65	98.08
$Li(BH_4)_{0.875}I_{0.125}$	4.17	4.17	6.75	1.88	1.22	1.99	2.48	2.77	101.53
$Li(BH_4)_{0.75}I_{0.25}$	4.23	4.23	6.75	1.89	1.22	1.97	2.48	2.72	104.31
$Li(BH_4)_{0.625}I_{0.375}$	4.28	4.28	6.82	1.90	1.22	1.96	2.48	2.73	107.99

with plane wave pseudo potential method (PWSCF) as implemented in the Quantum Espresso code. All pseudopotentials are constructed using the ultrasoft pseudopotential method, with cutoff kinetic energy of 50 Ry and the k-point grids for the Brillouin zone integration are sited to be 8x8x8. These values give good convergence of the total energy within $1meV/atom$. The atomic positions and the cell parameters, including the cell volume, are fully optimized by minimizing the Hellmann-Feynman forces and stresses without any symmetry constraint. All structures are fully relaxed when the Hellmann-Feynman forces on the atoms are smaller than 0.01 eV $Å^{-1}$.

5.3 Structural optimization

Atomic relaxation has been performed for each phase in this study as preliminary results, the relaxed structure are presented in figure 5.1. The obtained equilibrium volume, lattice constant and interatomic distances are summarized in table 5.1. First of all, we note that Li-B, B-H, H-H and Li-H distances are almost similar for all systems. Furthermore, the interatomic distance between Li^+ nearest added halide anions varied from 1.80 to 2.77 Å. In particular, the transition from $Pnma \rightarrow P63mc$ induces a volume expansion of 50% per formula unit. Nevertheless, for the substituted structures, we find that there is a significant reduction in volume,

associated with an energy gain up to 15 Ry per formula unit. The volume reduction is due to a large contraction along the a and c-axis. c axis of the hexagonal structure HT decreases when the parameters of the cell are optimized. The substitution effect of halides can be explained on the basis of interatomic distance. Because the size of the doping ion is larger, the inter-thermal distance in the case of doped ions is reduced and, therefore, the contribution of entropy to stabilization is smaller. The effect of substituted halides in h-$LiBH_4$ can be explained based on the interatomic distance. As the size of the halide ion is larger, the interatomic distance during the substitution is reduced. According to figure 5.1, a reorientation of $[BH_4]^-$ is observed when $[BH_4]^-$ anions are randomly replaced by halide ions (F^-, Cl^-, Br^-, I^-). It becomes more pronounced with increasing substituent fraction x, while for low values of x a partial reorientation of the nearest $[BH_4]^-$ anion to the halide anion is observed, total reorientation of $[BH_4]^-$ anion to the halide anion occurs for x = 0.25 and 0.375.

5.4 The heat of formation

The Heat of formation is calcualted based on the following reaction:

$$Li(BH_4)_{(1-x)}X_x \rightarrow (1\text{-x})\,B + 2\cdot(1\text{-x})\,H_2 + Li + x\,X \qquad \{16\}$$

figure 5.2 shows the predicted heat of formation as function of the molar fraction halide, the heat of formation of o-$LiBH_4$ are also presented as reference. Overall, the formation enthalpy decreases by increasing the molar fraction of halide content in hexagonal framework. The structure with bromide and iodides are assumed to have the highest formation enthalpy with value of -202.87 and -195.75 for x=0.125, respectively.

5.5 Lattice dynamic stability

The phonon dispersion has been carried out to analyze structural stability of $LiBH_4$ substituted by halide. Figure 5.3 shows that phonon modes are imaginary in case of the substitution for x = 0.125 and lower than observed for h-LiBH4. Furthermore, the intensity of the imaginary modes decreases when the halide anion fraction is

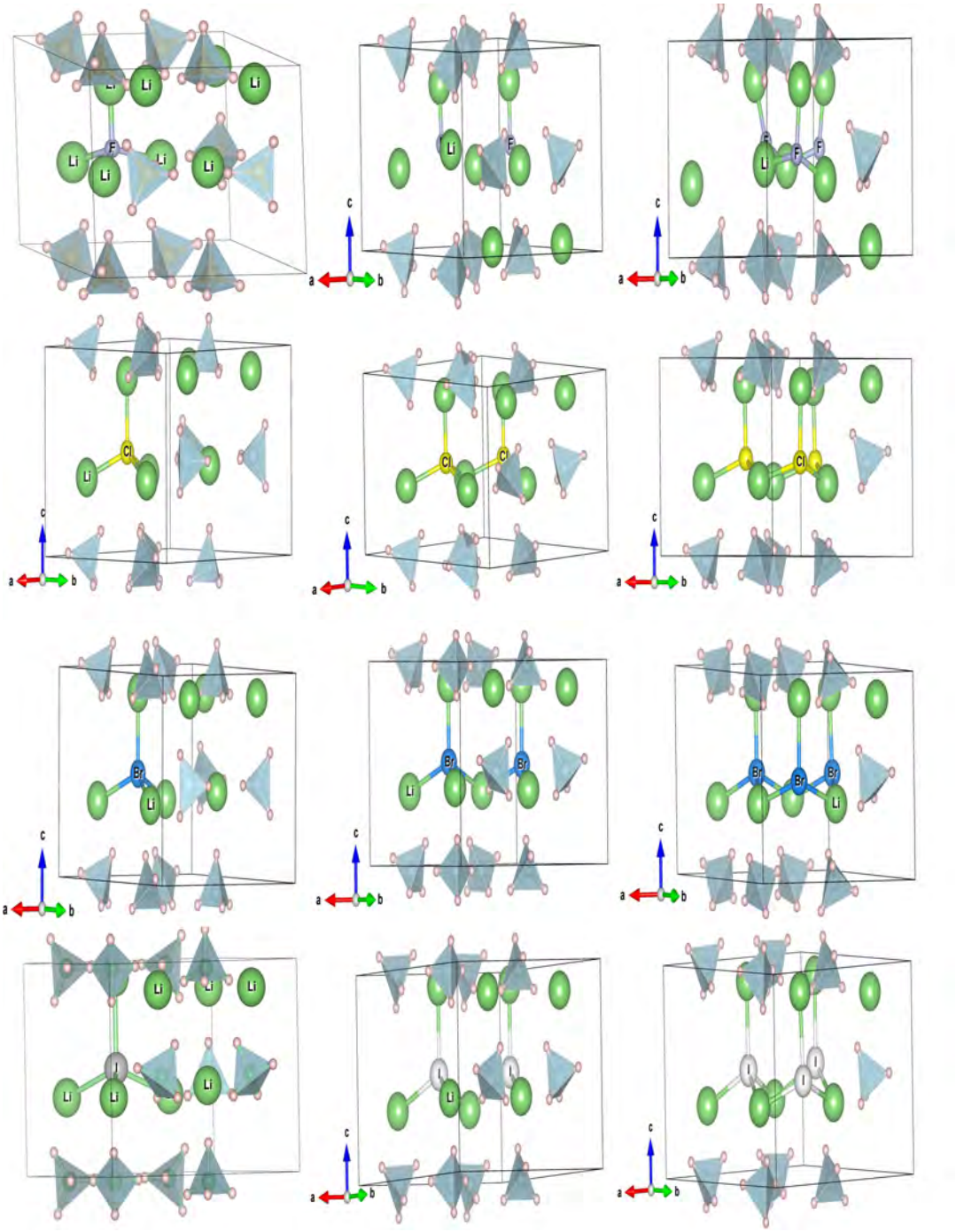

FIGURE 5.1: The optimized crystal structures of 2x2 supercells: Perspective views of LiBH4/LiX (with X= F, Cl, Br, I) systems

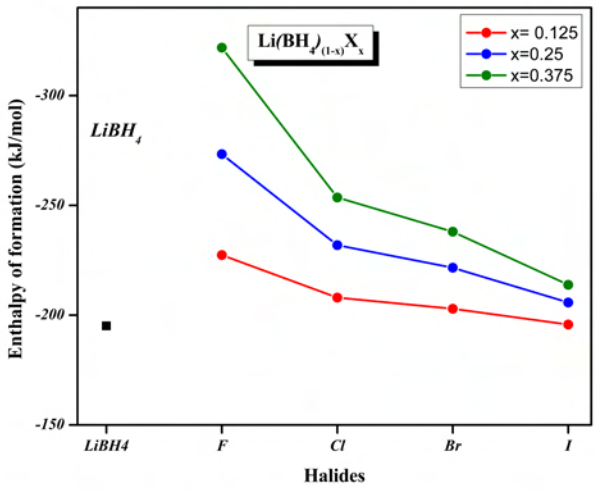

FIGURE 5.2: The calculated formation enthalpy of o-$LiBH_4$ and $LiBH_4$:LiX (with X= F, Cl, Br, I)

increased. As a result, the disordered phase is favored, and the phase is more mechanically stable at low temperature, due to the reorientation disordering of anion which is a common behavior of $[B_nH_n]^-$ groups as described for different systems based on borohydrides. Additionally, the figure 5.3 shows an imaginary frequencies around -10 THz indicates that the structure is unstable. Therefore, the coexistence of both phases (hexagonal and orthorhombic) and the absence of imaginary frequencies in the case of 37.5% indicates the structure is dynamically stable. Also, the existense of imaginary frequencies in this case mention a structure transition to orthorhombic stucture. The negative phonon branches are mostly associated with H instabilities.

5.6 De/hydrogenation and pathways

Two main desorption decomosition can be distinguished for $LiBH_4$:LiX systems (with X= F, Cl, Br, I), they are generally described according to the following reactions:

$$Li(BH_4)_{(1-x)}X_x \rightarrow (1\text{-x})\,B + \frac{3}{2}\cdot(1+x)\,H_2 + xLiX + (1\text{-x})\,LiH \qquad \{17\}$$

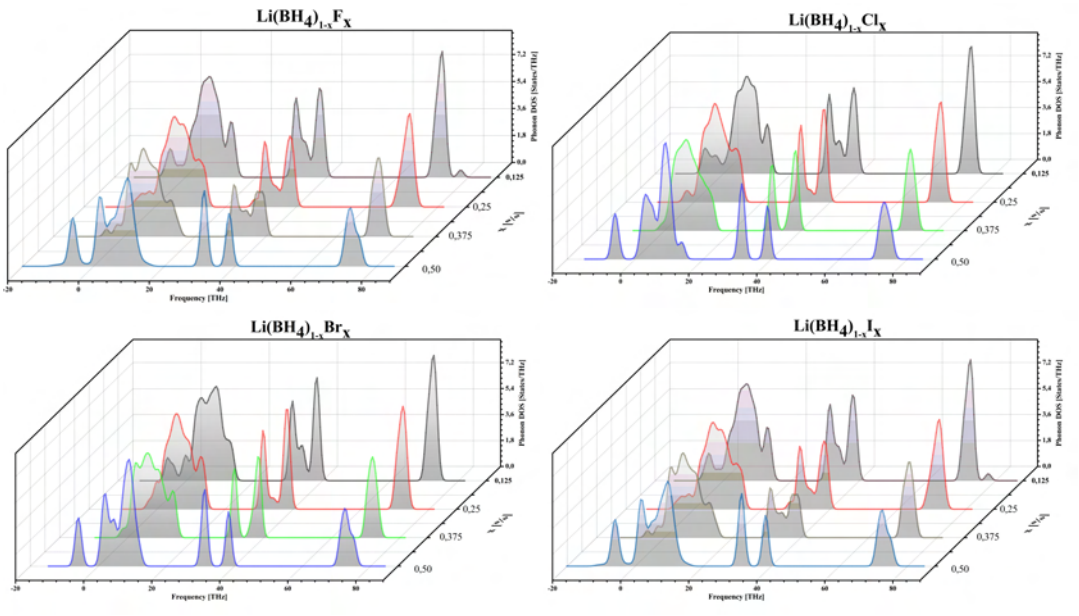

FIGURE 5.3: Total phonon density of states of $LiBH_4$:LiX (with X= F, Cl, Br, I)

$$Li(BH_4)_{(1-x)}X_x \rightarrow (1\text{-x})\,B + 2\cdot(1\text{-x})\,H_2 + (1\text{-x})\,Li + x\,LiX \qquad \{18\}$$

Where in the first step we defined LiX and LiH as product. Then we assume that the hydrogen content in LiH hydride is released. The enthalpy change accompanying a chemical change is independent of the route by which the chemical change occurs. The figure 5.4 shows theoretical hydrogen storage capacity of $LiBH_4$ based halide system. The table 5.2 is revealing the desorption enthalpy and temperature of studied systems. The substitution of the element $[BH_4]^-$ by fluorine reduces the stability of our system, which leads to an improvement of the desorption temperature. In addition, the desoption enthalpy decreases by increasing the fluorine content in hexagonal structure of $LiBH_4$. Nevertheless, it increases for the systems substituted by Clorine, Bromine and iodine. Thus, we conclude that the substiution by fluorine halide is mor intersing than other halides (Cl, Br, I) from point of view of hydrogen storage traget. Additionally, the reaction 17 exhibits a desorption temperature in the range of 500-600 K. Though, the reaction 18 exhibits a high temperature range of 680- 730 K due to formed hydride (LiH) which provide a very high stability. The compounds formed during the desorption of LiBH:LiX are not yet very clearly identified. X-ray and NMR investigations could be able to

TABLE 5.2: The enthalpy enthalpy and the corresponding desorption temperature of $LiBH_4$:LiX (with X= F, Cl, Br, I)

System	Reaction 17		Reaction 18	
	Edes (kJ mol^{-1} H_2)	Tdes (K)	Edes(kJ mol^{-1} H_2)	Tdes (K)
$Li(BH_4)_{0.875}F_{0.125}$	65.00	499.99	89.33	687.14
$Li(BH_4)_{0.75}F_{0.25}$	62.52	480.90	87.47	672.82
$Li(BH_4)_{0.625}F_{0.375}$	61.76	475.04	86.90	668.42
$Li(BH_4)_{0.875}Cl_{0.125}$	70.27	540.53	93.28	717.56
$Li(BH_4)_{0.75}Cl_{0.25}$	72.36	556.63	94.85	729.64
$Li(BH_4)_{0.625}Cl_{0.375}$	72.99	561.43	95.32	733.24
$Li(BH_4)_{0.875}Br_{0.125}$	70.66	543.56	93.58	719.83
$Li(BH_4)_{0.75}Br_{0.25}$	73.24	563.37	95.51	734.69
$Li(BH_4)_{0.625}Br_{0.375}$	74.41	572.38	96.39	741.46
$Li(BH_4)_{0.875}I_{0.125}$	70.97	545.91	93.81	721.60
$Li(BH_4)_{0.75}I_{0.25}$	72.56	558.16	95.00	730.79
$Li(BH_4)_{0.625}I_{0.375}$	72.69	559.12	95.10	731.51

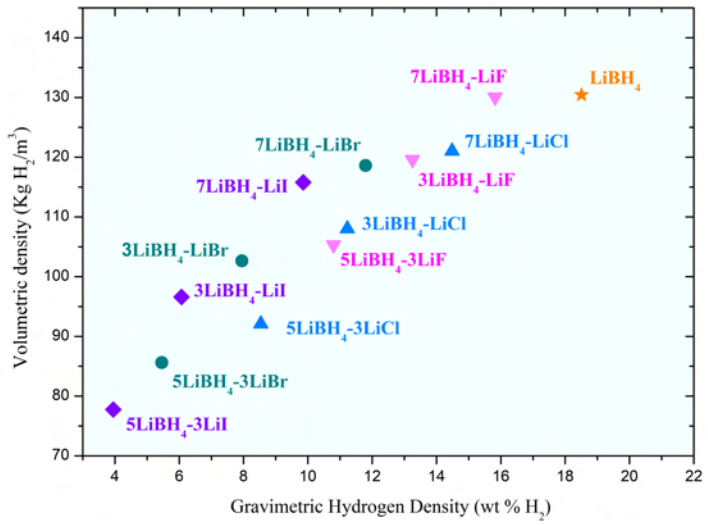

FIGURE 5.4: Theoretical hydrogen storage capacity of $LiBH_4$:LiX (with X= F, Cl, Br, I)

provide some evidence.

5.7 Conclusion

In this chapter, the hydrogen storage materials based on complex halide-borohydride. have been investigated. The properties of these systems, such as thermodynamics, crystal structure, lattice stability and energy barriers were analyzed, in order to understand its dehydrogenation behaviour and reaction pathways during the decomposition. From the obtained results, we can conclude that the substitution of lithium borohydride framework by halides is not interesting as solid-state for hydrogen storage. Since the desoption enthlpies and temperature increased in some cases reaching values far from DOE target.

General Conclusion

Conclusion

Due to the limited quantity of fossil fuels and their effects on the climate and the environment, it is becoming a global priority to explore alternative energy sources which are clean, abundant and durable. While sustainable energy such as solar, wind and hydrogen can meet the demand for energy, current challenges remain to find materials capable of storing and/or converting energy efficiently and at low cost. Hydrogen offers an elegant solution to the environment crucible. As a very flexible energy carrier, hydrogen can offer a global, clean, integrated and multisectoral energy approach, which will allow to make a contribution to solving the environmental problem and to guarantee of the Earth's energy future. However, the massive adoption of the economy hydrogen is slow due to lack of incentives and technical difficulties in hydrogen storage. The objective of this thesis was to improve the conditions for storing hydrogen in complex hydride-based tanks. According to the literature, the complex hydride $LiBH_4$ considerable interest for applications storage of hydrogen in solid state. Due to their large gravimetric and volumetric hydrogen capacities. For example, lithium borohydride ($LiBH_4$) has highest capacities among other solid storage materials 18.3% wt. However, the partial release of hydrogen requires pressures and high temperatures (up to 600 K, 10 MPa). Decomposition of complex hydride $LiBH_4$ is carried out in two stages of desorption. Boron and LiH are first formed, followed by the release of hydrogen bound to lithium. Ultimately, giving Li, B and hydrogen, the LiH formed during the first reaction of the desorption is a very stable compound. This hydride is difficult to decompose, and in practice, decomposition of $LiBH_4$ stops after LiH is formed, leaving bound hydrogen in the final products. The accessible hydrogen capacity of $LiBH_4$ is then reduced to 13.8 % by weight. Measuring the stability of hydride is inversely proportional to its energy training. As the enthalpy of formation increases, the stability of the hydride decreases. In order to use lithium

borohydride as an energy carrier in mobile applications, it is necessary to improve the thermodynamic properties of the storage of hydrogen in $LiBH_4$ without reducing its high gravimetric capacity (18.3 % wt). In our study, the role of biaxial stain on the structure of h-$LiBH_4$ and their effect on stability, thermodynamic properties and kinetics have been studied. Our results show that, the bi-axial strain results a decrease of desorption enthalpy of Lithium borohydride. Which could beneficial for improving the properties thermodynamics of $LiBH_4$. We should note also that movement of hydrogen atom inside the $LiBH_4$ frameworks was affected by the biaxial strain. Thus, enhance its kinetics propereties. The second strategy used to improve the properties of de/rehydrogenation is the substitution of boron by the lithium atom in the stable structure of borohydride lithium. First, the possibility of manufacturing these systems has been confirmed by the negative value of the formation enthalpies and the weak imaginary modes in the dispersion of phonons from all systems. In addition, the dehydrogenation temperature is reduced to 521.52 K for fully released hydrogen for the system $Li_{1.75}B_{0.25}H_4$. The significantly improved hydrogen storage properties of substituted systems are attributed to the decrease in boron atoms as part of the lithium borohydride, which leads to weaker hybridization between atoms of boron and hydrogen, and subsequently to a high gravimetric capacities. Our calculations Theories provide a new approach for efficient thermodynamic control $LiBH_4$, a leading candidate for high hydrogen storage The experimental evidence for these theoretical predictions may open up a new way to look for improved hydrogen storage properties of $LiBH_4$ and other related complex hydrides. In general, we have done a thorough study on the influence of different strategies used to improve the properties of $LiBH_4$. These studies have examined many properties; which we have shown to be the bi-axial constraint or substitution of $LiBH_4$ improves the de / hydrogenation properties of lithium borohydride either by the remarkable decrease in enthalpies of hydrogen desorption, and consequently the dehydrogenation temperature decrease towards the ambient, either in point of view kinetics or the activation energies of diffusion of hydrogen atom in $LiBH_4$ is also decreased. These thermodynamic and kinetic improvements could lead to use lithium borohydride $LiBH_4$ in storage applications hydrogen.

Lithium borohydrides have the potential to be used as anboard storage media for hydrogen in modile applications, on condition that the hydrogen desorption kinetics and reversibility

Bibliography

[1] United Nations, *World Population Prospects 2019*, **2019**, pp. 49–78.

[2] E. S. Hanley, J. P. Deane, B. P. Gallachóir, *Renewable and Sustainable Energy Reviews* **2018**, *82*, 3027–3045.

[3] IEA, Global Energy & CO₂ Statuts Report, tech. rep. March, **2018**.

[4] U.S. EIA, *Annual Energy Outlook 2019 with projections to 2050* **2019**, *44*, 1–64.

[5] British Petroleum Company, *The Editor BP Statistical Review of World Energy* **2019**.

[6] M. R. Allen, O. P. Dube, W. Solecki, F. Aragón–Durand, W. Cramer, S. Humphreys, M. Kainuma, J. Kala, N. Mahowald, Y. Mulugetta, R. Perez, M. Wairiu, K. Zickfeld, 1-Farming and Context, tech. rep., **2018**, pp. 47–92.

[7] R. Tuckett, *US EIA - Short-Term Energy Outlook* **2018**, 1–48.

[8] British Petroleum, BP statistical review of world energy. London, tech. rep., **2018**, p. 40.

[9] J. Burck, U. Hagen, F. Marten, N. Höhne, C. Bals, **2019**.

[10] L. H. U. W. Abeydeera, J. W. Mesthrige, T. I. Samarasinghalage, *Sustainability (Switzerland)* **2019**, *11*, 1–25.

[11] Freeman, *Journal of Chemical Information and Modeling* **2013**, *53*, 1689–1699.

[12] IRENA, *Hydrogen: a renewable energy perspective*, **2019**, pp. 1–52.

[13] U.S. Energy Information Administration, **2020**.

[14] H. Cavendish, *Philosophical Transactions of the Royal Society of London* **1766**, *56*, 141–184.

[15] F. G. Brickwedde, *Physics Today* **1982**, *35*, 34–39.

[16] M. L. Oliphant, P. Harteck, Rutherford, Transmutation effects observed with heavy hydrogen [1], **1934**.

[17] U.S. Department of Energy, Hydrogen Storage | Department of Energy, tech. rep. 1, **2012**, n/a.

[18] A. Züttel, *Naturwissenschaften* **2004**, *91*, 157–172.

[19] Y. Manoharan, S. E. Hosseini, B. Butler, H. Alzhahrani, B. T. F. Senior, T. Ashuri, J. Krohn, *Applied Sciences (Switzerland)* **2019**, *9*, DOI 10.3390/app9112296.

[20] J. O. Abe, A. P. Popoola, E. Ajenifuja, O. M. Popoola, *International Journal of Hydrogen Energy* **2019**, *44*, 15072–15086.

[21] B. James, **2017**.

[22] US Department of Energy, *U.S Drive* **2017**, 1–29.

[23] DOE Technical Targets for Fuel Cell Systems and Stacks for Transportation Applications | Department of Energy, **2020**.

[24] M. M. Whiston, I. L. Azevedo, S. Litster, K. S. Whitefoot, C. Samaras, J. F. Whitacre, *Proceedings of the National Academy of Sciences of the United States of America* **2019**, *116*, 4899–4904.

[25] U.S. Department of Energy, **2014**, 1–8.

[26] H Barthelemy, M Weber, F Barbier, *International Journal of Hydrogen Energy* **2017**, *42*, 7254–7262.

[27] D Mori, K Hirose, *International Journal of Hydrogen Energy* **2009**, *34*, 4569–4574.

[28] Linde AG, Cryogenic tanks | Linde Engineering, **2012**.

[29] J. R. Travis, D. Piccioni Koch, *Journal of Energy Storage* **2015**, *2*, 47–53.

[30] R. Krishna in, **2012**.

[31] R. Ahluwalia, T. Hua, J.-K Peng, S. Lasher, K. McKenney, J. Sinha, M. Gardiner, *International Journal of Hydrogen Energy* **2011**, *35*, 4171–4184.

[32] H. Barthelemy, M. Weber, F. Barbier, *International Journal of Hydrogen Energy* **2017**, *42*, 7254–7262.

[33] M. A. CHIKDENE, **1989**, 22.

[34] M. G. Nijkamp, J. E. Raaymakers, A. J. Van Dillen, K. P. De Jong, *Applied Physics A: Materials Science and Processing* **2001**, *72*, 619–623.

[35] D. Langohr, **2005**.

[36] R. Ströbel, J. Garche, P. T. Moseley, L. Jörissen, G. Wolf, *Journal of Power Sources* **2006**, *159*, 781–801.

[37] M. Hirscher, B. Panella, *Journal of Alloys and Compounds* **2005**, *404-406*, 399–401.

[38] Y. Xia, Z. Yang, Y. Zhu, *Journal of Materials Chemistry A* **2013**, *1*, 9365–9381.

[39] H. Kabbour, T. F. Baumann, J. H. Satcher, A. Saulnier, C. C. Ahn, *Chemistry of Materials* **2006**, *18*, 6085–6087.

[40] C. W. Huang, H. C. Wu, Y. Y. Li, *Separation and Purification Technology* **2007**, *58*, 219–223.

[41] S. Isobe, T. Ichikawa, J. I. Gottwald, E. Gomibuchi, H. Fujii in Journal of Physics and Chemistry of Solids, *Vol. 65*, Pergamon, **2004**, pp. 535–539.

[42] A. Chambers, C. Park, R. T. K. Baker, N. M. Rodriguez, *Journal of Physical Chemistry B* **1998**, *102*, DOI 10.1021/jp9801141.

[43] M. Hirscher, M. Becher, M. Haluska, A. Quintel, V. Skakalova, Y. M. Choi, U. Dettlaff-Weglikowska, S. Roth, I. Stepanek, P. Bernier, A. Leonhardt, J. Fink in Journal of Alloys and Compounds, *Vol. 330-332*, Elsevier, **2002**, pp. 654–658.

[44] T. Heine, L. Zhechkov, G. Seifert, *Physical Chemistry Chemical Physics* **2004**, *6*, 980–984.

[45] H. Imamura, N. Sakasai, T. Fujinaga, *Journal of Alloys and Compounds* **1997**, *253-254*, 34–37.

[46] O. V. Pupysheva, A. A. Farajian, B. I. Yakobson, *Nano Letters* **2008**, *8*, 767–774.

[47] N. S. Venkataramanan, A. Suvitha, H. Mizuseki, Y. Kawazoe, **2012**, 43.

[48] C. Liu, Y. Chen, C. Z. Wu, S. T. Xu, H. M. Cheng, *Carbon* **2010**, *48*, 452–455.

[49] H. M. Cheng, Q. H. Yang, C. Liu, *Carbon* **2001**, *39*, 1447–1454.

[50] A. D. Lucking, L. Pan, D. L. Narayanan, C. E. Clifford, *Journal of Physical Chemistry B* **2005**, *109*, 12710–12717.

[51] A. D. Lueking, R. T. Yang, N. M. Rodriguez, R. T. K. Baker, *Langmuir* **2004**, *20*, 714–721.

[52] H. Imamura, M. Kusuhara, S. Minami, M. Matsumoto, K. Masanari, Y. Sakata, K. Itoh, T. Fukunaga, *Acta Materialia* **2003**, *51*, 6407–6414.

[53] H. Imamura, S. Tabata, N. Shigetomi, Y. Takesue, Y. Sakata in Journal of Alloys and Compounds, *Vol. 330-332*, Elsevier, **2002**, pp. 579–583.

[54] F. H. Yang, R. T. Yang, *Carbon* **2002**, *40*, 437–444.

[55] D. Qu, *ACS National Meeting Book of Abstracts* **2010**, 1–26.

[56] Q. Lai, Y. Sun, T. Wang, P. Modi, C. Cazorla, U. B. Demirci, J. R. Ares Fernandez, F. Leardini, K. F. Aguey-Zinsou, *Advanced Sustainable Systems* **2019**, *3*, 1–64.

[57] J. K. Bristow, J. M. Skelton, K. L. Svane, A. Walsh, J. D. Gale, *Physical Chemistry Chemical Physics* **2016**, *18*, 29316–29329.

[58] V. R. Bakuru, M. E. DMello, S. B. Kalidindi, *ChemPhysChem* **2019**, *20*, 1177–1215.

[59] J. Liang, Y. B. Huang, R. Cao, *Coordination Chemistry Reviews* **2019**, *378*, 32–65.

[60] T. B. Lee, D. Kim, D. H. Jung, S. B. Choi, J. H. Yoon, J. Kim, K. Choi, S. H. Choi, *Catalysis Today* **2007**, *120*, 330–335.

[61] Y. Basdogan, S. Keskin, *CrystEngComm* **2015**, *17*, 261–275.

[62] A. C. Dillon, M. J. Heben, *Applied Physics A: Materials Science and Processing* **2001**, *72*, 133–142.

[63] A. C. Dillon, K. M. Jones, T. A. Bekkedahl, C. H. Kiang, D. S. Bethune, M. J. Heben, *Nature* **1997**, *386*, 377–379.

[64] M. Dornheim in *Thermodynamics - Interaction Studies - Solids, Liquids and Gases*, InTech, **2011**.

[65] J. Huot, F. Cuevas, S. Deledda, K. Edalati, Y. Filinchuk, T. Grosdidier, B. C. Hauback, M. Heere, T. R. Jensen, M. Latroche, S. Sartori, *Materials* **2019**, *12*, DOI 10.3390/ma12172778.

[66] P. Adelhelm, P. E. De Jongh, *Journal of Materials Chemistry* **2011**, *21*, 2417–2427.

[67] C. Weidenthaler, *Journal of Energy Chemistry* **2020**, *42*, 133–143.

[68] N. A. Rusman, M. Dahari, *International Journal of Hydrogen Energy* **2016**, *41*, 12108–12126.

[69] J. Bellosta von Colbe, J. R. Ares, J. Barale, M. Baricco, C. Buckley, G. Capurso, N. Gallandat, D. M. Grant, M. N. Guzik, I. Jacob, E. H. Jensen, T. Jensen, J. Jepsen, T. Klassen, M. V. Lototskyy, K. Manickam, A. Montone, J. Puszkiel, S. Sartori, D. A. Sheppard, A. Stuart, G. Walker, C. J. Webb, H. Yang, V. Yartys, A. Züttel, M. Dornheim, *International Journal of Hydrogen Energy* **2019**, *44*, 7780–7808.

[70] J. Bellosta von Colbe, J. R. Ares, J. Barale, M. Baricco, C. Buckley, G. Capurso, N. Gallandat, D. M. Grant, M. N. Guzik, I. Jacob, E. H. Jensen, T. Jensen, J. Jepsen, T. Klassen, M. V. Lototskyy, K. Manickam, A. Montone, J. Puszkiel, S. Sartori, D. A. Sheppard, A. Stuart, G. Walker, C. J. Webb, H. Yang, V. Yartys, A. Züttel, M. Dornheim, *International Journal of Hydrogen Energy* **2019**, *44*, 7780–7808.

[71] M. Dornheim, *Thermodynamics - Interaction Studies - Solids Liquids and Gases* **2011**, DOI 10.5772/21662.

[72] B. Łosiewicz, M. Popczyk, I. Napłoszek, A. Budniok in Solid State Phenomena, *Vol. 228*, **2015**, pp. 16–22.

[73] B. D. MacDonald, A. M. Rowe, *Journal of Power Sources* **2006**, *161*, 346–355.

[74] J. Chen, N. Kuriyama, H. T. Takeshita, H. Tanaka, T. Sakai, M. Haruta, *Electrochemical and Solid-State Letters* **2000**, *3*, 249–252.

[75] G. Mohan, M. Prakash Maiya, S. Srinivasa Murthy, *International Journal of Hydrogen Energy* **2007**, *32*, 4978–4987.

[76] B. Sakintuna, F. Lamari-Darkrim, M. Hirscher, Metal hydride materials for solid hydrogen storage: A review, **2007**.

[77] H. Cao, Y. Zhang, J. Wang, Z. Xiong, G. Wu, P. Chen, Materials design and modification on amide-based composites for hydrogen storage, **2012**.

[78] H. Yamamoto, H. Miyaoka, S. Hino, H. Nakanishi, T. Ichikawa, Y. Kojima, *International Journal of Hydrogen Energy* **2009**, *34*, 9760–9764.

[79] H. Y. Leng, T. Ichikawa, S. Hino, N. Hanada, S. Isobe, H. Fujii, *Journal of Power Sources* **2006**, *156*, 166–170.

[80] S. S. Murthy, **2016**, 200.

[81] V. A. Yartys, M. V. Lototskyy, E. Akiba, R. Albert, V. E. Antonov, J. R. Ares, M. Baricco, N. Bourgeois, C. E. Buckley, J. M. Bellosta von Colbe, J. C. Crivello, F. Cuevas, R. V. Denys, M. Dornheim, M. Felderhoff, D. M. Grant, B. C. Hauback, T. D. Humphries, I. Jacob, T. R. Jensen, P. E. de Jongh, J. M. Joubert, M. A. Kuzovnikov, M. Latroche, M. Paskevicius, L. Pasquini, L. Popilevsky, V. M. Skripnyuk, E. Rabkin, M. V. Sofianos, A. Stuart, G. Walker, H. Wang, C. J. Webb, M. Zhu, *International Journal of Hydrogen Energy* **2019**, *44*, 7809–7859.

[82] C. Liang, Y. Liu, H. Fu, Y. Ding, M. Gao, H. Pan, Li-Mg-N-H-based combination systems for hydrogen storage, **2011**.

[83] H. Y. Leng, T. Ichikawa, S. Isobe, S. Hino, N. Hanada, H. Fujii, *Journal of Alloys and Compounds* **2005**, *404-406*, 443–447.

[84] J. Wang, H. W. Li, P. Chen, *MRS Bulletin* **2013**, *38*, 480–487.

[85] B. Bogdanovic, M. Felderhoff, G. Streukens, *Journal of the Serbian Chemical Society* **2009**, *74*, 183–196.

[86] B. Bogdanović, M. Felderhoff, S. Kaskel, A. Pommerin, K. Schlichte, F. Schüth, *Advanced Materials* **2003**, *15*, 1012–1015.

[87] M. Ismail, Y. Zhao, X. B. Yu, A. Ranjbar, S. X. Dou, *International Journal of Hydrogen Energy* **2011**, *36*, 3593–3599.

[88] L. George, S. K. Saxena, Structural stability of metal hydrides, alanates and borohydrides of alkali and alkali- earth elements: A review, **2010**.

[89] M. J. Van Setten, G. A. De Wijs, V. A. Popa, G. Brocks, *Physical Review B - Condensed Matter and Materials Physics* **2005**, *72*, DOI 10.1103/PhysRevB.72.073107.

[90] D. Pukazhselvan, D. P. Fagg, O. N. Srivastava in International Journal of Hydrogen Energy, *Vol. 40*, Elsevier Ltd, **2015**, pp. 4916–4924.

[91] H. Morioka, K. Kakizaki, S. C. Chung, A. Yamada, *Journal of Alloys and Compounds* **2003**, *353*, 310–314.

[92] D. L. Anton in Journal of Alloys and Compounds, *Vol. 356-357*, Elsevier, **2003**, pp. 400–404.

[93] J. R. Ares, K. F. Aguey-Zinsou, F. Leardini, I. J. Ferrer, J. F. Fernandez, Z. X. Guo, C. Sanchez, *Journal of Physical Chemistry C* **2009**, *113*, 6845–6851.

[94] Y. Liu, Y. Yang, Y. Zhou, Y. Zhang, M. Gao, H. Pan, *International Journal of Hydrogen Energy* **2012**, *37*, 17137–17145.

[95] H. W. Li, Y. Yan, S. I. Orimo, A. Züttel, C. M. Jensen, *Energies* **2011**, *4*, 185–214.

[96] J. Mao, D. H. Gregory, *Energies* **2015**, *8*, 430–453.

[97] I. Dovgaliuk, D. A. Safin, N. A. Tumanov, F. Morelle, A. Moulai, R. Černý, Z. Łodziana, M. Devillers, Y. Filinchuk, *ChemSusChem* **2017**, *10*, 4725–4734.

[98] C. Milanese, T. R. Jensen, B. C. Hauback, C. Pistidda, M. Dornheim, H. Yang, L. Lombardo, A. Zuettel, Y. Filinchuk, P. Ngene, P. E. de Jongh, C. E. Buckley, E. M. Dematteis, M. Baricco, *International Journal of Hydrogen Energy* **2019**, *44*, 7860–7874.

[99] L. F. Chanchetti, D. R. Leiva, L. I. Lopes de Faria, T. T. Ishikawa, *International Journal of Hydrogen Energy* **2020**, *45*, 5356–5366.

[100] D. J. Griffiths, D. F. Schroeter, *Introduction to quantum mechanics*, Cambridge University Press, **2018**.

[101] E. Schrödinger, *Phys. Rev.* **1926**, *28*, 1049–1070.

[102] U. Peskin, N. Moiseyev, *The Journal of Chemical Physics* **1993**, *99*, 4590–4596.

[103] M Born, R Oppenheimer, *Annalen der Physik* **1927**, *389*, 457–484.

[104] D. R. Hartree, *Mathematical Proceedings of the Cambridge Philosophical Society* **1928**, *24*, 111–132.

[105] J. C. Slater, *Physical Review* **1928**, *32*, 339–348.

[106] J. A. Gaunt, *Mathematical Proceedings of the Cambridge Philosophical Society* **1928**, *24*, 328–342.

[107] J. C. Slater, Note on hartree's method [5], **1930**.

[108] V. Fock, *Zeitschrift für Physik* **1930**, *61*, 126–148.

[109] V. Fock, *Zeitschrift für Physik* **1930**, *62*, 795–805.

[110] L. H. Thomas, *Mathematical Proceedings of the Cambridge Philosophical Society* **1927**, *23*, 542–548.

[111] E. Teller, *Reviews of Modern Physics* **1962**, *34*, 627–631.

[112] R. G. Parr, Density-functional theory [9], **1990**.

[113] R. G. Parr in *Horizons of Quantum Chemistry*, Springer Netherlands, Dordrecht, **1980**, pp. 5–15.

[114] S. Seriy, *Open Journal of Modelling and Simulation* **2015**, *03*, 96–103.

[115] J.-L. Calais, *International Journal of Quantum Chemistry* **1993**, *47*, 101–101.

[116] P. Hohenberg, W. Kohn, *Physical Review* **1964**, *136*, B864.

[117] D. M. Ceperley, B. J. Alder, *Phys. Rev. Lett.* **1980**, *45*, 566–569.

[118] F. Bloch, *Zeitschrift für Physik* **1929**, *52*, 555–600.

[119] A. Dal Corso in, Springer, Berlin, Heidelberg, **1996**, pp. 155–178.

[120] QUANTUM ESPRESSO, QUANTUMESPRESSO - QUANTUMESPRESSO.

[121] P Giannozzi, O Andreussi, T Brumme, O Bunau, M. B. Nardelli, M Calandra, R Car, C Cavazzoni, D Ceresoli, M Cococcioni, N Colonna, I Carnimeo, A. D. Corso, S de Gironcoli, P Delugas, R. A. DiStasio, A Ferretti, A Floris, G Fratesi, G Fugallo, R Gebauer, U Gerstmann, F Giustino, T Gorni, J Jia, M Kawamura, H.-Y. Ko, A Kokalj, E Küçükbenli, M Lazzeri, M Marsili, N Marzari, F Mauri, N. L. Nguyen, H.-V. Nguyen, A Otero-de-la Roza, L Paulatto, S Poncé, D Rocca, R Sabatini, B Santra, M Schlipf, A. P. Seitsonen, A Smogunov, I Timrov, T Thonhauser, P Umari, N Vast, X Wu, S Baroni, *Journal of Physics: Condensed Matter* **2017**, *29*, 465901.

[122] S. Baroni, P. Giannozzi, A. Testa, *Physical Review Letters* **1987**, *59*, 2662–2665.

[123] P. Giannozzi, S. De Gironcoli, P. Pavone, S. Baroni, *Physical Review B* **1991**, *43*, 7231–7242.

[124] K. Parlinski, Z. Q. Li, Y. Kawazoe, *Phys. Rev. Lett.* **1997**, *78*, 4063–4066.

[125] F. Buda, **2008**, DOI 10.1007/978-1-4020-8250-4_24.

[126] J. P. Perdew, K. Burke, M. Ernzerhof, *Physical Review Letters* **1996**, *77*, 3865–3868.

[127] P. Giannozzi, S. Baroni, N. Bonini, M. Calandra, R. Car, C. Cavazzoni, D. Ceresoli, G. L. Chiarotti, M. Cococcioni, I. Dabo, A. Dal Corso, S. De Gironcoli, S. Fabris, G. Fratesi, R. Gebauer, U. Gerstmann, C. Gougoussis, A. Kokalj, M. Lazzeri, L. Martin-Samos, N. Marzari, F. Mauri, R. Mazzarello, S. Paolini, A. Pasquarello, L. Paulatto, C. Sbraccia, S. Scandolo, G. Sclauzero, A. P. Seitsonen, A. Smogunov, P. Umari, R. M. Wentzcovitch, *Journal of Physics Condensed Matter* **2009**, *21*, DOI 10.1088/0953-8984/21/39/395502.

[128] A Togo, I Tanaka, *Scr. Mater.* **2015**, *108*, 1–5.

[129] Y. Zhang, T. Shao, *Journal of Physics D: Applied Physics* **2013**, *46*, DOI 10.1088/0022-3727/46/23/235304.

[130] J. H. Liao, Y. J. Zhao, X. B. Yang, *International Journal of Hydrogen Energy* **2015**, *40*, 12063–12071.

[131] J. P. Soulié, G. Renaudin, R. Erný, K. Yvon, *Journal of Alloys and Compounds* **2002**, DOI 10.1016/S0925-8388(02)00521-2.

[132] J. Weiqing, C. Shilong, *International Journal of Hydrogen Energy* **2016**, DOI 10.1016/j.ijhydene.2016.10.147.

[133] Y Bouhadda, S Djellab, M Bououdina, N Fenineche, Y Boudouma, *Journal of Alloys and Compounds* **2012**, *534*, 20–24.

[134] T. J. Frankcombe, G.-J. Kroes, A. Züttel, *Chemical Physics Letters* **2005**, *405*, 73–78.

[135] N. Ohba, K. Miwa, M. Aoki, T. Noritake, S. I. Towata, Y. Nakamori, S. I. Orimo, A. Züttel, *Physical Review B - Condensed Matter and Materials Physics* **2006**, *74*, 2–8.

[136] X. Mo, W. Jiang, S. Cao, *Results in Physics* **2017**, *7*, 3236–3242.

[137] J. Weiqing, C. Shilong, *International Journal of Hydrogen Energy* **2017**, *42*, 6181–6188.

[138] S. Yu, X. Ju, C. Wan, S. Li, *International Journal of Hydrogen Energy* **2015**, *40*, 6365–6372.

[139] K. Miwa, N. Ohba, S. I. Towata, Y. Nakamori, S. I. Orimo, *Physical Review B - Condensed Matter and Materials Physics* **2004**, *69*, 1–8.

[140] F. Buchter, Z. Łodziana, P. Mauron, A. Remhof, O. Friedrichs, A. Borgschulte, A. Züttel, D. Sheptyakov, T. Strässle, A. J. Ramirez-Cuesta, *Physical Review B - Condensed Matter and Materials Physics* **2008**, *78*, 094302.

[141] T. J. Frankcombe, G. J. Kroes, *Physical Review B - Condensed Matter and Materials Physics* **2006**, *73*, 1–9.

[142] R. Gremaud, A. Züttel, A. Borgschulte, A. J. Ramirez-Cuesta, K. Refson, D. Colognesi, *Chemical Physics* **2013**, *427*, 22–29.

[143] A. M. Racu, J. Schoenes, Z. Lodziana, A. Borgschulte, A. Züttel, *Journal of Physical Chemistry A* **2008**, *112*, 9716–9722.

[144] D. J. Siegel, C. Wolverton, V. Ozoliņš, *Physical Review B - Condensed Matter and Materials Physics* **2007**, *75*, 014101.

[145] Z. Lodziana, T. Vegge, *Physical Review Letters* **2004**, *93*, 145501.

[146] A. El Kharbachi, E. Pinatel, I. Nuta, M. Baricco, *Calphad: Computer Coupling of Phase Diagrams and Thermochemistry* **2012**, *39*, 80–90.

[147] A. El Kharbachi, I. Nuta, F. Hodaj, M. Baricco, *Thermochimica Acta* **2011**, *520*, 75–79.

[148] V. Dmitriev, Y. Filinchuk, D. Chernyshov, A. V. Talyzin, A. Dzwilevski, O. Andersson, B. Sundqvist, A. Kurnosov, *Physical Review B - Condensed Matter and Materials Physics* **2008**, *77*, 174112.

[149] P. Mauron, F. Buchter, O. Friedrichs, A. Remhof, M. Bielmann, C. N. Zwicky, A. Züttel, *The Journal of Physical Chemistry B* **2008**, *112*, 906–910.

[150] P. Mauron, F. Buchter, O. Friedrichs, A. Remhof, M. Bielmann, C. N. Zwicky, A. Züttel, *Journal of Physical Chemistry B* **2008**, *112*, 906–910.

[151] L. Yin, P. Wang, Z. Fang, H. Cheng, *Chemical Physics Letters* **2008**, *450*, 318–321.

[152] M. Corno, E. Pinatel, P. Ugliengo, M. Baricco, *Journal of alloys and compounds* **2011**, *509*, S679–S683.

[153] L. M. Arnbjerg, D. B. Ravnsbæk, Y. Filinchuk, R. T. Vang, Y. Cerenius, F. Besenbacher, J.-E. Jørgensen, H. J. Jakobsen, T. R. Jensen, *Chemistry of Materials* **2009**, *21*, 5772–5782.

[154] H. Maekawa, M. Matsuo, H. Takamura, M. Ando, Y. Noda, T. Karahashi, S. I. Orimo, *Journal of the American Chemical Society* **2009**, *131*, 894–895.

[155] I. Cascallana-Matias, D. A. Keen, E. J. Cussen, D. H. Gregory, *Chemistry of Materials* **2015**, *27*, 7780–7787.

[156] V. Gulino, M. Brighi, E. M. Dematteis, F. Murgia, C. Nervi, R. Cerny, M. Baricco, *Chemistry of Materials* **2019**, *31*, 5133–5144.

ROYAUME DU MAROC
Université Mohammed V - RABAT -
جامعة محمد الخامس – الرباط –
Faculté des sciences
كلية العلوم
CENTRE D'ETUDES DOCTORALES - SCIENCES ET TECHNOLOGIES

Année Universitaire : 2020-2021

Résume

L'hydrogène offre une solution élégante à le creuset de l'environnement. En tant que vecteur d'énergie très flexible, l'hydrogène peut offrir une approche énergétique globale, propre, intégrée et multisectorielle, qui permettra contribuer de manière décisive à la résolution du problème environnemental et à la garantie de l'avenir énergétique de la Terre. Cependant, l'adoption massive de l'économie de l'hydrogène est lente en raison d'un manque d'incitations et de difficultés techniques dans le stockage de l'hydrogène. Les complexes d'hydrures de $LiBH_4$ suscitent un intérêt considérable pour plusieurs applications. Notamment, le stockage de l'hydrogène à l'état solide, en raison de leurs nombreuses propriétés remarquables. Basé sur ceci, nous avons décidé faire une étude approfondie sur l'influence des différentes stratégies utilisé pour améliorer les propriétés de $LiBH_4$. Ces études ont examiné de nombreuses propriétés ; dont nous avons montré que soit le contrainte biaxiale ou substitution de $LiBH_4$ améliore les propriétés de dé/hydrogénation de borohydrure de lithium soit par la diminution remarquable des enthalpies de désorption d'hydrogène, et par conséquent la diminution température de déshydrogénation vers l'ambiante, soit en point de vue cinétique ou les énergies d'activation de diffusion d'atome d'hydrogène en LiBH4 est également diminué. Ces améliorations thermodynamiques et cinétique pourraient conduire à utiliser le borohydrure de lithium $LiBH_4$ dans les applications de stockage de l'hydrogène.

Mots-clefs : Stockage de l'hydrogène, Borohydrure de lithium, la théorie de la densité fonctionnelle, stockage des energies.

Abstract

Hydrogen is the perfect fuel, it is abundant, the most efficient and produces no emissions when used in a fuel cell or combustion engine. However, hydrogen potential has not been realized even partially mainly because up of storage and commercial production difficulties. A complex hydride LiBH4 is a favorable prospect for solid-state hydrogen storage material capable of releasing the DOE target, because of the attractive volumetric capacity 121 kg.H2/m3, and the highest gravimetric capacity at room temperature exists 18.3 wt% . Based on this, we decided to do an in-depth study on the influence of the different strategies used to improve the properties of LiBH4. These studies have examined many properties; in which it shows that either the biaxial constraint or substitution of LiBH4 improves the de/hydrogenation properties of lithium borohydride; by the remarkable decrease in enthalpies of hydrogen desorption, and consequently the decrease in dehydrogenation temperature towards the ambient, either in kinetic point of view or the activation energies of diffusion of hydrogen atom in LiBH4 is also decreased. These thermodynamic and kinetic improvements could lead to the use of lithium borohydride LiBH4 in hydrogen storage applications.

KeyWords : Lithium borohydride, Hydrogen storage, First-principles calculation, Strain effect Desorption enthalpy, Activation energies